

Experimental Quantum Information

Hartmut Häffner

June 19, 2007

Important note: these are just notes on a lecture on experimental quantum information in the summer semester 2006 at the University of Innsbruck. Hopefully nothing less, but certainly nothing more.

Questions/remarks/criticism:

- e-mail: hartmut.haeffner@uibk.ac.at
- phone: +43 512 507-4729, -6398 or -6371

Contents

1	Introduction	4
1.1	What is quantum information?	4
1.2	Why quantum information?	7
1.3	Literature	7
2	Qubits	9
2.1	Two-level systems	9
2.2	The Schrödinger equation for a two-level system	12
2.3	The Bloch picture	12
2.4	Single qubit operations	14
2.5	The measurement process	15
2.6	Rabi oscillations	16
3	Two and more qubits	20
3.1	No-cloning theorem	20
3.2	Tensor product	20
3.3	Entanglement	21
3.4	Experimental investigation of entanglement	22
3.5	Entangled states of Atom–Photon pairs	25
3.6	Bell inequalities	26
3.7	The -1-sign of the $SU(2)$	30
3.8	Two-qubit gates	30
4	Quantum computers	34
4.1	The power of QC	34
4.2	Status of QC	34
4.3	DiVincenzo criteria	36

CONTENTS	2
-----------------	----------

4.4 Decoherence	36
4.4.1 Density matrix formalism	38
4.4.2 Decoherences	39
5 Trapped ions	40
5.1 Two-qubit gates	42
5.1.1 The Cirac&Zoller-approach	43
5.1.2 A geometrical phase gate	47
5.2 Scaling the ion trap approach	48
6 Neutral atoms	55
6.1 Atoms in 3-D optical lattices	56
6.2 A neutral atom quantum register	58
6.3 Optical tweezers approach	59
7 Cavity QED	67
7.1 Some experimental details for the Paris-experiment	67
7.2 The DiVincenzo-criteria for the Paris-experiment	70
7.3 Experiments	71
8 Superconducting qubits	78
8.1 Josephson-junctions	78
8.2 The DiVincenzo-criteria for charged qubits	81
8.3 Coupling of charged qubit to a cavity	84
9 Spin-qubits with quantum dots	93
9.1 The DiVincenzo-criteria for spin-qubits	94
9.2 Single shot readout of spins in quantum dots	95
10 Nuclear Magnetic Resonance	103
10.1 The DiVincenzo-criteria for NMR	105
11 Linear optics	112
12 Deutsch-Josza algorithm	113
13 Teleportation	121
13.1 Photon experiments	123
13.2 Ion trap experiment(s)	123

14 Simulation of quantum systems	129
---	------------

Chapter 1

Introduction

1.1 What is quantum information?

Quantum information is information stored in quantum systems. To make life easier, we will use mostly two-level systems. Processing such information is called quantum information processing!

Comparison of quantum information processing with classical computing:

	classical	quantum
Bits	physical object which is either in state 0 or 1.	superposition of two orthogonal quantum states. In particular that means that qubits can be in states where they are neither in 0 nor in 1 alone, but sort of in both simultaneously.
Register	a row of 0's and 1's.	a collection of 2-level systems.
Computation	switching of bits	rotations in the Hilbert-space.

A qubit is usually described mathematically as:

$$|\Psi\rangle_{\text{qubit}} = \alpha|0\rangle + \beta|1\rangle \quad (1.1)$$

with α and β being complex numbers and $|\alpha|^2 + |\beta|^2 = 1$. What's the difference to an analogue bit (e.g. a voltage)? You will be able to answer this after the lecture!

The most general state of a (three) qubit (quantum) register is the superposition: $|\Psi\rangle_{\text{register}} = c_{000}|000\rangle + c_{001}|001\rangle + c_{010}|010\rangle + c_{011}|011\rangle + c_{100}|100\rangle + c_{101}|101\rangle + c_{110}|110\rangle + c_{111}|111\rangle$.

Thus a three-qubit register lives in an 8-dimensional Hilbert space. Now, operations on the quantum register can be described by matrices.

Suppose we want to increment our qubit register by one. We just have to implement the following matrix:

$$\begin{array}{c}
 \text{Input} \\
 \Downarrow \\
 \left(\begin{array}{cccc|ccccc}
 |000\rangle & |001\rangle & |010\rangle & |011\rangle & |100\rangle & |101\rangle & |110\rangle & |111\rangle & \\
 \hline
 0 & 0 & 0 & 0 & 0 & 0 & 0 & -1 & |000\rangle \\
 1 & 0 & 0 & 0 & 0 & 0 & 0 & 0 & |001\rangle \\
 0 & 1 & 0 & 0 & 0 & 0 & 0 & 0 & |010\rangle \\
 0 & 0 & 1 & 0 & 0 & 0 & 0 & 0 & |011\rangle \\
 0 & 0 & 0 & 1 & 0 & 0 & 0 & 0 & |100\rangle \\
 0 & 0 & 0 & 0 & 1 & 0 & 0 & 0 & |101\rangle \\
 0 & 0 & 0 & 0 & 0 & 1 & 0 & 0 & |110\rangle \\
 0 & 0 & 0 & 0 & 0 & 0 & 1 & 0 & |111\rangle
 \end{array} \right) \Rightarrow \text{Output}
 \end{array} \tag{1.2}$$

What is happening to a state $\frac{1}{\sqrt{3}}(|001\rangle + |010\rangle + |110\rangle)$? Just apply the matrix to this state and we get: $\frac{1}{\sqrt{3}}(|010\rangle + |011\rangle + |111\rangle)$ Message: operations can be performed on different "numbers" simultaneously.

This would be really great: suppose you want to factor $2^{58919405739217} - 1$. We just put the quantum register in a superposition of all numbers between 2 and $2^{29459702869608}$ and try to divide through all these numbers with our quantum computer simultaneously and get all factors immediately.

But: a measurement (in the logical basis) yields one of the states (e.g. $|011\rangle$ in the small example above)! We can obtain only one result at a time. On top of this is only probabilistic if the quantum computer is in a superposition state at the read-out! So how do we gain anything from quantum computing? Trick: measure only in the end and in a particular basis such that the result is deterministic. We will see later how to perform these basis transformations.

This is what a (simple) quantum computation looks like:

1. Initialization (classical): often $|00\cdots 0\rangle$
2. Computation (quantum): matrix multiplication
3. Measurement (classical): projection onto one of the measurement eigenstates

(pointless remarks: we humans are too simple minded to feed anything else than classical information into a computer as well as to read off anything else (interface to our classical world). Note: Most error-correction protocols require a measurement and a feedback during the computation.)

Some specialities about quantum information?

- Quantum information processing is reversible. The reason is that all operations can be described by unitary operations (rotations in the Hilbert-space). No information is destroyed! We only look at it from another side. Have a look at the solution of the time-independent Schrödinger equation $i\hbar \frac{d}{dt}|\Psi\rangle = H|\Psi\rangle$

$$|\Psi(t)\rangle = \exp(-iHt/\hbar)|\Psi(0)\rangle \quad (1.3)$$

However, this holds only if the environment is included. If you don't want to do that (or you can't) you have to use the density matrix formalism (later). Remarks: to erase one bit you have to generate $kT \ln 2$ heat. This is not necessary for both a classical and a quantum computer.

- Quantum information cannot be copied (The no-cloning theorem: Wootters & Zurek "A Single quantum cannot be cloned", Nature 299, 802-803 (1982)).
- Still, quantum information can be transferred with almost perfect fidelity, however, the source has to be destroyed. This is what physicists call teleportation.
- A measurement removes most of the information. This information is "lost" in the environment.
- Most measurements have no definite outcome.

1.2 Why quantum information?

- Bits get smaller and smaller till the information is quantum whether we want it or not.
- Factorization of large numbers (Shor, P. W.: Algorithms for quantum computation: discrete log and factoring. Proceedings of the 35th IEEE FOCS, 124134 (1994)) factorization of a number with L digits: classical computer: $t \sim \exp(L^{1/3})$, quantum computer: $t \sim L^2$
- Search of large unsorted data bases search data base with N entries (Grover, L. K.: A fast quantum mechanical algorithm for database search. Proceedings of the 28th ACM STOC, 212219 (1996)): classical computer: $O(N)$, quantum computer: $O(N^{1/2})$
- Simulation of quantum systems (Feynman, R. P.: Simulating physics with computers. International Journal of Theoretical Physics 21, 467488 (1982))
- Test of quantum mechanics (quantum – classical transition): why can't we be in a superposition of being in bed and at work?
- Quantum computer as atomic "state synthesizer": optical clocks, "super atoms"
- Provides a new view on quantum mechanics and on information science
- For the fun of it (Gedanken experiments): explore the weirdness of quantum mechanics experimentally (wavefunction collapse, entanglement, teleportation ...)

1.3 Literature

Often I will give the references on the spot. Here are some references (books) which cover a broader range:

- "Quantum Computation and Quantum Information", M. A. Nielsen and I. L. Chuang, Cambridge (2000).

- ”A short introduction to Quantum Information and Quantum Computation”, M. Le Bellac, Cambridge University Press (2006).
- ”The Physics of Quantum Information”, D. Bouwmeester (editor), (Springer, 2000).
- H.-K. Lo, T. Spiller, S. Popescu, Introduction to Quantum Computation and Information (World Scientific, 1998).
- ”Introduction to Quantum Computers”, G. P. Berman (editor), (World Scientific, 1998).
- See also links on
”<http://heart-c704.uibk.ac.at/LV/Quanteninformation/Quanteninformation.html>”

Chapter 2

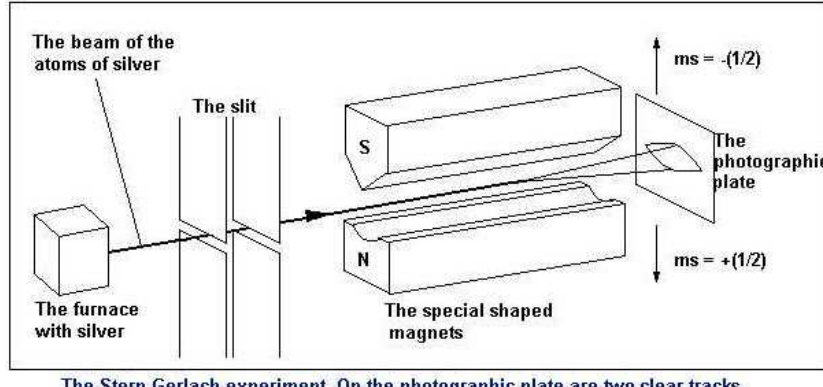
Qubits

Qubits are represented by two level systems.

2.1 Two-level systems

Examples for qubits:

- Electron spin
Stern-Gerlach experiment What happens if an atomic beam passes a Z -oriented Stern-Gerlach apparatus? What happens for ZX and finally for ZXZ ?
- Zeeman-levels of atoms
- Polarization of (single) photons \Rightarrow Quantum cryptography
Experiment:
 1. A $|0\rangle = |V\rangle$ polarized laser beam hits a polarizer oriented horizontally. Complete darkness \Rightarrow the probability to find the laser beam in $|1\rangle = |H\rangle$ is 0.
 2. We insert another polarizer (oriented differently at some other angle) in the path \Rightarrow we get light! The beam is now prepared in $|H\rangle$!
- Time bins of single photons \Rightarrow Quantum cryptography.



The Stern-Gerlach experiment. On the photographic plate are two clear tracks.

Figure 2.1: Sketch of the Stern-Gerlach experiment (from: <http://library.thinkquest.org/19662/low/eng/exp-stern-gerlach.html>).

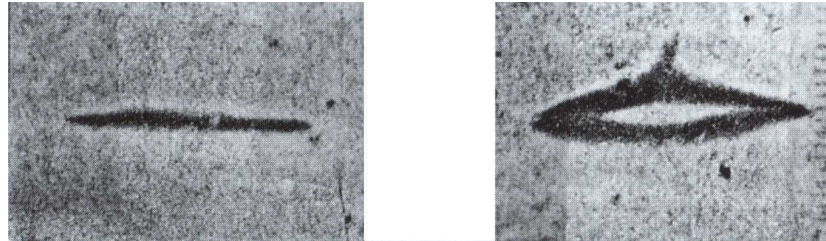


Figure 2.2: Original data from the Stern-Gerlach experiment. (a): no magnetic field, (b) with magnetic field. (from: <http://www.physik.unibas.ch/Praktikum/VPII/SternGerlach/SternGerlach.html> / Original publications: W. Gerlach und O. Stern, "Der experimentelle Nachweis der Richtungsquantelung im Magnetfeld", Zeitschrift für Physik **9**, 349 (1922) und W. Gerlach und O. Stern, "Das magnetische Moment des Silberatoms", Zeitschrift für Physik **9**, 353 (1922))

- A pair of electrons (cooper pair) or not in a small superconducting volume (charge qubit).
- Two levels of an atom
Hyperfine states or (meta) stable states (see 2.3).

Qubits live in two dimensional Hilbert-spaces. An arbitrary quantum state of a two-level system is given by

$$|\Psi\rangle = \alpha|0\rangle + \beta|1\rangle \quad (2.1)$$

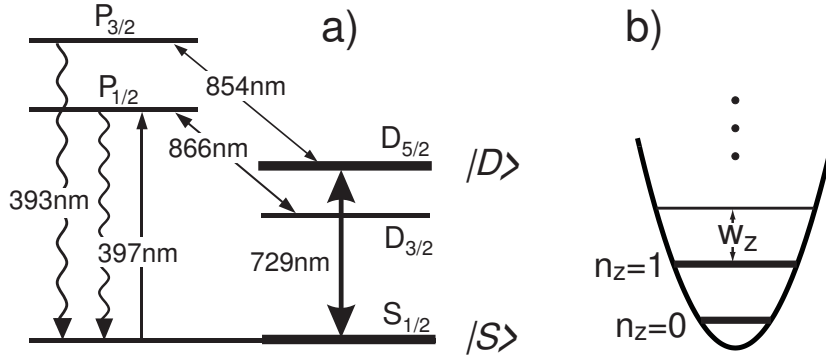


Figure 2.3: Level scheme of Calcium.

with $|\alpha|^2 + |\beta|^2 = 1$. This might be rewritten as

$$|\Psi\rangle = e^{i\gamma} \left(\cos \frac{\theta}{2} |0\rangle + e^{i\varphi} \sin \frac{\theta}{2} |1\rangle \right). \quad (2.2)$$

Which operations are allowed to transform a valid state into another valid state? 2×2 matrices which conserve the norm (i.e. unitary, $A^\dagger A = I$). In addition we want $\det(A) = 1$. These objects form a group called SU(2). We can write

$$A = e^{-iH}. \quad (2.3)$$

H is traceless and Hermitian. Then any H yields an A within the SU(2). The H 's form the so-called Lie-Algebra of the SU(2). As a basis we have the important matrices: $\sigma_x = \begin{pmatrix} 0 & 1 \\ 1 & 0 \end{pmatrix}$, $\sigma_y = \begin{pmatrix} 0 & -i \\ i & 0 \end{pmatrix}$, $\sigma_z = \begin{pmatrix} 1 & 0 \\ 0 & -1 \end{pmatrix}$

Thus we can write

$$A = e^{-i(a\sigma_x + b\sigma_y + c\sigma_z)}. \quad (2.4)$$

Remark: the Lie-algebra is the derivative of the group at the identity. To convince yourself take the derivative of Eq. 2.3. the Lie-algebra yields information about the group around the identity. The nice thing about groups is that, once you know what it looks like locally, you know (almost) everything about the group.

2.2 The Schrödinger equation for a two-level system

$$i\hbar \frac{d}{dt} |\Psi\rangle = H |\Psi\rangle \quad (2.5)$$

For a magnetic moment in a magnetic field H is $-\vec{\mu} \cdot \vec{B}$. For a spin-1/2 particle:

$\vec{\mu} = \mu \vec{\sigma}$, $\vec{\sigma} = \begin{pmatrix} \sigma_x \\ \sigma_y \\ \sigma_z \end{pmatrix}$. This yields the Schrödinger equation (Schrödinger-Pauli equation):

$$i\hbar \begin{pmatrix} \dot{C}_1 \\ \dot{C}_2 \end{pmatrix} = -\mu \left(\begin{pmatrix} 0 & B_x \\ B_x & 0 \end{pmatrix} + \begin{pmatrix} 0 & -iB_y \\ iB_y & 0 \end{pmatrix} + \begin{pmatrix} B_z & 0 \\ 0 & -B_z \end{pmatrix} \right) \begin{pmatrix} C_1 \\ C_2 \end{pmatrix} \quad (2.6)$$

The Pauli-matrices appear. They tell how the spin should change from each time-step to the next one. Or in other words: how its motion should differ from doing nothing. Here we are: the Lie-algebra. We also see that a magnetic field along the x and the y axes can induce transitions between the two logical eigenstates spin up $0 = |\uparrow\rangle$ and spin down $1 = |\downarrow\rangle$.

The solution to the Schrödinger-Equation Eq. 2.5 is given by (its time independent):

$$|\Psi(t)\rangle = \exp\left(-i\frac{Ht}{\hbar}\right) |\Psi(0)\rangle \quad (2.7)$$

$\exp\left(-i\frac{Ht}{\hbar}\right)$ is the time evolution operator. Note that the Hamiltonian H is in the SU(2)'s Lie-algebra. Thus $\exp\left(-i\frac{Ht}{\hbar}\right)$ automatically is an element of the SU(2).

2.3 The Bloch picture

Can we visualize the SU(2)? Difficult. But there exists an epimorphism from the SU(2) to the SO(3) (group of rotations in a three dimensional space). These groups have the same Lie-algebra (Spin (SU(2)) and angular

momentum ($\text{SO}(3)\text{SU}(2)$ operations as rotations in a three dimensional space.

Now, have a look at Eq. 2.2. It is difficult to observe the overall phase γ (only the modulus of a wave function can be measured). Two angles remain: θ and $\phi \Rightarrow$ point on a sphere.

$$\vec{R} = \begin{pmatrix} \cos \varphi \sin \theta \\ \sin \varphi \sin \theta \\ \cos \theta \end{pmatrix} \quad (2.8)$$

We call it Bloch sphere. Note, that we are in danger to mix different things: the states of a qubit (they live on the Bloch sphere) and the operation on the state (rotations of the Bloch sphere).

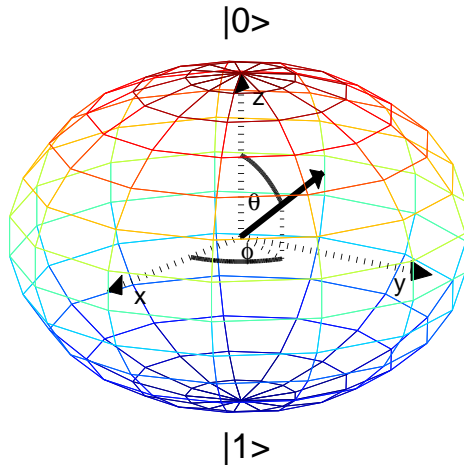


Figure 2.4: The Bloch sphere.

In Eq. 2.2 we inserted the strange factor of 2. The reason is that a full rotation ($\theta = 2\pi$) on the Bloch sphere doesn't bring the state back only within a factor of -1 . We will discuss later an experiment which verifies this. But we can get some hints with the laser-PBS experiment:

- Note that we have to rotate by 90 degrees to change from $|H\rangle$ to $|V\rangle$. However, to rotate from $|H\rangle$ to $|V\rangle$ on the Bloch sphere, we need $\theta = \pi$.
- A rotation around 180 degrees in real space (a 2π -pulse) changes the sign (the phase of the electric field).

- We can interpret the phase ϕ as the relative phase of the $|H\rangle$ - and $|V\rangle$ -basis states.

Remark without explanation: Laser light itself is not a qubit! We need to quantize it first and that means single photons.

2.4 Single qubit operations

Rotations around any of the three axis: X, Y and Z -gates. Example:

$$R_x(\theta) = e^{i\frac{\theta}{2}\sigma_x} = \cos \frac{\theta}{2}I + i \sin \frac{\theta}{2}\sigma_x = \begin{pmatrix} \cos \frac{\theta}{2} & i \sin \frac{\theta}{2} \\ i \sin \frac{\theta}{2} & \cos \frac{\theta}{2} \end{pmatrix} \quad (2.9)$$

$$R_y(\theta) = e^{i\frac{\theta}{2}\sigma_y} = \cos \frac{\theta}{2}I + i \sin \frac{\theta}{2}\sigma_y = \begin{pmatrix} \cos \frac{\theta}{2} & \sin \frac{\theta}{2} \\ -\sin \frac{\theta}{2} & \cos \frac{\theta}{2} \end{pmatrix} \quad (2.10)$$

$$R_z(\theta) = e^{i\frac{\theta}{2}\sigma_z} = \cos \frac{\theta}{2}I + i \sin \frac{\theta}{2}\sigma_z = \begin{pmatrix} e^{i\theta/2} & 0 \\ 0 & e^{-i\theta/2} \end{pmatrix} \quad (2.11)$$

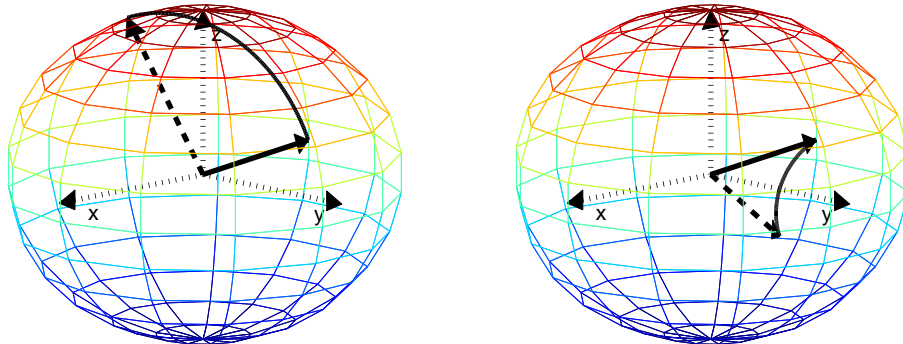


Figure 2.5: Rotation around the X and the Y axis visualized on the Bloch-sphere.

Any rotations around an axis in the x - y -plane can now be written as

$$R(\theta, \phi) = \exp \left(i\theta/2 (e^{i\phi}\sigma_+ + e^{-i\phi}\sigma_-) \right), \quad (2.12)$$

where $\sigma_+ = \begin{pmatrix} 0 & 1 \\ 0 & 0 \end{pmatrix}$ and $\sigma_- = \begin{pmatrix} 0 & 0 \\ 1 & 0 \end{pmatrix}$ are the raising and lowering operators. Rotations around the z axis can be decomposed into rotations around the x and the y axis.

2.5 The measurement process

A measurement of a qubit yields only one result: either $|0\rangle$ or $|1\rangle$. What else would we expect of a bit? After all the photon gets absorbed or not in the polarizer. Or an atom is either fluorescing or not (That requires that a fluorescence measurement measures the qubit)! Mathematically, we say that

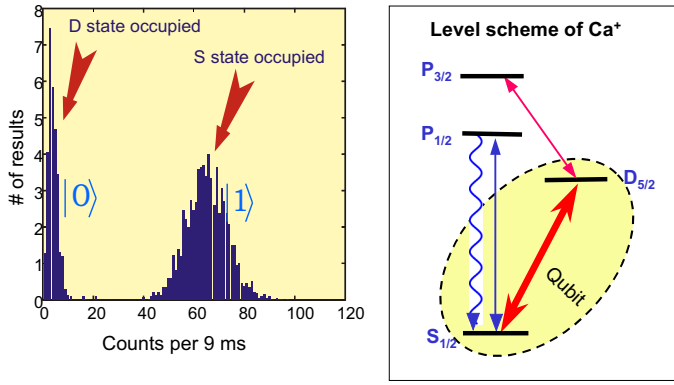


Figure 2.6: State detection in a Calcium-40 ion via the so-called electron shelving method. The ion fluoresces only when it is in the ground state $|1\rangle = |S\rangle$. If the qubit is in $|0\rangle = |D\rangle$ the ion remains dark.

the qubit (the Bloch vector) is projected onto the eigen-basis of the operator corresponding to the measurement process. Often we measure energies. Then we deal with the eigenstates of the Hamiltonian or for qubits the σ_z -operator.

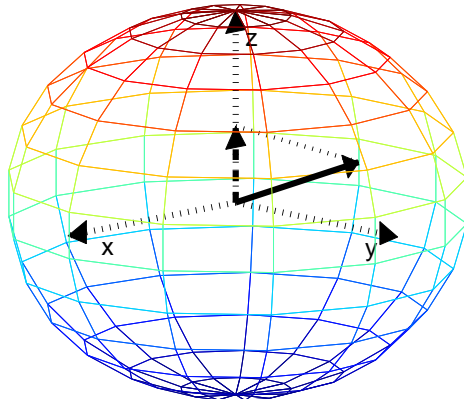


Figure 2.7: A measurement is described by a projection onto the z -axis of the Bloch sphere.

2.6 Rabi oscillations

Resonant coupling between the two levels of a qubit is described by the (Schrödinger-) equation:

$$i \begin{pmatrix} \dot{C}_1 \\ \dot{C}_2 \end{pmatrix} = \begin{pmatrix} 0 & \Omega/2 \\ \Omega/2 & 0 \end{pmatrix} \begin{pmatrix} C_1 \\ C_2 \end{pmatrix} \quad (2.13)$$

Solve this either by e^{-Ht} or solve the differential equation. Choose $C_1(t = 0) = 1$, $C_0(t = 0) = 0$ and you get:

$$\ddot{C}_1 = -i\frac{\Omega}{2}\dot{C}_2 = -(\Omega/2)^2 C_1 . \quad (2.14)$$

This equation has the solutions:

$$C_1(t) = \cos \frac{\Omega}{2}t \quad \text{and} \quad C_2(t) = i \sin \frac{\Omega}{2}t . \quad (2.15)$$

What do we measure?

$$|C_1(t)|^2 = \cos^2 \frac{\Omega}{2}t = \frac{1}{2}(1 + \cos \Omega t) \quad (2.16)$$

$$|C_2(t)|^2 = \sin^2 \frac{\Omega}{2}t = \frac{1}{2}(1 - \cos \Omega t) \quad (2.17)$$

The system driven around the Bloch sphere.

What do we learn from this:

- $\pi/2$ -pulse \Rightarrow system in a superposition $\frac{1}{\sqrt{2}}(|0\rangle + ie^{i\varphi}|1\rangle)$, where in Eq. 2.13 the Ω 's have to be replaced by $e^{\pm i\varphi}\Omega$. The phase which appears here can be understood as the relative phase between the atomic polarization and the lasers phase (see Fig. 2.9). Thus we can draw an analogy to a driven harmonic oscillator to understand what is going on for different phases.
- π -pulse \Rightarrow population is inverted.
- 2π -pulse ($t = 2\pi/\Omega$) \Rightarrow population is not changed, but the sign of the wavefunction is inverted ($|\Psi\rangle \rightarrow -|\Psi\rangle$)! Experiment: later when we have means to detect it experimentally!

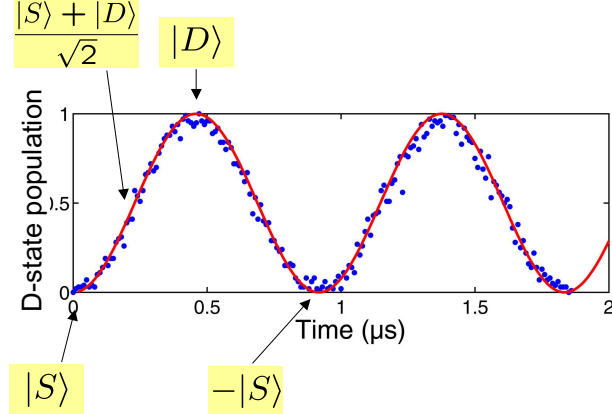


Figure 2.8: Rabi-flops between the $|S\rangle$ and the $|D\rangle$ states of a Calcium-40-ion. First the ion was prepared in the $|S\rangle$ state and the coupling (a laser connecting the $|S\rangle$ and the $|D\rangle$ states) was switched on for a time indicated at the x-axis. For each dot the experiment is repeated 100 times. Finally the ions state was measured by driving the $|S\rangle \rightarrow |P\rangle$ transition: For the $|S\rangle$ -state fluorescence, for the $|D\rangle$ -state complete darkness.

The last operation is the most important single qubit operation. It realizes the transformation:

$$\begin{matrix} |0\rangle & |1\rangle \\ |0\rangle & \left| \frac{1}{\sqrt{2}}, \frac{i}{\sqrt{2}} \right. \\ |1\rangle & \left| \frac{i}{\sqrt{2}}, \frac{1}{\sqrt{2}} \right. \end{matrix} \quad (2.18)$$

In Eq. 2.12 this corresponds to $R(\pi/2, 0)$.

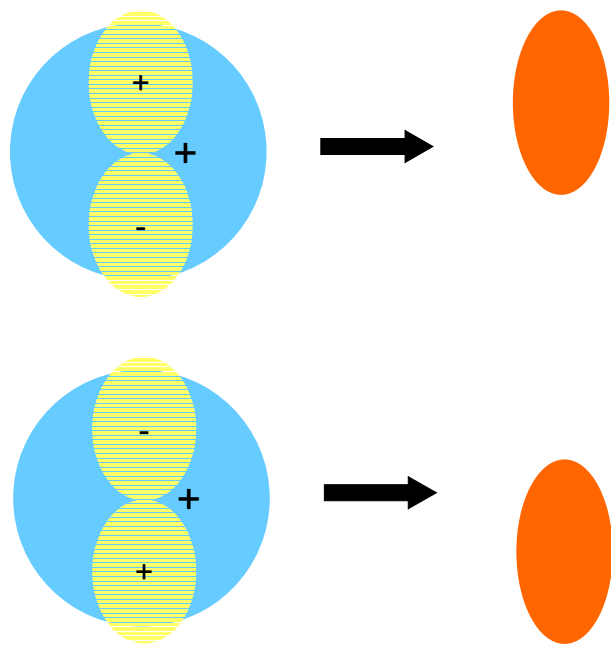


Figure 2.9: The emergence of a dipole from a relative phase of the atomic wave functions. As time goes on the realative phase of the atomic wave functions (connected to the S and P-level) evolve according to the Schrödinger equation. Thus the dipole oscillates.

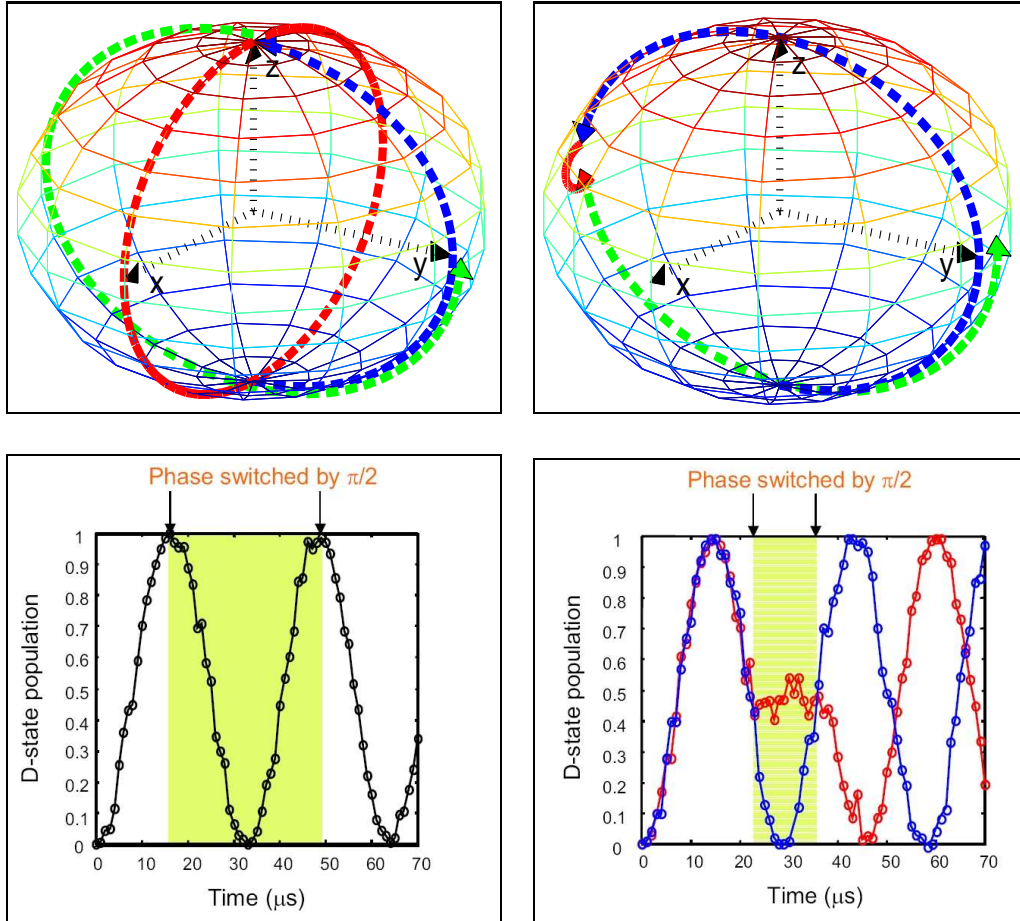


Figure 2.10: Single qubit rotations. Left: $R(\pi, 0)R(2\pi, \pi/2)R(\pi, 0)$, right: $R(3\pi/2, 0)R(\pi, \pi/2)R(3\pi/2, 0)$, top: traces of the Bloch vector, bottom: the corresponding measurement results.

Chapter 3

Two and more qubits

3.1 No-cloning theorem

Unlike classical information quantum information cannot be copied (W.K. Wootters and W.H. Zurek, Nature London **299**, 802 (1982)). The usual method of measuring on bit and then preparing another one fails, because we never can gain full information on a quantum bit (unless we know in which state it is).

3.2 Tensor product

Composite quantum systems (qubits) are described as the tensor product (or the inner product) of the descriptions of the corresponding subsystems:

$$|BA\rangle = |B\rangle \otimes |A\rangle . \quad (3.1)$$

Why is this a good way to do it? Suppose both qubits are in an equal superposition of the basis states $|0\rangle$ and $|1\rangle$. What is the probability to find both qubits in $|0\rangle$? Our intuition suggests $\frac{1}{4}$. Formally the probability now is given by

$$|\langle 00|BA\rangle|^2 = |(\langle 0| \otimes \langle 0|)(|B\rangle \otimes |A\rangle)|^2 = |\langle 0|B\rangle \times \langle 0|A\rangle|^2 = \frac{1}{4} , \quad (3.2)$$

where we assumed $|A\rangle = |B\rangle = (|0\rangle + |1\rangle)/\sqrt{2}$. With other words, the tensor product structure ensures that the combined probability of events is the product of the single event probabilities. How does it work if you want to describe the state space with matrices?

$$|A\rangle = \begin{pmatrix} a_1 \\ a_2 \end{pmatrix}, |B\rangle = \begin{pmatrix} b_1 \\ b_2 \end{pmatrix} \Rightarrow |B\rangle \otimes |A\rangle = \begin{pmatrix} b_1 a_1 \\ b_1 a_2 \\ b_2 a_1 \\ b_2 a_2 \end{pmatrix}. \quad (3.3)$$

3.3 Entanglement

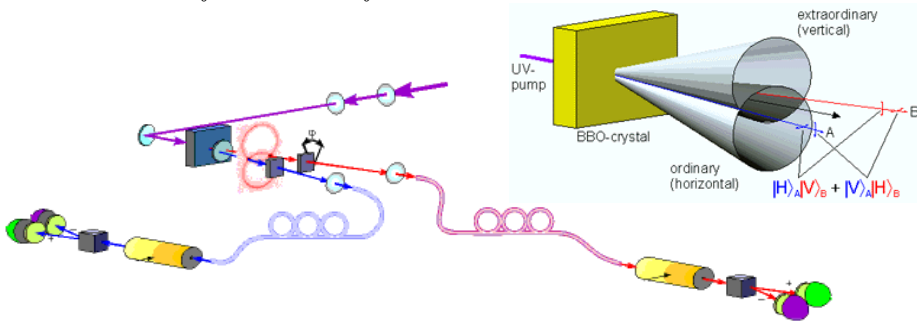
Entangled states are non-separable states. What does that mean? Suppose we have two systems (e.g. qubits) $|A\rangle$ and $|B\rangle$. Two examples for valid states are $|00\rangle + |01\rangle$ and $|00\rangle + |11\rangle$ (from here on we sometimes leave out the normalization). The first state we can write also as $|0\rangle \otimes (|0\rangle + |1\rangle)$. Then according to the rule for tensor products (c.f. Eq. 3.2) the probability of finding the total system in a particular state is just the product of the probabilities for each subsystem. But what for $|00\rangle + |11\rangle$? Here it doesn't work, because we cannot write this state as a tensor product of two states. This is called non-separability. We call every state which cannot be written as a tensor product entangled. The probability to find one result in one subsystem depends on what you would find in the other system. Attention: whether a state is entangled or not depends on your point of view. Suppose you change the basis from $\{|00\rangle, |01\rangle, |10\rangle, |11\rangle\}$ to $\{|oo\rangle = |00 + 11\rangle, |oI\rangle = |00 - 11\rangle, |Io\rangle = |01 + 10\rangle, |II\rangle = |01 - 10\rangle\}$ (this is the so-called Bell-basis). Then $|oo\rangle = |00 + 11\rangle$ can be written as $|o\rangle \otimes |o\rangle$ seems not to be entangled anymore! Therefore the concept of subsystems is crucial for entanglement. Now: Are the spins of two electrons in a ground-state Helium-atom entangled? Their spin state is $|\uparrow\downarrow\rangle - |\downarrow\uparrow\rangle$ (the total wavefunction has to be antisymmetric with respect to the exchange of the two particles). Here, we won't call this an entangled state as we are not able to observe the electrons independently. Question: is the state $|00\rangle + |01\rangle + |10\rangle + |11\rangle$ entangled? No, because it can be written as $(|0\rangle + |1\rangle) \otimes (|0\rangle + |1\rangle)$. Nevertheless $|00\rangle + |01\rangle + |10\rangle - |11\rangle$ is entangled. You can convince yourself by trying to write it as a product state. Now we try to understand entanglement:

Parametric down conversion

(excerpt from: "<http://www.quantum.univie.ac.at/research/photonentangle/teleport/tpsource.htm>" l")

Inside a nonlinear crystal (BBO) an ultraviolet photon (wavelength 490nm) may spontaneously split into two infrared photons (780 nm). The down-conversion photons (A and B) have orthogonal polarizations ($|H\rangle$ or $|V\rangle$). In the two beams along the intersections of the cones we observe a polarization-entangled two-photon state.

For the experimental realization of quantum teleportation it was necessary to use pulsed down-conversion. Only if the pulse width of the UV-light, and thus the time of generating photon pairs is shorter than the coherence time of the down-converted photons, interferometric Bell-state analysis can be performed. In the experiment the pulses from a mode-locked Ti:Saphire laser have been frequency doubled to give pulses of 200 fs duration. The interfering light was observed after passage through IR-filters of 4 nm bandwidth giving a coherence time of about 520 fs.



3.4 Experimental investigation of entanglement

Parametric down-conversion (see inset on page 22) leads to entangled photon pairs of the form $|VH\rangle e^{i\alpha} |HV\rangle$ (an entangled state with horizontal $|H\rangle$ and vertical $|V\rangle$ polarizations as a single photon basis) (see Kwiat et al., Phys. Rev. Lett. 75, 4337 - 4341 (1995)).

How do we verify that this is an entangled state? Suppose party A (Alice) measures in the $\{|H\rangle, |V\rangle\}$ basis and party B (Bob), too. Each of the two find apparently random results. But if they compare their results later, then

whenever Alice measures $|H\rangle$ Bob measures $|V\rangle$ and vice-versa. Is that the heart of entanglement? No! This could be explained with a source, which randomly sends balls marked with $|H\rangle$ in one direction and with $|V\rangle$ in the opposite direction. There is nothing quantum mechanical about a source like this.

Now, suppose Alice and Bob choose to apply each to rotate their qubit prior to their measurement. That is they place a half-wave plate in the path and thus measure in the $\{|+\rangle, |-\rangle\} \equiv \{|H\rangle + |V\rangle, |H\rangle - |V\rangle\}$ basis. What will they find? For simplicity we investigate now the state $|VH + HV\rangle$ (What would happen to $|VH - HV\rangle$, what would we have to do to get the same result as in the following lines for the singlet state?).

$$\begin{aligned} |VH + HV\rangle &\xrightarrow{R_2(\pi/2,0), R_1(\pi/2,0)} \\ &|(V + iH)(H + iV) + (H + iV)(V + iH)\rangle \\ &= |VH + iVV + iHH - HV + HV + iHH + iVV - VH\rangle \\ &= i|HH + VV\rangle. \end{aligned}$$

That means, only by choice of the basis, we switched from a perfectly anti-correlated to a perfectly correlated state. At first glance this is also not difficult to believe, because in a classical picture Alice could have inverted all their photons. But here both of them applied only half the rotation. Additionally some parts of the states interfere destructively whereas other interfere constructively. This interference happens for a state which is delocalized (the photons can be really far apart). In the end Alice's and Bob's results can be still perfectly correlated (i.e. a (partially) deterministic) result.

The situation becomes even more intriguing if Alice and Bob decide to switch their measurement basis independently and randomly. When they then later compare their data, they find anti-correlation when they both have chosen to measure in the logical basis, correlation when they have measured in the $\{|+\rangle, |-\rangle\}$ basis and no correlation at all when they measured in different basis sets. Note that unless Alice and Bob tell each other in which basis they measured when they have no information what the other measured. Otherwise information would have been transmitted instantaneously. However, if they tell each other, they (and only they) know what the other measured when they both measured in the same basis. This can be used for quantum cryptography (secure transmission of a secret key), because an observer tabbing the line would destroy the perfect correlation and thus would be

detected. Of course Alice and Bob have to test from time to time whether they have perfect correlation and thus throw away some part of their keys ...

What happens if we scan the phase ϕ of the second analysis pulse in Eq. 3.4?

$$\begin{aligned}
 |VH + HV\rangle &\xrightarrow{R_2(\pi/2,\phi), R_1(\pi/2,0)} \\
 &|(V + ie^{i\phi}H)(H + iV) + (H + ie^{-i\phi}V)(V + iH)\rangle \\
 &= |VH + iVV + ie^{i\phi}HH - e^{i\phi}HV + HV + iHH + ie^{-i\phi}VV - e^{-i\phi}VH\rangle \\
 &= |(1 - e^{-i\phi})VH + i(1 + e^{-i\phi})VV + i(1 + e^{i\phi})HH + (1 - e^{i\phi})HV\rangle.
 \end{aligned}$$

The we change between correlated and anti-correlated results.

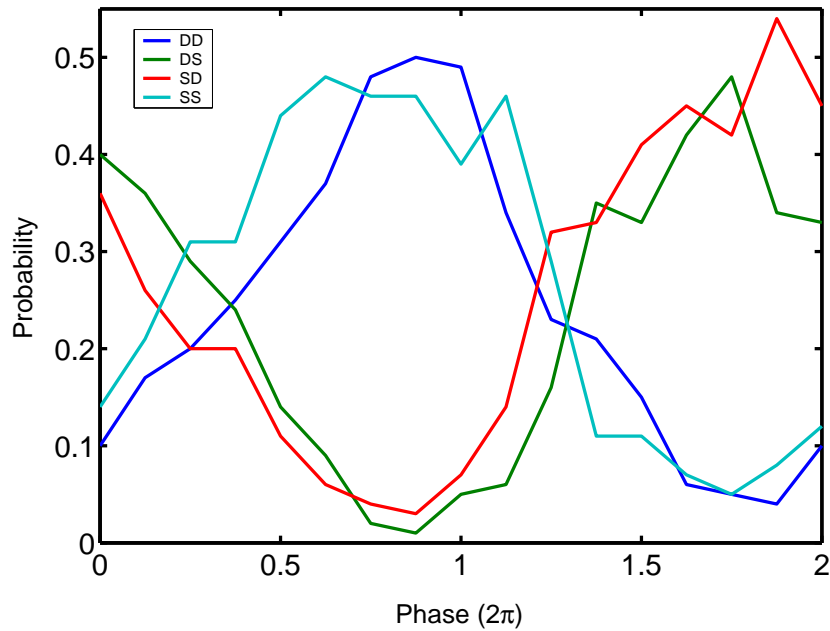


Figure 3.1: Recent results on the ion trap experiment. The Bell state $|SD + e^{i\phi}DS\rangle$ of two Calcium ions was analyzed with two $\pi/2$ -pulses. The phase of the pulse onto the second ion was scanned. The oscillation is a proof of the interference of the state and thus of entanglement. From the contrast the maximum overlap with a Bell state of the form $|SD + e^{i\phi}DS\rangle$ (the fidelity) can be deduced to amount to at least 0.85.

3.5 Entangled states of Atom–Photon pairs

Experiments carried out by C. Monroe (Ann Arbor, US) with ions (Fig. 3.2) and by H. Weinfurter (Munich) with atoms (Fig. 3.3).

photon, or the $^2S_{1/2} |1,0\rangle$ ground state (defined as $| \uparrow \rangle$) while emitting a σ^- -polarized photon (Fig. 2b). The single photon pulses are collected with an $f/2.1$ imaging lens whose axis is perpendicular to the quantization axis. Along this direction, the states of polarization of the σ^+ and the π photons are orthogonal; the former (defined as $|H\rangle$) is polarized perpendicular to the quantization axis,

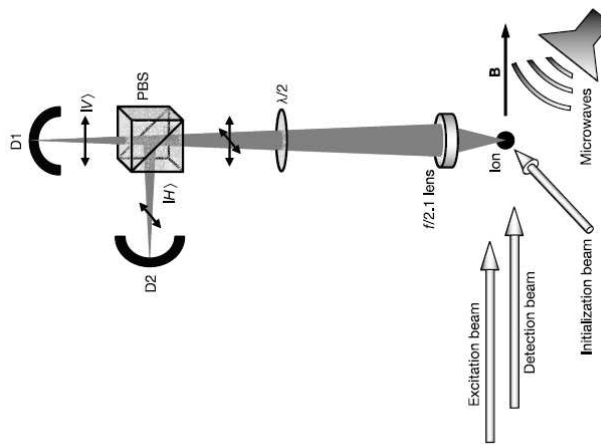


Figure 3.2: From B. B. Blinov *et al.*, Nature **428** 153 (2004). How to entangle single photons with a single Cadmium ion.

Figure 2 The experimental procedure (time axis not to scale). **a**, The atomic qubit is initialized to the $| \uparrow \rangle$ hyperfine ground state, following a $30\text{-}\mu\text{s}$ π -polarized optical pumping pulse and a $15\text{-}\mu\text{s}$ microwave (μw) rotation. **b**, The atom is weakly excited with a 50-ns σ^+ -polarized optical pulse, resulting in spontaneous emission to either state $| \uparrow \rangle$ or state $| \downarrow \rangle$ (separated by frequency $\delta \approx 2\pi(1.0\text{ MHz})$), accompanied by emission and detection of a photon polarized in state $|H\rangle$ or state $|V\rangle$, respectively. **c**, After a delay of $\tau \approx 1\text{ }\mu\text{s}$, a $15\text{-}\mu\text{s}$ microwave rotation pulse prepares the atomic qubit for measurement in any basis, and finally a $200\text{-}\mu\text{s}$ σ^+ -polarized optical detection pulse provides efficient measurement of the atomic qubit.

Figure 1 The experimental apparatus. The π -polarized initialization beam propagates perpendicular to the quantization axis defined by a magnetic field **B**, while the σ^- -polarized excitation and detection beams propagate along the quantization axis. The scattered photons are collected by an imaging lens and directed to a polarizing beam splitter (PBS), and two photo-counting detectors D1 and D2 register the V- and H-polarized photons, respectively. The $\lambda/2$ -waveplate is used to rotate the photon polarization for photonic qubit measurements in different bases. A microwave horn is located near the tap to drive coherent transitions between the hyperfine levels of the atomic ground state, at a frequency near 14.5 GHz .

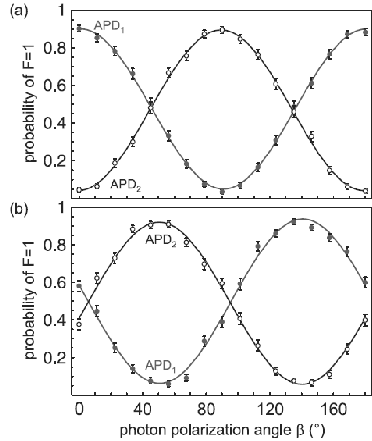


FIG. 3 (color online). Probability of detecting the atom in the ground level $F = 1$ (after the STIRAP pulse) conditioned on the detection of the photon in detector APD₁ (●) or APD₂ (○) as the linear polarization of the photonic qubit is rotated by an angle β . (a) The atomic qubit is measured in $\hat{\sigma}_z$ and (b) in $\hat{\sigma}_y$, whereas the photonic qubit is projected onto the states $1/\sqrt{2}(|\sigma^+\rangle \pm e^{i\beta}|\sigma^-\rangle)$.

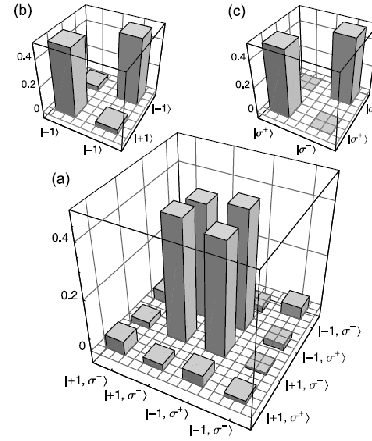


FIG. 4 (color online). (a) Graphical representation of the real part of the measured density matrix of the entangled atom-photon state. The fidelity (overlap with the expected state $|\Psi^+\rangle$) from this measurement is $\mathcal{F} = 0.87 \pm 0.01$. Insets (b) and (c) show the single particle density matrices for the atom and photon state, respectively, indicating that the single particles when observed on their own are found in a completely mixed state.

Figure 3.3: From J. Volz *et al.*, Phys. Rev. Lett. **96**, 030404 (2006). These results are with neutral Rb-atoms.

3.6 Bell inequalities

Many people were/are not happy with the (philosophical) consequences of entanglement, because entanglement was thought to imply some instantaneous remote interaction between the subsystems. Most of the alternative explanation attempts postulated hidden variables for each subsystem with the information in which state the subsystem should be found in case it is measured. Bell could prove that certain quantities are always smaller than 2 for these scenarios but could be larger than 2 in the framework of quantum mechanics. Thus violations of Bell inequalities were used to rule out (classical) explanations for the strange consequences of entanglement. If you're more interested in this, here is some literature concerning Bell-inequalities:

- Einstein, B. Podolsky, N. Rosen, Phys. Rev. 47 (1935) 777 u. N. Bohr, following article, "Can Quantum-Mechanical Description of Physical Reality Be Considered Complete?" Bell's Inequalities, Concept and Experimental Tests:

- J. S. Bell: "Speakable and unspeakable in quantum mechanics", Collected Papers Cambridge Univ. Press 1987 and later reprints
 - G. Alber, M. Freyberger: "Quantenkorrelationen und die Bell'schen Ungleichungen", Phys. Blätter 55 (1999) 23-27 Summary of the so-called "Aspect-type" Correlated Two-Particle Experiments:
 - A. Aspect: "Experimental Tests of Bell's Inequalities", Europhys. News 22 (1991) 73
 - A. Aspect: "Bell's inequality test: more ideal than ever", Nature 390 (1999) 189
- Einstein, Podolsky, and Rosen.

MAY 15, 1935

PHYSICAL REVIEW

VOLUME 47

Can Quantum-Mechanical Description of Physical Reality Be Considered Complete?A. EINSTEIN, B. PODOLSKY AND N. ROSEN, *Institute for Advanced Study, Princeton, New Jersey*

(Received March 25, 1935)

In a complete theory there is an element corresponding to each element of reality. A sufficient condition for the reality of a physical quantity is the possibility of predicting it with certainty, without disturbing the system. In quantum mechanics in the case of two physical quantities described by non-commuting operators, the knowledge of one precludes the knowledge of the other. Then either (1) the description of reality given by the wave function in

quantum mechanics is not complete or (2) these two quantities cannot have simultaneous reality. Consideration of the problem of making predictions concerning a system on the basis of measurements made on another system that had previously interacted with it leads to the result that if (1) is false then (2) is also false. One is thus led to conclude that the description of reality as given by a wave function is not complete.

■ Bohr.

OCTOBER 15, 1935

PHYSICAL REVIEW

VOLUME 48

Can Quantum-Mechanical Description of Physical Reality be Considered Complete?N. BOHR, *Institute for Theoretical Physics, University, Copenhagen*

(Received July 13, 1935)

It is shown that a certain "criterion of physical reality" formulated in a recent article with the above title by A. Einstein, B. Podolsky and N. Rosen contains an essential ambiguity when it is applied to quantum phenomena. In this connection a viewpoint termed "complementarity" is explained from which quantum-mechanical description of physical phenomena would seem to fulfill, within its scope, all rational demands of completeness.

Figure 3.4: Publications starting the discussion about hidden-variable theories (from Ulrich Hohenester's lecture on the interpretation of quantum mechanics: <http://physik.uni-graz.at/uxh/>).

In the following, we follow the lecture notes of R. Werner / Braunschweig (<http://www.imaph.tu-bs.de/ftp/werner/qm9596.dvi>) in order to find boundaries for certain experimental values which can be explained by a classical theory. Of course we want to investigate a setting where the experiment violate these boundary. The setting is as follows: we have two (entangled) particles (e.g. photons (Weihs et al., Phys. Rev. Lett. **81** 5039 (1998)) or ions (see e.g. Rowe et al., nature **409** 791 (2001)) which are measured each independently (e.g. both systems are very far from each other) in either 0 or 1 by an apparatus A and B for each respective particle. We have four possible outcomes with the probabilities $P(0, 0|A, B)$, $P(0, 1|A, B)$, $P(1, 0|A, B)$, $P(1, 1|A, B)$. Note that we avoid to use kets, because we want to construct a classical theory. We define now the parity $C(A, B)$ (C for correlation coefficient) as

$$\begin{aligned} C(A, B) &= \sum_{a,b} abP(a, b|A, B) \\ &= P(0, 0|A, B) - P(0, 1|A, B) - P(1, 0|A, B) + P(1, 1|A, B) \end{aligned}$$

where $a, b \in \{-1, 1\}$ are the possible measurement results. From this, we have $-1 \leq C(A, B) \leq 1$.

We (or the respective parties) make now four of such parity measurements (of course we have to repeat them independently over and over for each setting) where we choose all four combinations of two measurement settings $\{A_1, A_2\}, \{B_1, B_2\}$ for each particle. We sum the results of the four measurement settings in the following way up:

$$\beta = C(A_1, B_1) + C(A_1, B_2) + C(A_2, B_1) - C(A_2, B_2). \quad (3.5)$$

We have now four random variables a_1, a_2, b_1, b_2 representing the possible measurement values ± 1 . We assume now that each of these 16 possibilities has a certain value when a measurement is done (and in contradiction to quantum mechanics also the quantity not measured). Thus for the Bell correlation in Eq. 3.5, we have

$$\beta = a_1 b_1 + a_1 b_2 + a_2 b_1 - a_2 b_2. \quad (3.6)$$

For each single realisation, $a, b \in \{-1, 1\}$, there is no way that $|\beta| > 2$. Thus we have also for statistical mixtures as the expectation value is a linear function $|\beta| \leq 2$. This a Bell inequality, derived in this form by Clauser, Horne, Shimony and Holt (Phys. Rev. Lett. **23**, 880 (1969)).

What is our quantum mechanical expectation. Lets assume we start with two ions (photons) in the state $\Psi = (|00\rangle + |11\rangle)/\sqrt{2}$. We have now to calculate the expectation values $a_n b_n$ for all four measurement settings: doing nothing before the measurement, rotating one particle by $\pi/4$ before the measurement, and finally rotating both by $\pi/4$ before the measurement.

The measurement settings A_1 and B_1 are in the logical eigen basis and we have $\langle a_1 \rangle = \langle b_1 \rangle = 0$, but $\langle a_1 b_1 \rangle = 1$, because both measurement yield always the same sign. Applying the rotation on just one of the ions leads to the following state:

$$\begin{aligned} &(|00\rangle + |11\rangle)/\sqrt{2} \xrightarrow{R_a(\pi/4,0)} \\ &((\cos \frac{\pi}{8}|0\rangle + i \sin \frac{\pi}{8}|1\rangle)|0\rangle + (\cos \frac{\pi}{8}|1\rangle + i \sin \frac{\pi}{8}|0\rangle)|1\rangle)/2. \end{aligned} \quad (3.7)$$

This state is of the form $c_1|00\rangle + c_2|01\rangle + c_3|10\rangle + c_4|11\rangle$ with $c_1 = \cos \frac{\pi}{8}$ and $c_2 = i \sin \frac{\pi}{8}$. We get now for the parity of this state:

$$2c_1^2 - 2c_2^2 = \cos^2 \frac{\pi}{8} - \sin^2 \frac{\pi}{8} = \cos \frac{\pi}{4} = \frac{1}{\sqrt{2}}, \quad (3.8)$$

where we used the identity $\cos(\alpha + \beta) = \cos \alpha \cos \beta - \sin \alpha \sin \beta$.

Furthermore, a calculation analogous to Eq. 3.4 (or applying a $R_b(\pi/4, 0)$ pulse to the result of Eq. 3.7) shows that applying a pulse $R(\frac{\pi}{4}, 0)$ to both particles prior to the measurement (corresponding to the situation where we measure in A_2 and B_2), yields $|00\rangle + i|01\rangle + i|10\rangle + |11\rangle$, whose parity is 0 ($a_2 b_2 = 0$).

Thus we finally have for these measurement settings from Eq. 3.6:

$$\beta = 1 + \frac{1}{\sqrt{2}} + \frac{1}{\sqrt{2}} - 0 = 2 + (\sqrt{2} - 1). \quad (3.9)$$

There have been plenty of experimental tests where values of $\beta > 2$ were found. Most notably by A. Aspect (reference???). However, it is very difficult to experimentally avoid loopholes. For instance, one can be tempted to argue that during the measurement process information leaks out to the other particle telling it which way to behave. Therefore quite some effort was made to do the measurement within the time it takes light to travel between the two measurement locations. Zeilinger (reference) where the first

to realize this setup. In these experiments, however, only a fraction of the entangled photons could be analysed because of finite detector efficiencies. Therefore we can argue that by some mysterious selection process only a certain class of particles could be detected which violate the Bell inequality. An ion trap experiment ruled this out (Rowe et al., Nature **409** 791 (2001)) by creating entanglement deterministically and collecting all measurement results, however, at the expense that the measurements were not separated light-like. Now we can argue again that ... well we simply have to do the experiment.

3.7 The -1-sign of the $SU(2)$

Now we are going to investigate the strange property that the sign of the wavefunction is changed, when we apply 2π -pulse (see Sec. 2.6). Suppose the following experiment: We split a quantum state into two halves with $R(\pi/2, 0)$ -pulse, wait for some time and finally recombine it then again with a $R(\pi/2, \pi)$ -pulse (a Ramsey experiment). If everything goes well, we end with the same state we started with. Now we perform a 2π -rotation on one of the "populations" in between the Ramsey pulses. What do we expect? The phase of the part of the wavefunction which undergoes the Rabi-oscillation gets a minus sign! This means that we now have acquired an additional phase factor of -1. Thus the last $R(\pi/2, \pi)$ -pulse effectively acts as a $R(\pi/2, 0)$ -pulse and in total we should have inverted to total population.

As an example Fig. 3.5 discusses an experiment realized in the ion-trap set-up at Innbruck. Fig. 3.6 shows the relevant level scheme of a single ion in a trap.

3.8 Two-qubit gates

A two qubit gate (+ single qubit gates) whith which you can realize any unitary transformation in the Hilbert space is called universal. Three prominent examples:

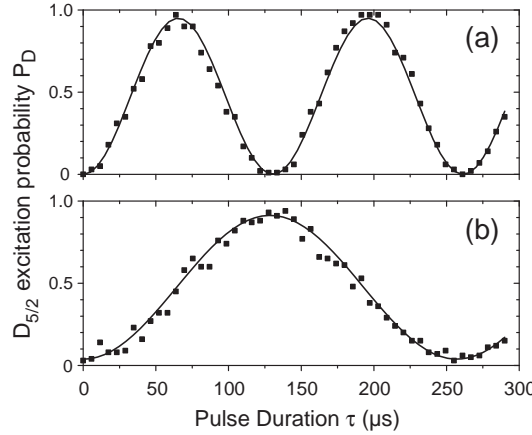


Figure 3.5: (a) Resonant Rabi oscillations on the blue sideband of the $|S\rangle - |D\rangle$ transition. The period of the population oscillation is 131(1) μs , as found from the fit to the data. (b) Ramsey $\pi/2$ pulses on the $|S\rangle - |D\rangle$ carrier transition enclose the Rabi flopping on the sideband. The phase of the $|S\rangle$ state is revealed to oscillate with a period of 257(2) μs . The ratio of both periods is 1.96(3) and agrees well with the expected value of 2. (from "Precision measurement and compensation of optical Stark shifts for an ion-trap quantum processor", H. Häffner et al., Phys. Rev. Lett. **90**, 143602-1-4 (2003).)

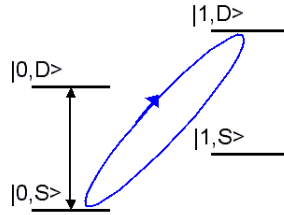


Figure 3.6: level scheme of a single trapped ion. The electronic (internal) states are labelled S and D . The first two motional excitations of the ion are labelled 0 and 1. Thus only for $|0, S\rangle$ -state a blue sideband transition is possible.

1. Phase gate ($\Phi(\pi)$):

$$\Phi(\pi) = \left(\begin{array}{c|cccc} & 00 & 01 & 10 & 11 \\ \hline 00 & 1 & 0 & 0 & 0 \\ 01 & 0 & 1 & 0 & 0 \\ 10 & 0 & 0 & 1 & 0 \\ 11 & 0 & 0 & 0 & -1 \end{array} \right) . \quad (3.10)$$

2. CNOT gate:

	00	01	10	11
00	1	0	0	0
01	0	1	0	0
10	0	0	0	1
11	0	0	1	0

(3.11)

The second bit (the left most bit) in Eq. 3.11, or ' b ' in Eq. 3.3, is called the control bit, because it controls whether the first bit (the target bit) is flipped or not. What happens if we apply a CNOT to a state Ψ , where the control bit is in a superposition of the two logical eigenstates and the target bit is in an eigenstate ($\Psi = \frac{1}{\sqrt{2}}(|0\rangle + |1\rangle) \otimes |0\rangle$)? The control bit remains unchanged, however the target bit is put in the same state as the control bit. Thus we arrive at the entangled state $(|00\rangle + |11\rangle)/\sqrt{2}$. However, note that this is not copying quantum information. A copy machine would have created the state $\frac{1}{2}(|0\rangle + |1\rangle) \otimes (|0\rangle + |1\rangle)$.

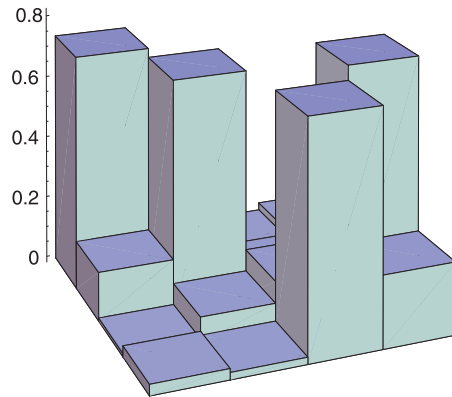


Figure 3.7: Truth table of a CNOT realized in an ion trap setup (from: F. Schmidt-Kaler et al., Nature 422, 408-411 (2003).).

3. $\sqrt{\text{SWAP}}$ gate:

	00	01	10	11
00	1	0	0	0
01	0	$\frac{1}{\sqrt{2}}$	$\frac{1}{\sqrt{2}}$	0
10	0	$-\frac{1}{\sqrt{2}}$	$\frac{1}{\sqrt{2}}$	0
11	0	0	0	1

(3.12)

With single qubit operations these gates are all equivalent. Example: what does the pulse sequence $R_1(\pi/2, \pi)\Phi R_1(\pi/2, 0)$ (time flows from right to left):

$$R_1(\pi/2, \pi)\Phi R_1(\pi/2, 0) =$$

$$\begin{pmatrix} 1 & -i & 0 & 0 \\ -i & 1 & 0 & 0 \\ 0 & 0 & 1 & -i \\ 0 & 0 & -i & 1 \end{pmatrix} \begin{pmatrix} 1 & 0 & 0 & 0 \\ 0 & 1 & 0 & 0 \\ 0 & 0 & 1 & 0 \\ 0 & 0 & 0 & -1 \end{pmatrix} \begin{pmatrix} 1 & i & 0 & 0 \\ i & 1 & 0 & 0 \\ 0 & 0 & 1 & i \\ 0 & 0 & i & 1 \end{pmatrix} \quad (3.13)$$

For the first qubit (upper left 2×2 matrix) we have the identity, because $R(\pi/2, \pi)R(\pi/2, 0) = \exp(-i\frac{\pi}{2}\sigma_x)\exp(i\frac{\pi}{2}\sigma_x) = I$. Alternatively you see that by looking on the Blochsphere! For the lower right part we have

$$\begin{aligned} \exp(-i\frac{\pi}{2}\sigma_x)\exp(i\pi\sigma_z)\exp(i\frac{\pi}{2}\sigma_x) &= \frac{1}{\sqrt{2}} \begin{pmatrix} 1 & -i \\ -i & 1 \end{pmatrix} \begin{pmatrix} 1 & 0 \\ 0 & -1 \end{pmatrix} \frac{1}{\sqrt{2}} \begin{pmatrix} 1 & i \\ i & 1 \end{pmatrix} \\ &= \frac{1}{\sqrt{2}} \begin{pmatrix} 1 & -i \\ -i & 1 \end{pmatrix} \frac{1}{\sqrt{2}} \begin{pmatrix} 1 & i \\ -i & -1 \end{pmatrix} \\ &= \begin{pmatrix} 0 & i \\ -i & 0 \end{pmatrix} \end{aligned} \quad (3.14)$$

Thus we have

$$R_1(\pi/2, \pi)\Phi(\pi)R_1(\pi/2, 0) = \begin{pmatrix} 1 & 0 & 0 & 0 \\ 0 & 1 & 0 & 0 \\ 0 & 0 & 0 & i \\ 0 & 0 & -i & 0 \end{pmatrix}. \quad (3.15)$$

We have transferred a phase gate into a CNOT gate. That means: what you can do with one gate, you can do with the other gate, too, just by using additional single qubit gates. Thus the phase gate has also entangling capability and is as universal as a CNOT. Similarly the $\sqrt{\text{SWAP}}$ gate in Eq. 3.12 can be transferred into a CNOT and is therefore also universal.

Chapter 4

Quantum computers

4.1 The power of QC

Hilbert space is big! Example: 30 qubits: $2^{30} \approx 10^9$ dimensions. This corresponds to $\sim 10\text{ GB}$ for the state vector only (5 bytes/number) A more impressive example: 300 qubits: $2^{300} \approx 10^{90}$ dimensions. Well, the universe has only 10^{80} atoms...

4.2 Status of QC

Major routes to build a quantum computer:

- **Trapped ions** Beginning of experimental QC, proposal by Cirac and Zoller in 1995, first CNOT in 1995 by Wineland et al., 4-ion entangled states (2000), algorithms with up to four qubits (2006), 8-ion entangled states (2005).
- **NMR** First quantum algorithms in 1997, so far seven qubits, factorization of 15 with Shor's algorithm by Chuang et al. (2001). No real quantum computing, because it works with a mixture of states \Rightarrow signal to noise gets worse with an increasing number of qubits and thus problem for large qubit registers ($n \gtrsim 10$).

- **Cavity QED** Probabilistic entanglement of three atoms by Haroche et al. (2000).
- **Linear optics** First entangled states (1967, demonstrated 1972). Probabilistic entanglement of up to six photons (Pan), demonstration of a probabilistic CNOT gate. Already in use for quantum cryptography.
- **Neutral atoms** Possible creation of entangled states (I. Bloch / T.W. Hänsch) from a Mott-insulator phase, but so far no proof of entanglement in these systems. Single qubit operations on a register by Meschede (2004).
- **Solid state** Many proposals, so far Rabi-oscillations, read-out of a single quantum dot (Vandersypen 2004). Still many problems with decoherence properties. Claim of good scalability, but not clear at all, since usually only next neighbor interaction.
- **Superconducting qubits** One and two qubit gates demonstrated (Nakamura). But problems with coherence, and read-out. Bell state and its tomography have been implemented (Martinis, 2006). Claim to have run a quantum algorithm with 16 qubits. Scientifically not verifiable.
- **Continuous variables** Not easy to specify. Some entanglement seen, teleportation experiments. Very interesting properties, especially since these systems are in some aspects easier to handle and offer a completely different point of view on quantum information. However, we wont talk about these here.

Important realized quantum algorithms:

- **Deutsch-Josza algorithm** First quantum algorithm to be found. Also the first to be simulated by NMR (Chuang et al. / IBM Almaden Research Center 1998), First quantum algorithm to be realized on a quantum computer (ion trap experiment / Blatt et al. / Innsbruck 2001)
- **Shor's factoring algorithm** Factorization of 15 with by Chuang et al. / IBM Almaden Research Center, 2001).
- **Teleportation** First realization with photons by Zeilinger et al. / Innsbruck 1997. Other experiments by Martini and Gisin. However, all

only probabilistic (post-selection). Performed also on a NMR-system and with continuous variables (photons). First deterministic teleportation on demand with atoms by Wineland et al. / Boulder and Blatt et al. / Innsbruck, both in 2004 with trapped ions.

- **Error correction** Simulation with NMR-systems. First quantum version of error correction by Wineland et al. / Boulder in 2004.

4.3 DiVincenzo criteria

How will we evaluate the different experimental approaches? DiVincenzo criteria (D. P. DiVincenzo, Quant. Inf. Comp. 1 (Special), 1 (2001)). According to DiVincenzo a useful quantum computer must fullfill the following criteria:

1. a scalable physical system with well characterized qubits,
2. the ability to initialize the state of the qubits,
3. a coherence time much longer than operation time,
4. an universal set of quantum gates: single qubit and two-qubit gates.
5. a qubit-specific measurement.

Additionally:

6. Ability to interconvert stationary and flying qubits,
7. Ability to faithfully transmit flying qubits between specified locations.

4.4 Decoherence

According to quantum mechanics every closed system can be described by a wavefunction. Are we happy with this? No! In order to do this, we have to write down the wavefunction for the whole universe. Example: We want to describe an ensemble of atoms (qubits) which where brought into a superposition of two internal levels and move (randomly) in an inhomogeneous

Table 4.0-1
The Mid-Level Quantum Computation Roadmap: Promise Criteria

QC Approach	The DiVincenzo Criteria					QC Networkability
	#1	#2	#3	#4	#5	
NMR	●	○	○	●	○	●
Trapped Ion	○	●	○	●	●	○
Neutral Atom	○	●	○	○	○	○
Cavity QED	○	●	○	●	●	○
Optical	○	○	●	●	○	○
Solid State	○	○	○	●	○	●
Superconducting	○	●	○	●	○	●
Unique Qubits	This field is so diverse that it is not feasible to label the criteria with "Promise" symbols.					

Legend: ● = a potentially viable approach has achieved sufficient proof of principle

○ = a potentially viable approach has been proposed, but there has not been sufficient proof of principle

● = no viable approach is known

The column numbers correspond to the following QC criteria:

- #1. A scalable physical system with well-characterized qubits.
- #2. The ability to initialize the state of the qubits to a simple fiducial state.
- #3. Long (relative) decoherence times, much longer than the gate-operation time.
- #4. A universal set of quantum gates.
- #5. A qubit-specific measurement capability.
- #6. The ability to interconvert stationary and flying qubits.
- #7. The ability to faithfully transmit flying qubits between specified locations.

Figure 4.1: Status of quantum computing approaches according to the ARDA roadmap (2004).

magnetic field. Each atom evolves according to

$$\Psi\rangle_i = \frac{1}{\sqrt{2}} (|0\rangle + e^{i\mu\Delta B_i t} |1\rangle) . \quad (4.1)$$

What is the measurement result? The probabilities to find any qubit in one of the two eigenstates are equal. However, after some time the qubits seem to have different (random) phases. In the quantum information language we apply different z -rotations to the atoms. This is called dephasing and can be made visible when we apply a $\pi/2$ -pulse prior to the measurement. How can we describe this averaging (interaction with the environment)?

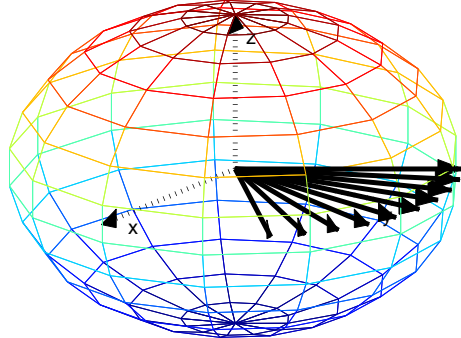


Figure 4.2: Dephasing and averaging of the Bloch-vector

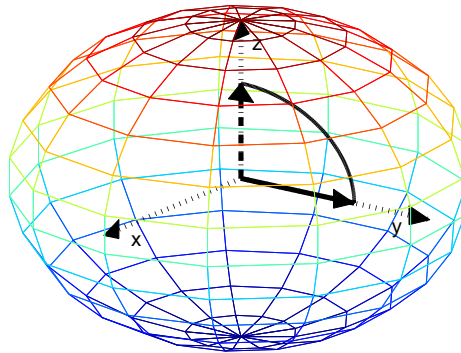


Figure 4.3: Detecting dephasing. In the Bloch picture a dephased qubit has a shorter Bloch vector.

4.4.1 Density matrix formalism

The density matrix of a qubit $\alpha|0\rangle + \beta|1\rangle$ can be written as:

$$\rho = \begin{pmatrix} |0\rangle\langle 0| & |0\rangle\langle 1| \\ |1\rangle\langle 0| & |1\rangle\langle 1| \end{pmatrix} = \begin{pmatrix} |\alpha|^2 & \rho_{12} \\ \rho_{21} & |\beta|^2 \end{pmatrix} \quad (4.2)$$

The diagonal terms correspond to the probabilities to find the system in this particular state. ρ_{12} and ρ_{21} are the coherences. They tell us about the "quantum nature" of the qubit. We always have $\text{Tr}(\rho) = 1$ ($|\alpha|^2 + |\beta|^2 = 1$). The coherences obey $\rho_{12} = \rho_{12}^*$. For pure states we have in addition $\text{Tr}(\rho^2) = 1$. The phase information corresponds to the phase of ρ_{21} . We can write the density matrix also in terms of the angles (on the Bloch-sphere, c.f. Eq. 2.8)

$$\rho = \begin{pmatrix} \cos^2(\theta/2) & r \sin \theta e^{-i\varphi} \\ r \sin \theta e^{i\varphi} & \sin^2(\theta/2) \end{pmatrix}, \quad (4.3)$$

with $0 \leq r \leq 1$.

4.4.2 Decoherences

There are two single qubit decoherence processes:

1. bit flips: The Bloch vector's length shrinks and/or is displaced (e.g. for spontaneous decay). This is often also referred to as a T_1 process (especially in NMR).
2. (pure) dephasing: The Bloch vector's length shrinks along the (x, y) -plane (The T_2 process).

We always have

$$T_2 \leq 2T_1 \quad (4.4)$$

Here T_1 and T_2 are the coherence times of the respective processes. Equation 4.4 expresses the fact that a (uncontrolled) bit flip necessarily destroys the phase information.

Chapter 5

Trapped ions

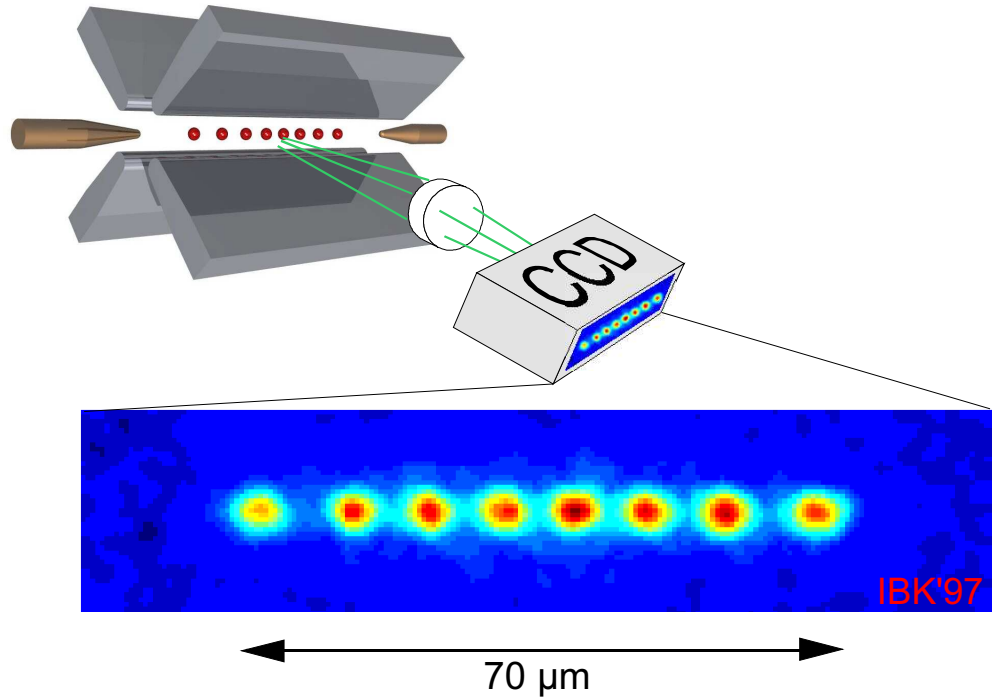


Figure 5.1: Image of an ion string (Innsbruck 1997)

Evaluation of the ion trap approach according to the DiVincenzo criteria:

1. **A scalable physical system with well characterized qubits** \Rightarrow qubits are stored in the internal levels of the ions. The qubits are driven with laser pulses either directly between the levels (Innsbruck) or in case of a pure ground state encoding (everybody else) Raman pulses. The scaling can be achieved either by storing more and more ions in the same (linear) trap. A better approach is to segment the trap and shuttle the ions back and forth.
 2. **The ability to initialize the state of the qubits** \Rightarrow optical pumping
 3. **A coherence time much longer than operation time** \Rightarrow a coherence time of 30 Minutes has been demonstrated by Wineland et al. (P. T. H. Fisk et al., IEEE Trans. on Instrum. and Meas. 44, 113 (1995).), more typical are 1 ms, usually limited by magnetic field noise.
 4. **An universal set of quantum gates:**
 - (a) Single qubit gates \Rightarrow Rabi oscillations driven by laser pulses (X, Y -gates). For a Z -gate you can either use an XY -operation or directly an off-resonant laser.
 - (b) Two-qubit gates \Rightarrow Use the Coulomb interaction: The motion of one of the ions is shared between all ions in the string. In the most simple approach the quantum information of one ion is swapped into the motional degree of freedom (Cirac and Zoller, Phys. Rev. Lett. **74**, 4091 (1995)). Then conditioned on the motional state a 2π -pulse is applied (c.f. Fig. 3.5) \Rightarrow phase gate. Another way is to apply a state dependent force with a laser field onto the ions (very much like in an optical dipole trap). If both ions feel the same force nothing is happening, however, if the ions are in different states, the distance between them changes. Thus a phase is acquired \Rightarrow phase gate (for details see D. Leibfried et al., Nature 422, 412-415 (2003)).
 5. **A qubit-specific measurement** \Rightarrow Shelving method. One of the qubit-levels is dark while the other one fluoresces if we apply laser light.
- Additionally:
6. **Ability to interconvert stationary and flying qubits** \Rightarrow move the ions into a high-finesse cavity and couple them to photons.

7. Ability to faithfully transmit flying qubits between specified locations \Rightarrow use the photons and couple them again into a high-finesse cavity with an ion inside.

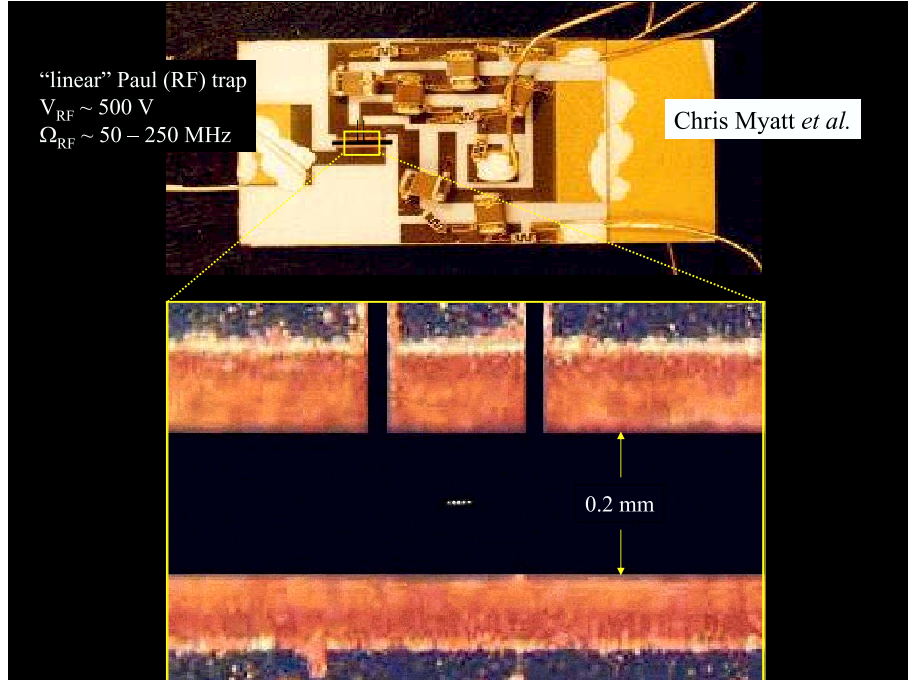


Figure 5.2: Boulder-ion trap

5.1 Two-qubit gates

The weakest point in trapped ion quantum computing is the implementation of two-qubit gates. All other DiVincenzo criteria can be easily scaled to thousands of ions. Therefore will concentrate here on two-qubit gates (in particular the publication "How to realize a universal quantum gate with trapped ions", F. Schmidt-Kaler et al., Appl. Phys. B: Lasers and Optics 77, 789 - 796 (2003)) and "Experimental demonstration of a robust, high-fidelity geometric two ion-qubit phase gate", D. Leibfried et al., Nature 422, 412-415 (2003). A good source for information is also "<http://www.lkb.ens.fr/recherche/qedcav/houches/Blattwineland.htm>".

5.1.1 The Cirac&Zoller-approach

The conditional dynamics between ions is usually achieved via the Coulomb-coupling. Fig. 5.3 shows the extended level scheme of an ion (a qubit) close to the ground state of a harmonic trap. The idea of I. Cirac and P. Zoller was

1. to map the internal state of one ion to the motion of an ion string,
2. to change the phase of an other ion depending on the motion of the ion string,
3. to map the motion of the ion string back onto the original ion.

If we can achieve this, we have realized a phase gate!

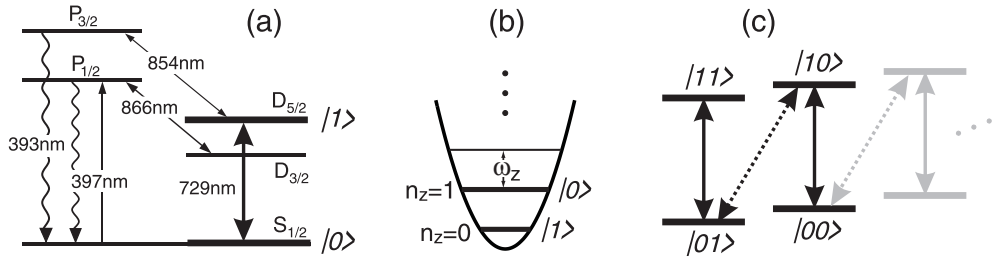


Figure 5.3: Level scheme(s) of a trapped Calcium-40-ion.

The operations which modify individual qubits and connect a qubit to the bus (the center-of mass mode) are performed by applying laser pulses on the carrier ¹ or the “blue” sideband ² of the S→D transition. Qubit rotations can be written as unitary operations in the following way: carrier rotations are given by

$$R^C(\theta, \varphi) = \exp \left[i \frac{\theta}{2} (e^{i\varphi} \sigma^+ + e^{-i\varphi} \sigma^-) \right], \quad (5.1)$$

whereas transitions on the blue sideband are denoted as

$$R^+(\theta, \varphi) = \exp \left[i \frac{\theta}{2} (e^{i\varphi} \sigma^+ a^\dagger + e^{-i\varphi} \sigma^- a) \right]. \quad (5.2)$$

¹ $|S, n\rangle \rightarrow |D, n\rangle$ transition, i.e. no change of vibrational quantum number n , laser on resonance

² $|S, n\rangle \rightarrow |D, n+1\rangle$, laser detuned by $+\omega$

Here σ^\pm are the atomic raising and lowering operators which act on the electronic quantum state of an ion by inducing transitions from the $|S\rangle$ to $|D\rangle$ state and vice versa (notation: $\sigma^+ = |D\rangle\langle S|$). The operators a and a^\dagger denote the annihilation and creation of a phonon at the trap frequency ω , i.e. they act on the motional quantum state. The parameter θ depends on the strength and the duration of the applied pulse and φ the relative phase between the optical field and the atomic polarization.

For the two-qubit CNOT operation, Cirac and Zoller proposed to use the common vibration of an ion string to convey the information for a conditional operation (bus-mode). Accordingly, the gate operation can be achieved with a sequence of three steps after the ion string has been prepared in the ground state $|n_b = 0\rangle$ of the bus-mode. First, the quantum information of the control ion is mapped onto this vibrational mode, the entire string of ions is moving and thus the target ion participates in the common motion. Second, and conditional upon the motional state, the target ion's qubit is inverted. Finally, the state of the bus-mode is mapped back onto the control ion. Note, that this gate operation is not restricted to a two-ion crystal since the vibrational bus mode can be used to interconnect any of the ions in a large crystal, independent of their position.

We realize this gate operation with a sequence of laser pulses. A blue sideband π -pulse, $R^+(\pi, 0)$, on the control ion transfers its quantum state to the bus-mode. Next, we apply the CNOT operation R_{CNOT} to the target ion, see sect. 3.10. Finally, the bus-mode and the control ion are reset to their initial states by another π -pulse $R^+(\pi, \pi)$ on the blue sideband.

We now address the problem to perform a CNOT (or a phase gate) on a single ion with the motion as a control bit. For this we will drive an effective 2π -pulse on the two two-level systems ($|S, 0\rangle \leftrightarrow |D, 1\rangle$) and ($|S, 1\rangle \leftrightarrow |D, 2\rangle$) which changes the sign of all computational basis states except for $|D, 0\rangle$). Since the Rabi frequency depends on n ($\Omega_+(n) = \sqrt{n+1}\Omega_+(n=0)$), we need to use a composite-pulse sequence instead of a single blue sideband pulse. The sequence is composed of four sideband pulses $R_4 R_3 R_2 R_1$ and can be described by

$$\begin{aligned} R_{\text{phase}} &= R^+(\pi\sqrt{n+1}, 0) R^+(\pi\sqrt{\frac{n+1}{2}}, \pi/2) \\ &\quad \cdot R^+(\pi\sqrt{n+1}, 0) R^+(\pi\sqrt{\frac{n+1}{2}}, \pi/2) \end{aligned} \quad (5.3)$$

Figure 5.4 illustrates the evolution of the Bloch vectors during the phase gate and provides a step-by-step picture of the process³.

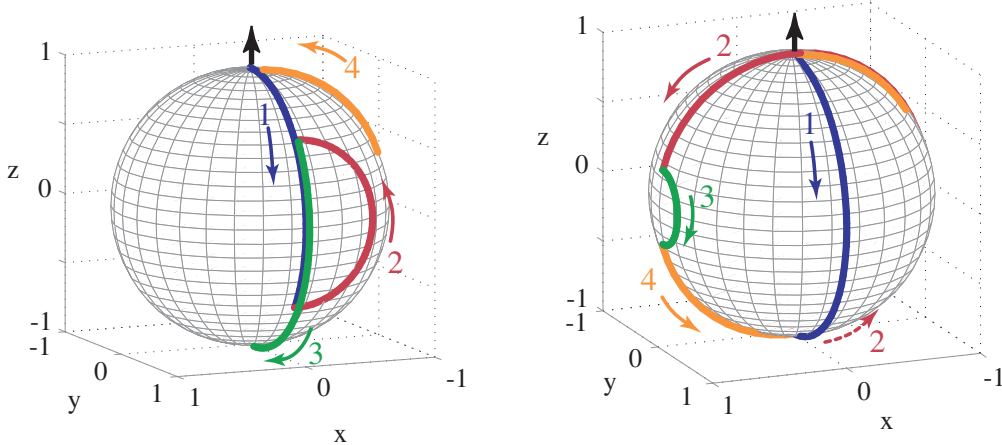


Figure 5.4: Bloch sphere trajectories for the composite phase gate, R_{phase} . Left: Bloch sphere for the quasi-two-level-system $|S, 0\rangle \leftrightarrow |D, 1\rangle$. The initial state is $|S, 0\rangle$, indicated by the black arrow. Pulse R_1 of the sequence rotates the state vector about the x -axis by $\pi/\sqrt{2}$. R_2 accomplishes a π -rotation about the y -axis. It therefore transforms the state to its mirror image about the x - y -plane. Consequently, R_3 , which is identical to R_1 , rotates the state vector all the way down to the bottom of the sphere. R_4 , just like R_2 , represents a π -rotation about the y -axis. The final state identical to the initial one, except the acquired phase factor -1 . Right: The same laser pulse sequence acting in the $|S, 1\rangle \leftrightarrow |D, 2\rangle$ subspace. Again, the final state identical to the initial one, except the acquired phase factor -1 .

However, note that in order to see the phase gate working in the experiment, we have to enclose the phase-gate by two $R^C(\frac{\pi}{2}, 0)$ -pulses to transfer the phase-gate into a CNOT-gate (c.f. Eq. 3.15 and Fig. 3.7).

We also can use the CNOT to entangle two ions: If the qubits are initialized in the superposition state $|\text{control, target}\rangle = |S + D, S\rangle$, the CNOT operation generates an entangled state $|S, S\rangle + |D, D\rangle$. The corresponding data are plotted in fig. 5.6, left side. At the end of the sequence, near

³The Bloch-sphere picture doesn't give complete information on the phases picked up during the evolution. Those have to be computed using a matrix representation.

$t=500\ \mu s$, only the states $|S, S\rangle$ and $|D, D\rangle$ are observed with $P_{SS}=0.42(3)$ and $P_{DD}=0.45(3)$. The phase coherence of both these components is verified by applying additional analysis $\pi/2$ -pulses on the carrier transition followed by the projective measurement (c.f. Eq. 3.4). From the observed populations prior to the analyzing pulses and the contrast of the oscillation, see fig. 5.7, we calculate the fidelity according to the prescription given in Sackett et al., and find a gate fidelity of 0.71(3).

Limitations The gate fidelity is well understood in terms of a collection of experimental imperfections. Most important is dephasing due to laser frequency noise and due to ambient magnetic field fluctuations that cause a Zeeman shift of the qubit levels. As quantum computing might be understood as a multi-particle Ramsey interference experiment, a faster execution of the gate operation would help to overcome this type of dephasing errors. However, a different type of error increases with the gate speed: With higher Rabi frequencies, the off-resonant excitation of the nearby and strong carrier transition is increasingly important even if the corresponding phase shift is compensated. Additional but minor errors are due the addressing imperfection, residual thermal excitation of the bus mode and spectator modes and laser intensity fluctuations.

To understand some of these limitations, we have a look at the Schrödinger-equation describing laser interaction in the level scheme in Fig. 5.3:

$$\begin{pmatrix} \dot{C}_1 \\ \dot{C}_2 \\ \dot{C}_3 \\ \dot{C}_4 \end{pmatrix} = \begin{pmatrix} 0 & \Omega_0 & 0 & i\eta\Omega_0 \\ \Omega_0 & \Delta & -i\eta\Omega_0 & 0 \\ 0 & i\eta\Omega_0 & \omega_t & (1-\eta^2)\Omega_0 \\ -i\eta\Omega_0 & 0 & (1-\eta^2)\Omega_0 & \Delta + \omega_t \end{pmatrix} \begin{pmatrix} C_1 \\ C_2 \\ C_3 \\ C_4 \end{pmatrix} \quad (5.4)$$

Here Ω_0 is the Rabi frequency, $\eta = \sqrt{\frac{a_0}{\lambda}}$ is the Lamb-Dicke factor, ω_t is the motional frequency of the ion and Δ the detuning of the laser with respect to the qubit transition. Note that the Lamb-Dicke parameter enters in the strength of the sideband transition. This can be understood as the Lamb-Dicke parameters is the square-root of the ratio of the size of the ions ground state wavefunction $a_0 = \sqrt{\frac{\hbar}{2m\omega}}$ and the photons wavelength λ (the phase gradient imprinted by the laser light induces the kick on the ion.)

General problems with this approach:

- It is slow $\eta \approx 0.02 - 0.1 \Rightarrow$ decoherence starts to set in. Mainly it is dephasing caused by laser frequency and magnetic field fluctuations. We cannot speed up the gate by simply increasing the laser power, because the carrier transition is only 1 MHz away. Therefore we would get an unacceptable amount of off-resonant excitations on the carrier transition.
- Addressing errors affect the neighboring ions. In this context this is particularly bad, because this means that the ion crystals motion gets affected additionally.
- This scheme is sensitive to heating of the ion crystal.

Part of these problems can be reduced by using a different encoding of the qubits: Use the ground state manifold (e.g. hyperfine structure or Zeeman manifold) as compared to an optical transition:

1. No sophisticated laser frequency stabilization is required, because only the frequency difference between the two laser beams is important (Raman transitions) \Rightarrow much improved coherence times possible
2. Two photons interact \Rightarrow a larger recoil to kick the ions (increased Lamb-Dicke factor).
3. More freedom in the laser interaction simply because there are two laser beams \Rightarrow other gate types possible.

5.1.2 A geometrical phase gate

A very promising two qubit-gate is the one realized by the Boulder-group (D. Leibfried et. al, Nature 422, 412-415 (2003)). Here they induce with a pair of laser beams a state dependent force (like in an optical dipole trap). They adjust the trap frequency such that the ion-ion distance is a multiple of the laser wavelength and drive the ion string with two Raman-beams with a difference frequency close to the stretch-mode. Then one gets the situation depicted in Fig. 5.8. Thus if the two ions are in a different electronic state the breathing mode is excited and we pick up a phase. If there is no differential force, the stretch-mode is not excited. The frequency difference is too far

away from the center-of-mass frequency and thus in this case nothing is happening. We therefore can get the following Hamiltonian:

$$\Phi'(\pi) = \left(\begin{array}{c|cccc} & 00 & 01 & 10 & 11 \\ \hline 00 & 1 & 0 & 0 & 0 \\ 01 & 0 & e^{i\pi/2} & 0 & 0 \\ 10 & 0 & 0 & e^{i\pi/2} & 0 \\ 11 & 0 & 0 & 0 & 1 \end{array} \right) = \left(\begin{array}{cccc} 1 & 0 & 0 & 0 \\ 0 & e^{i\pi/2} & 0 & 0 \\ 0 & 0 & e^{i\pi/2} & 0 \\ 0 & 0 & 0 & e^{-i\pi} \end{array} \right) \left(\begin{array}{cccc} 1 & 0 & 0 & 0 \\ 0 & 1 & 0 & 0 \\ 0 & 0 & 1 & 0 \\ 0 & 0 & 0 & e^{-i\pi} \end{array} \right). \quad (5.5)$$

The interaction is equivalent to a Z -gate with length $\pi/2$ on both ions plus a phase gate $\Phi(\pi)$. By choosing the detuning from the stretch-mode appropriately, one returns exactly to the ground state, if we have picked up the phase of $\pi/2$. First the drive increases the motional state and we get a coherent state and then the drive gets out of resonance and drives the system back to the ground state.

Since the qubit transition frequency does not show up in the laser light no off-resonant excitations are induced. Therefore this gate can be carried out quite fast. The Boulder group achieved fidelities of up to 0.97 with this gate.

5.2 Scaling the ion trap approach

As we increase the number of ions in the trap, it gets more and more difficult to kick the ion string with a single (or in the Raman approach with two) photons. In our mathematical description the Lamb-Dicke-parameter gets smaller ($\eta \sim \sqrt{N}$, where N is the number of ions).

There are at least three ideas to avoid this non-exponential dilemma:

1. Split up the ion string in small portions and move the ions around
⇒ segmented traps (D. Kielpinski, C.R. Monroe, and D.J. Wineland,
"Architecture for a Large-Scale Ion-Trap Quantum Computer," Nature
417, 709-711 (2002).).
2. Couple the ions via image charges to each other.
3. Couple the ions via cavities and photons.

Here we shortly address the idea of segmented traps: In a segmented trap ions can be moved by changing the voltages on the trap electrodes. Furthermore the ion strings can be merged and split. In this way the quantum registers size can be tailored to the actual need. These procedures have been successfully demonstrated by the Wineland-group and were already used in their experiment on teleportation (M. D. Barrett, et al., Nature **429**, 737-739 (2004)). However, in particular during the splitting and merging procedure the ion string is heated a little bit. Therefore additional cooling during the qubit operations is required. This can be, as also demonstrated by the Wineland group, achieved by sympathetic cooling with an additional ion species (Mg^+) without destroying the coherence of the qubits.

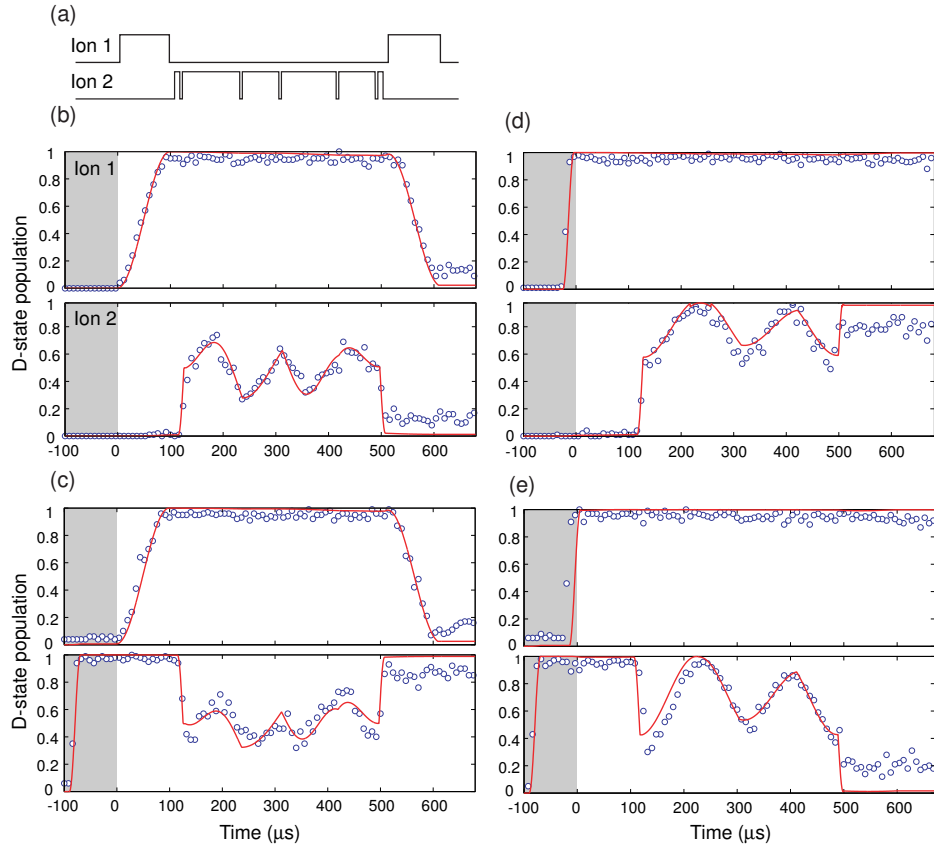


Figure 5.5: State evolution of both qubits $|control, target\rangle = |ion 1, ion 2\rangle$ under the CNOT operation. First, we initialize the quantum register in the state (b) $|S, S\rangle$, (c) $|S, D\rangle$, (d) $|D, S\rangle$, or (e) $|D, D\rangle$ (shaded area, $t \leq 0$). Then, the quantum gate pulse sequence (a) is applied: After mapping the first ion's state (control qubit) with a π -pulse of length $95\mu s$ to the bus-mode, the single-ion CNOT sequence (consisting of 6 concatenated pulses) is applied to the second ion (target qubit) for a total time of $380\mu s$. Finally, the control qubit and bus mode are reset to their initial values with the concluding π -pulse applied to the first ion. To follow the temporal evolution of both qubits during the gate, the pulse sequence (a) is truncated and the $|D\rangle$ state probability is measured as a function of time. The solid lines indicate the theoretically expected behavior. Input parameters for its calculation are the independently measured Rabi frequencies on the carrier and sideband transitions and the addressing error.

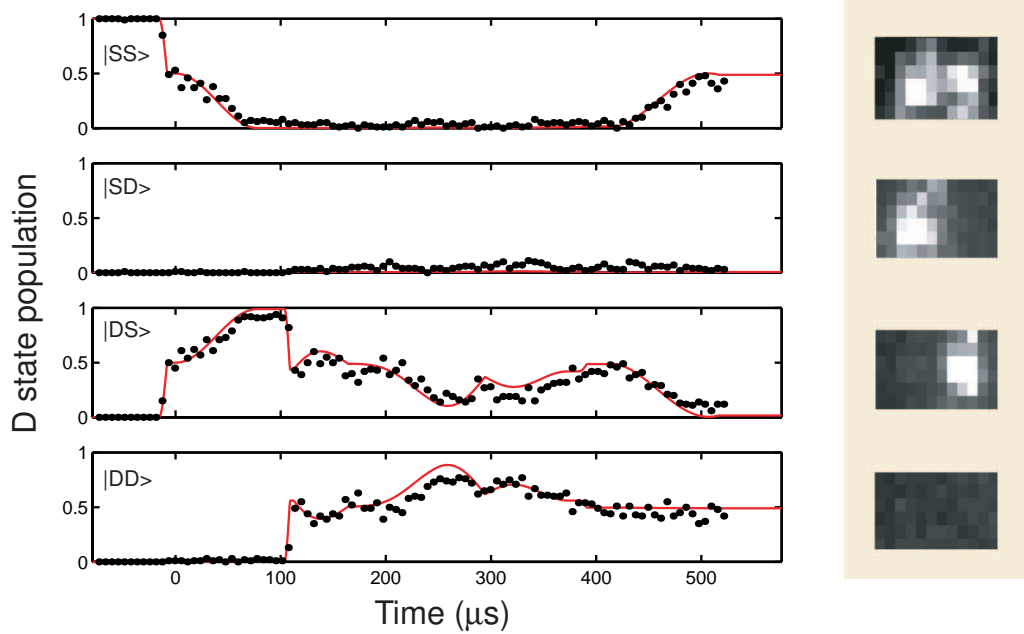


Figure 5.6: Left: the controlled-NOT gate operation R_{CNOT} is performed with ions initially prepared in $|S + D, S\rangle$. The data points represent the probability for the ion string to be in the state indicated on the right-hand side by the corresponding CCD image, during the execution of the gate. The measurement procedure is the same as in fig. 5.5. Right: CCD images of the fluorescence of the two-ion crystal as measured in different logic basis states: $|SS\rangle$, $|SD\rangle$, $|DS\rangle$, and $|DD\rangle$. The ion distance is 5.3 μm .

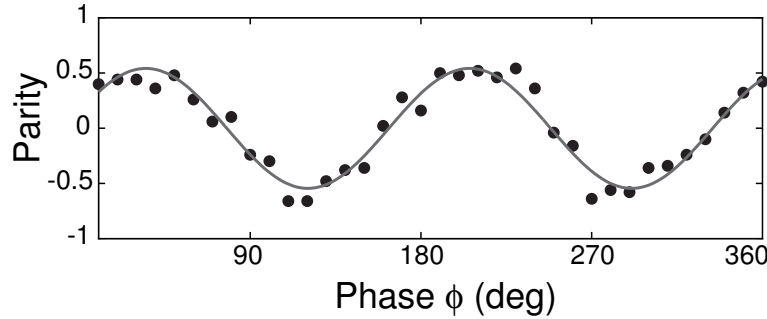


Figure 5.7: Analysis of the entangled output state of a CNOT: After the gate operation, we apply $\pi/2$ -pulses on the carrier transition, with a phase ϕ , to both ions, and measure the parity $P = P_{SS} + P_{DD} - (P_{SD} + P_{DS})$ as a function of the phase. The quantum nature of the gate operation is proved by observing oscillations with $\cos 2\phi$, whereas a non-entangled state would yield a variation with $\cos \phi$ only. The observed visibility is 0.54(3).

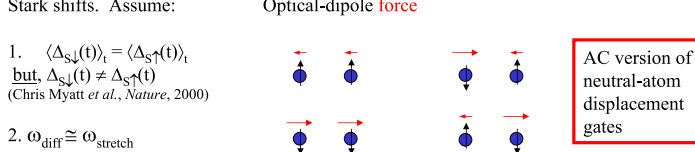
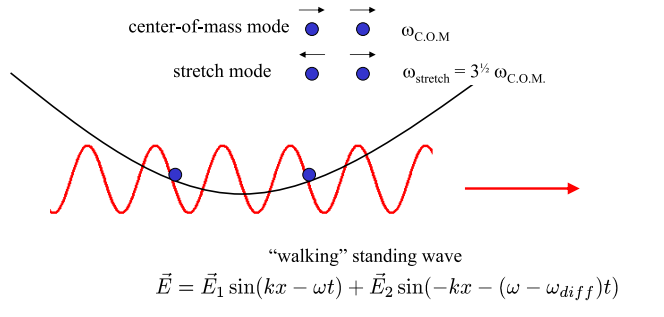


Figure 5.8: Illustration for the geometrical phase gate gate (taken from D. Wineland’s lecture in Les Houches 2003).

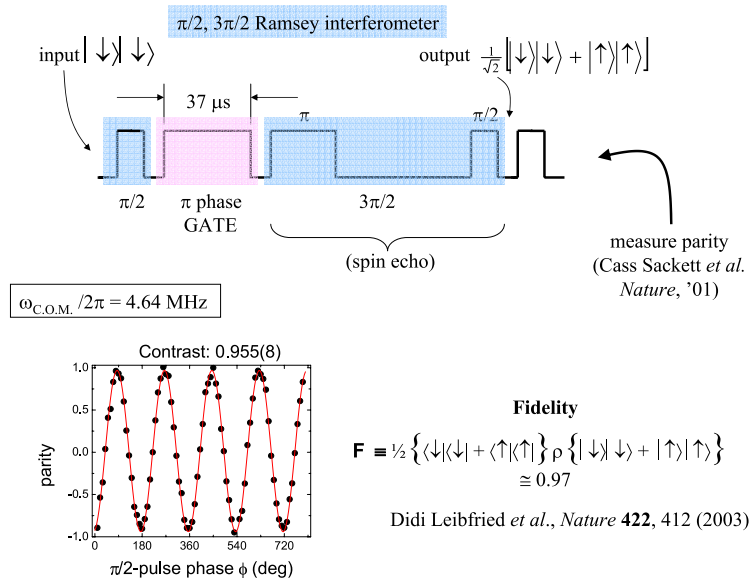


Figure 5.9: Illustration for the implementation of geometrical phase-gate (taken from D. Wineland's lecture in Les Houches 2003).

Multiplexing scheme

(DJW et al., NIST J. Res., '98; Dave Kielpinski et al. Nature, '02)

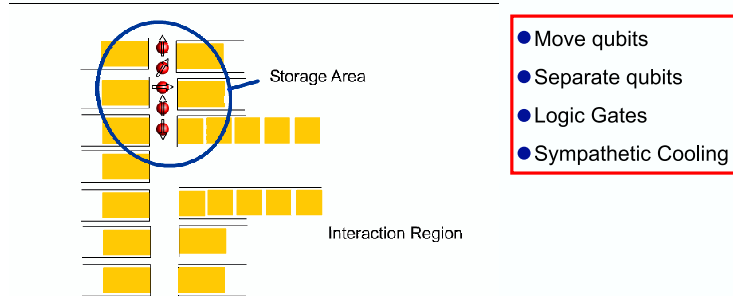
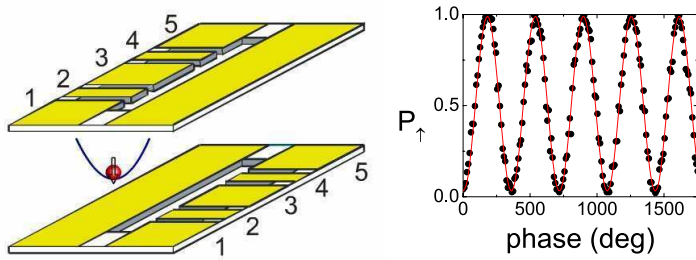


Figure 5.10: How to scale the ion trap approach to more qubits (taken from D. Wineland's lecture in Les Houches 2003).

Initial results

- $\tau(\text{transfer}) \approx 25 \mu\text{s}$ (motion heating < 1 quantum)
- qubit coherence preserved during transfer (0.5 % measurement accuracy)
- robust (no loss observed from transfer; $> 10^6$ consecutive transfers typical)
- two ions “split” to separate traps

M.A. Rowe *et al.*, Quant. Info. Compt., **4**, 257 (2002).

Figure 5.11: Coherent transport of quantum information between two traps (taken from D. Wineland’s lecture in Les Houches 2003).

Chapter 6

Neutral atoms

We will discuss here the experiments carried out by the groups of

- I. Bloch/T. Hänsch (O. Mandel et al., Nature **425**, 937-940 (2003))
- D. Meschede (D. Schrader et al., Phys. Rev. Lett. **93**, 150501)
- P. Grangier (Bergamini et al., J. Opt. Soc. Am. B, **21**, No. 11, p. 1889-1894 (2004))

Evaluation of the Divincenzo criteria for neutral atoms:

1. **A scalable physical system with well characterized qubits:** single atoms, scalability is in general good, but depends of course on the particular architecture.
2. **The ability to initialize the state of the qubits:** optical pumping
⇒ no problem here
3. **Coherence times much longer than operation time:** potentially as good as with ions.
4. **An universal set of quantum gates:**
 - single qubit operations: Either rf.-pulses or Raman-transitions.
 - two qubit operations: Usually people propose controlled collisions: However, so far only demonstrated for a collection of non addressable atoms. Another way is to mediate coupling via a high finesse

cavity.

5. **A qubit-specific measurement:** Shelving method, slightly more difficult as compared to ions: the traps for neutral atoms are usually shallower than the ones for ions. Thus they are easily heated out of the trap if detected. As an alternative one can use a destructive method: atoms in a particular state are ejected from the trap.

6.1 Atoms in 3-D optical lattices

The quantum mechanical ground state of atoms repelling each other in a deep three-dimensional lattice is an Mott-insulator state (M. P. A. Fisher et al., Phys. Rev. B **40**, 546 (1989), Jaksch et al. Phys. Rev. Lett. **81**, 3108 (1998)). In the simplest case each lattice site is occupied by exactly one atom. For quantum information purposes this is a very interesting state, as we seemingly have created a large quantum register. Additional appeal is given by the following theoretical investigations:

- D. Jaksch et al. showed in Phys. Rev. Lett. **82**, 1975 (1999) that atoms in different magnetic moments can be state selectively moved with respect to each other and in this way controlled collisions can be used to create entangled (cluster) states.
- Robert Raussendorf and Hans J. Briegel showed in Phys. Rev. Lett. **86**, 5188 (2001) that you can perform any quantum computation by creating an entangled state (a cluster state) and with subsequent local operations (i.e. single qubit operations and measurements).

But how can we achieve the Mott state? A very reasonable way is to start from a BEC (the ground state of Bosonic atoms in a single trap) and perform only slow (adiabatic with respect to all relevant time scales) changes to the systems Hamiltonian (keeping in mind that the Mott state is the ground state for atoms in a tightly confining lattice) towards our desired trapping Hamiltonian. In practice this corresponds to ramping up an optical lattice slowly to such a depth that the on-site interaction is larger than the kinetic energy associated with the tunneling process (the tunnelling time multiplied with \hbar). In this regime, it is for each atom energetically more favorable to stay at its site. Naively, the slowness of the ramp ensures that the atoms

(the wavefunction) have the time to adjust to the new bounding conditions before they are trapped in the lattice sites.

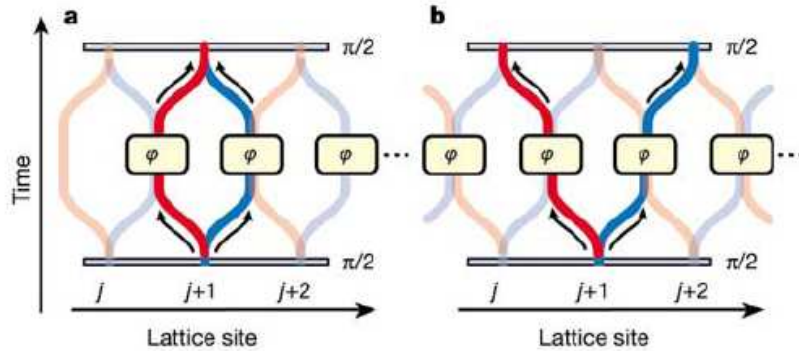


Figure 1 Schematic multiple quantum gate sequences based on controlled interactions. **a**, A chain of neutral atoms on different lattice sites is first placed in a coherent superposition of two spin-states $|0\rangle$ (red) and $|1\rangle$ (blue) with a $\pi/2$ microwave pulse. Then a spin-dependent transport is used to split the spatial wave packet of an atom, and move these two components along two opposite directions depending on their spin-state. The wave packets are separated by a lattice period such that each atom is brought into contact with its neighbouring atom. Owing to the collisional interaction between the atoms, a phase shift φ is acquired during a time t_{hold} that the atoms are held on a common lattice site depending on the spin-state of the atoms. After such a controlled collisional interaction, the wave packets of the individual atoms are returned to their original site and a final microwave $\pi/2$ pulse is applied to all atoms. This multiple quantum gate sequence can be equivalently described as a controllable quantum Ising interaction^{6,12}. **b**, In a slight modification of such a sequence, the atoms are not returned to their original lattice site $j+1$ but rather delocalized further over the j th and $(j+2)$ th lattice site after the controlled collisional interaction. The small arrows indicate the different paths that a single atom will follow during the multiple quantum gate sequence. Both sequences can be viewed as multi-particle interferometers, where the many-body output state of the interferometer can in general not be expressed as a product state of single-particle wavefunctions.

Figure 6.1: A controlled collisional phase shift (from O. Mandel et al., Nature **425**, 937-940 (2003)) can lead to an entangled state.

We turn now to the discussion of creating entangled atoms: as the logical basis, Rb-atoms with the states $|0\rangle = |F = 1, m_f = -1\rangle$ and $|1\rangle = |F = 2, m_f = -2\rangle$ are used. In the first step a $\pi/2$ -pulse ($R(\pi/2, \pi/2)$) was applied to all atoms simultaneously. In case of two atoms this yields the state $|\Psi_1\rangle = |00\rangle + |01\rangle + |10\rangle + |11\rangle$. Atoms in the state $|0\rangle$ will be trapped by σ^+ -light,

whereas atoms in the $|1\rangle$ -state will be trapped by σ^- -light (for this laser light at 785 nm tuned between the D1 and D2 line can be used). Now we should describe the affected lattice in terms of σ^\pm -lattices. In the next step the polarization of one of the lattice beams is rotated. The rotation of the polarization has now the effect that the minima of the lattices are shifted as compared to each other. If we move the lattices now by $\lambda/2$ with respect to each other, atoms in neighboring lattice sites meet if, and only if, they are in a particular state, e.g. $|01\rangle$, depending on the direction of the lattice shift. The realized interaction is a phase gate where all but one of the four logical eigenstates remain unchanged and one state acquires a phase. The hold time (interaction time) can be chosen such that one acquires a minus sign. Thus we have now: $|\Psi_2\rangle = |00\rangle - |01\rangle + |10\rangle + |11\rangle$. A last $\pi/2$ -pulse ($R(\pi/2, \phi)$) with variable phase ϕ tests now for the interference capability. For the unentangled state $|\Psi_1\rangle$ we would have full contrast, namely for $\phi = \pi/2$ we have $|11\rangle$ and for $\phi = 3/2\pi$ $|00\rangle$. However, for an entangled state of the form $|\Psi_2\rangle$ the final states oscillate between $|00\rangle - |01\rangle + |10\rangle + |11\rangle$ ($\phi = \pi/2$) and $((-1 + i)|01\rangle + (1 + i)|10\rangle)/2$ ($\phi = \pi$). That means that if we measure only the number of the atoms in $|0\rangle$ the signal does not oscillate. Thus we can verify the dynamics above experimentally. However, the problem of this method to detect entanglement is, that the loss of visibility could have many reasons, e.g. plain dephasing. This is essentially rebutted by the reappearance of the fringes if the hold time is doubled such that the induced phase is again 1. However, another problem is that no information on the amount of entanglement is obtained with this method, as the above reasoning for the loss of contrast is true also if more than 2 atoms are involved.

6.2 A neutral atom quantum register

The following text is taken from the home page of the Meschede-group (http://www.iap.uni-bonn.de/ag_meschede/english/index_eng.html): *Using the methods of laser cooling, we have realized a simple and controllable quantum system consisting of a few atoms. These atoms can be stored on the "optical conveyor belt".*

We use lasers and microwaves in order to manipulate the internal quantum states of atoms and store quantum information.

Recently we have realized a quantum register with a few neutral atoms. We can initialize, write and read out information from individual atoms of the register.

In order to realize quantum logic operations (quantum gates) with qubits in this quantum register we need a controlled interaction between these atoms. This interaction can be realized by making two atoms to exchange a single photon. This controlled exchange of a single photon can be done by placing the atoms using the "conveyor belt" inside a miniaturized optical resonator (a photon trap). The next goal of the experiment is to realize an entangled (not separable) state of two atoms.

6.3 Optical tweezers approach

The following text is taken from the home page of the Grangier-group (<http://www.iota.u-psud.fr/%7Egrangier/Dipolaire/microtrapgb.html>): *The main goal of this experiment consists in trapping a single atom at a very precise point. It is thus necessary to realize a trap too small to contain more than one atom. We use the interaction which exists between the laser light and the dipole momentum induced on the atoms to realize a dipole trap. In order to realize such a trap, we use a very powerful objective allowing to focus the trapping laser beam on a spot with a sub-micron size.*

Experimental setup (see Fig.6.7): The objective is placed in the center of an ultra-high vacuum chamber, it allows to focus the trapping laser beam in the center of the MOT. It collects also the fluorescence of the trapped atoms and images them on the CCD camera (1 micron \iff 1 CCD pixel) or on an avalanche photodiode to measure the evolution of the fluorescence with time. On the above experimental setup, the objective is placed in the center of the ultra-high vacuum chamber. With 6 laser beams and a magnetic field gradient, we realize a magneto-optical trap (MOT) around the focal point of the objective. The trapping laser beam is then focused in the center of this cloud of cold atoms to trap some of them around the focal point. Their fluorescence light, induced by the MOT beams, is collected by the same objective to image trapped atoms on a CCD camera such as ONE micron on the trap corresponds to ONE pixel on the CCD. We can also measure the evolution of the fluorescence of the trap with an avalanche photodiode.

A typical image observed on the CCD when both MOT and dipole trap are on is shown on the right (not shown here). Only one pixel is illuminated : this is the position of the dipole trap which size is only one micron.

Image observed on the CCD : one pixel corresponds to one micron

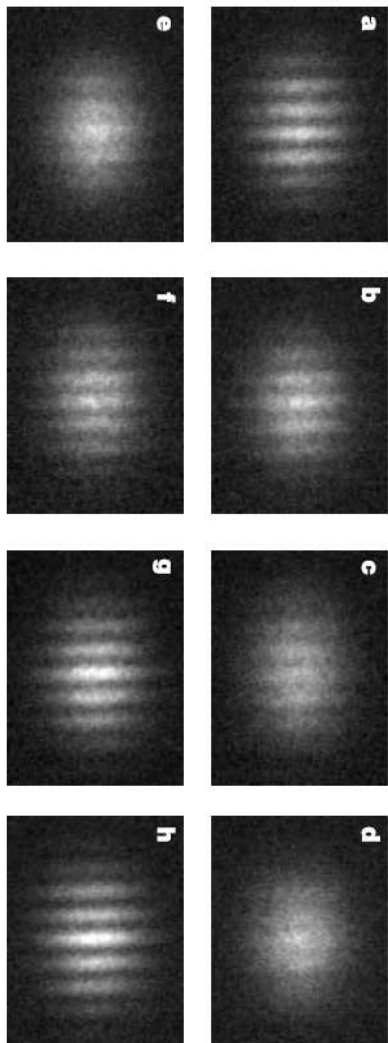


Figure 4 Spatial interference patterns recorded after applying the multiple quantum gate sequence of Fig. 1b for different collisional interaction times t_{hold} . The different hold times (μs) of 30 (a), 90 (b), 150 (c), 210 (d), 270 (e), 330 (f), 390 (g) and 450 (h), lead to different collisional phase shifts φ , ranging from $\varphi \approx 0$ (a) to just over $\varphi \approx 2\pi$ (h). The

vanishing and reappearance of the interference pattern is caused by the coherent entangling-disentangling dynamics in the many-body system due to the controlled collisions between neighbouring atoms. The state-selective absorption images were obtained after a time-of-flight period of 11 ms.

Figure 6.2: Images of the released atoms (from O. Mandel et al., Nature **425**, 937-940 (2003)). The reduced fringe contrast indicates the presence of entanglement. **Figure 4:** Spatial interference patterns recorded after applying the multiple quantum gate sequence of Fig. 1b for different collisional interaction times t_{hold} . The different hold times (μs) of 30 (a), 90 (b), 150 (c), 210 (d), 270 (e), 330 (f), 390 (g) and 450 (h) lead to different collisional phase shifts J , ranging from $J \approx 0$ (a) to just over $J \approx 2\pi$ (h). The vanishing and reappearance of the interference pattern is caused by the coherent entanglingdisentangling dynamics in the many-body system due to the controlled

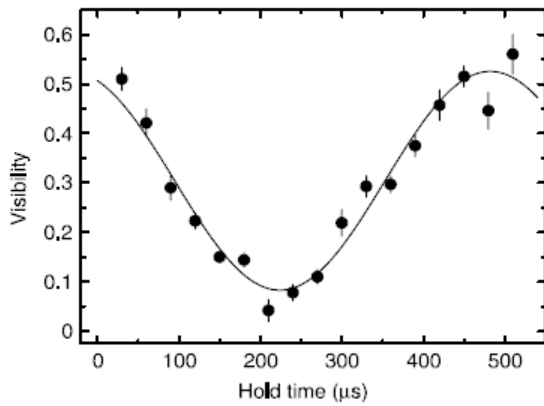


Figure 3 Visibility of Ramsey fringes versus hold times on neighbouring lattice sites for the experimental sequence similar to the one displayed in Fig. 1a. The solid line is a sinusoidal fit to the data including an offset and a finite amplitude. Such a sinusoidal behaviour of the visibility versus the collisional phase shift (determined by the hold time t_{hold}) is expected for a Mott insulating state with an occupancy of $n = 1$ atom per lattice site²³. The maximum observed visibility is limited to 55% by inhomogeneities and time-dependent fluctuations of the lattice potentials throughout the cloud of atoms that are not perfectly compensated by the applied spin-echo sequence (see text).

Figure 6.3: A vanishing fringe contrast is a necessary condition for the presence of entanglement (from O. Mandel et al., Nature **425**, 937-940 (2003))

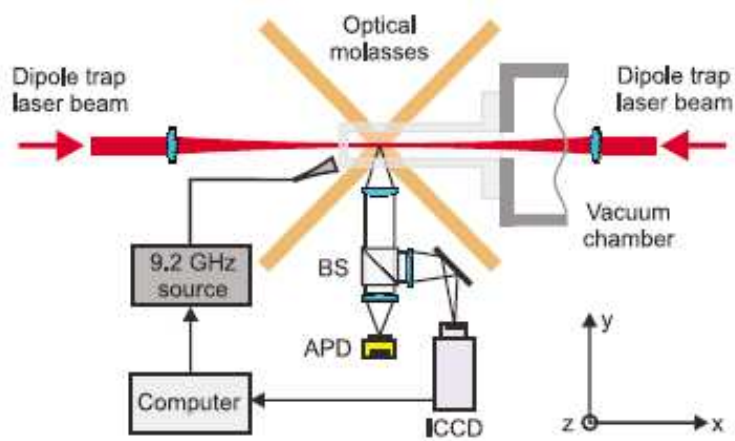


Figure 6.4: Source: D. Schrader et al., Phys. Rev. Lett. **93**, 150501: Scheme of the experimental setup. Two focused counterpropagating Nd:YAG laser beams form the dipole trap. We illuminate the trapped atoms by an optical molasses and split the fluorescence light with a beam splitter (BS) for imaging onto an avalanche photodiode (APD) and an ICCD camera. Using the information about the atom positions, a computer calculates the corresponding atomic resonance frequencies which are then transmitted to the microwave source.

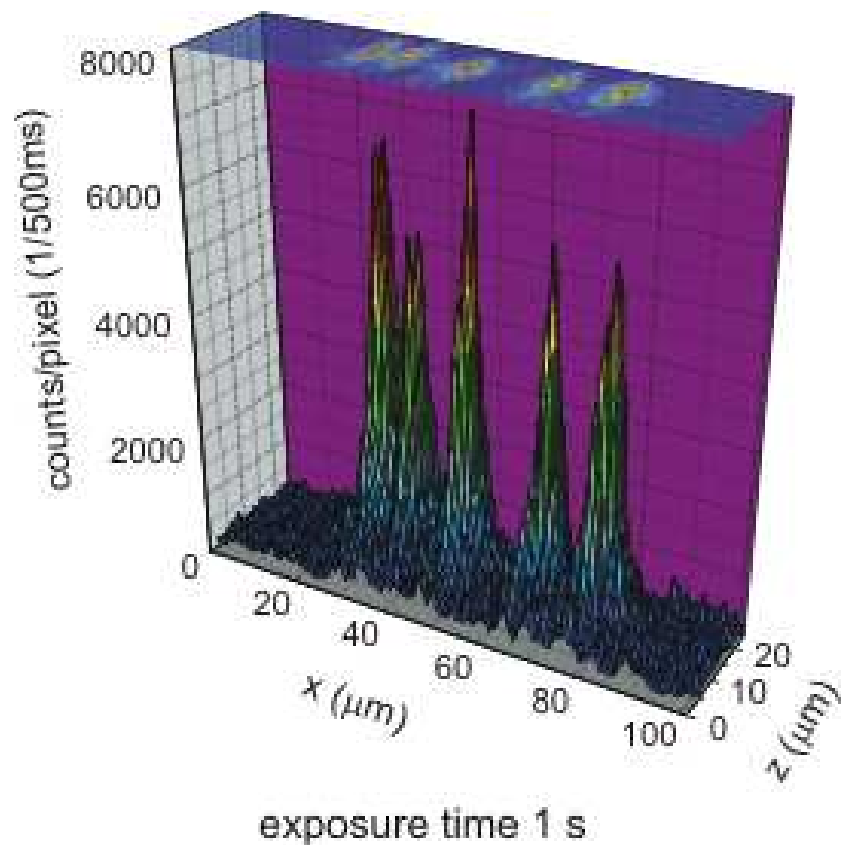


Figure 6.5: Five Cs atoms on the "Optical conveyor belt": a quantum register with five neutral atoms trapped by an optical lattice

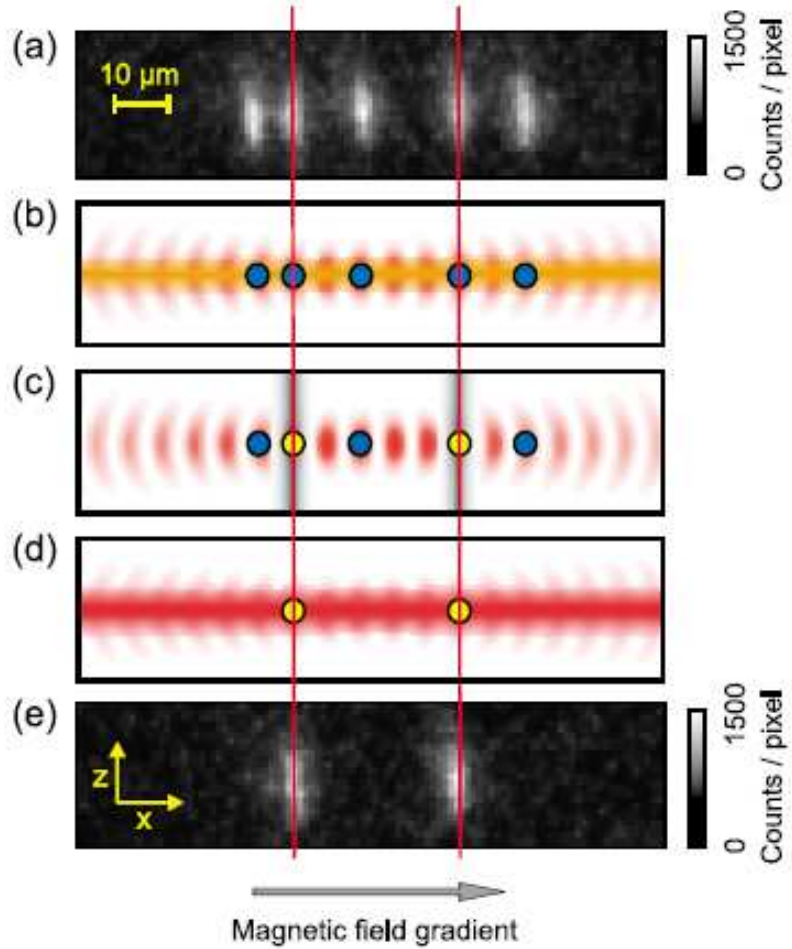


Figure 6.6: Source: D. Schrader et al., Phys. Rev. Lett. **93**, 150501: FIG. 2 (color). Five-atom quantum register. (a) Image of five neutral atoms trapped in separate potential wells of a standing wave dipole trap. The exposure time is 500 ms. One detected photon induces on average 350 counts on the CCD chip. (b) An optical pumping laser initializes the register in state $|00000\rangle$. (c) Two microwave pulses at the resonance frequencies of atoms 2 and 4 perform a spin flip on these atoms to switch to state $|01010\rangle$. The colors indicate the atomic states, blue corresponding to state $|0\rangle$ and yellow to state $|1\rangle$. (d) We state-selectively detect the atoms by applying a pushout laser which removes atoms in state $|0\rangle$ (*original text* $|1\rangle$) from the trap. (e) A final camera picture confirms the presence of atoms 2 and 4. Note that the spatial period of the schematic potential wells in (b) (d) is stretched for illustration purposes.

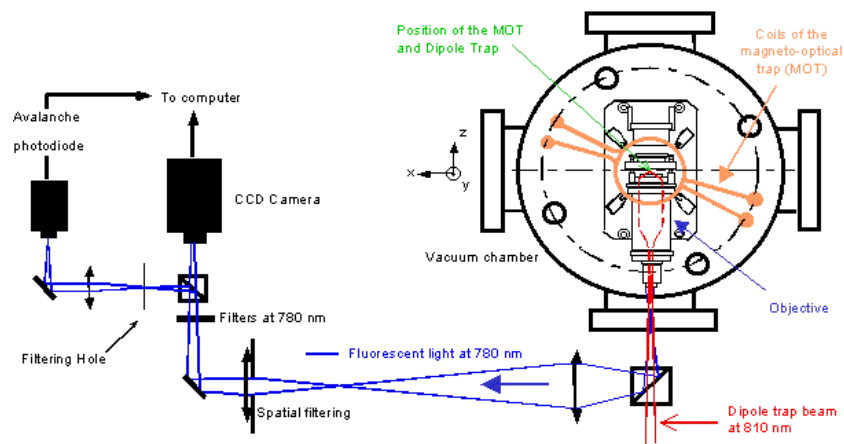


Figure 6.7: Experimental setup of the single atom trapping apparatus of the Grangier-group.

Chapter 7

Cavity QED

We discuss here mainly the work by S. Haroche and co-workers in Paris (Raimond, Brune, Haroche, Rev. Mod. Phys **73** 565 (2001)) (the work by A. Wallraff et al. is discussed later in chapter 8): In this pioneering work one of the first entangled states of massive particles were produced and detected. The experiment essentially is an atomic beam experiment: Oven, beam preparation, quantum state engineering outside and inside a super conducting cavity and read-out via field ionization.

7.1 Some experimental details for the Paris-experiment

- Preparation procedure

1. 0.2 atoms are excited to a Rydberg level ($n = \{49, 50, 51\}$), adiabatic microwave pulses transfer them to the target circular Rydberg level. The production time is known to within 2 μ s.
2. together with Doppler selective velocity selection of ± 2 m/s the position is known with a precision 1 mm.
3. On average 0.2 atoms are prepared per pulse. The pulses where no atoms are produced are rejected by the data analysis. The

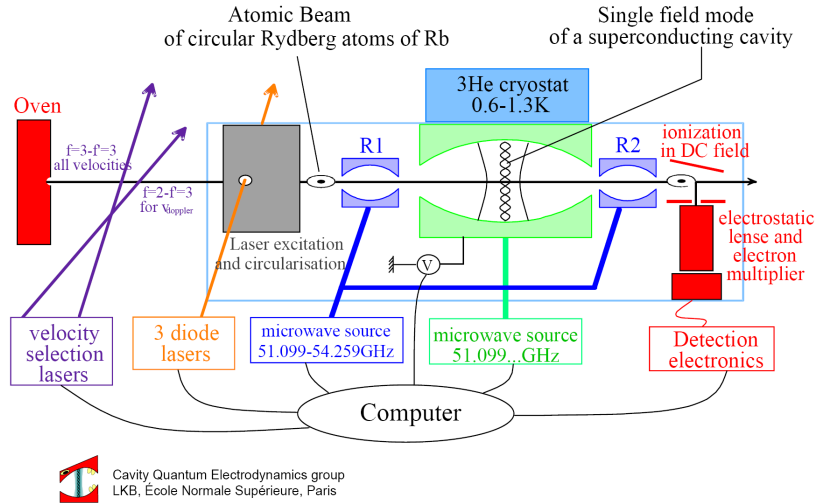


Figure 7.1: Experimental setup of the Paris-experiment. (from a talk by J.M. Raimond)

probability of having to atoms prepared is 0.2, half of these are detected as such events (detection efficiency of 0.4) and can also be excluded from the data analysis. Thus the preparation efficiency is 0.9.

- **single qubit operations** → microwave pulses
- **two qubit operations**

cavity of two carefully polished spherical niobium mirrors (diameters 50 mm, radius of curvature 40 mm) (all at 1 K). A static electric field along the cavity is used to tune the atoms into and out of resonance with the cavity. Two small holes allow to couple microwaves in. To increase the relaxations time a ring of aluminum is placed around the cavity (same symmetry axis). Thus Q values of up to 3×10^8 have been achieved. This corresponds to a relaxation time of 1 ms. However, now the atoms have to pass small holes drilled in the aluminum ring which leads to dephasing. Therefore the single qubit operations have to be driven inside the cavity. The cavity is "cooled" from the thermal population of 0.7 to 0.1 by sending atoms through the cavity in the lower qubit level.

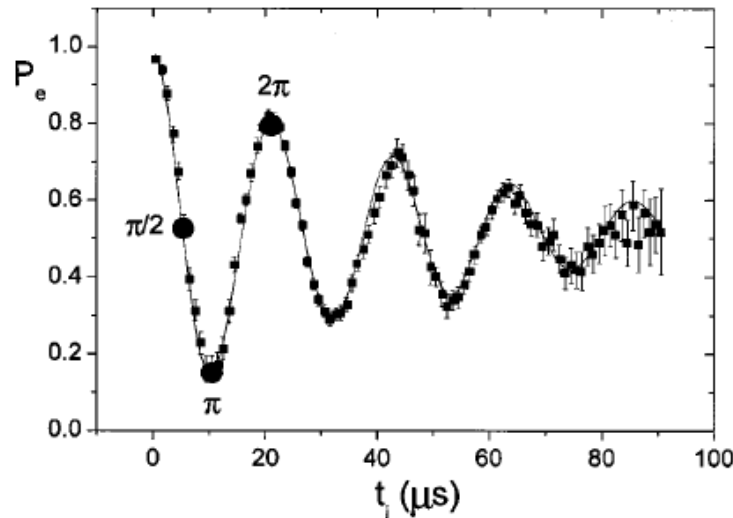


FIG. 3. Vacuum Rabi oscillations. The atom in state e enters an empty resonant cavity. P_e denotes the probability for detecting the atom in e as a function of the effective interaction time t_i . Three important interaction times (corresponding to the $\pi/2$, π , and 2π Rabi rotations) are indicated.

Figure 7.2: Vacuum Rabi oscillations in Haroche-experiment. (from Raïmond, Brune, Haroche, Rev. Mod. Phys **73** 565 (2001)). The system oscillates between $|0, e\rangle$ and $|1, g\rangle$, where the numbers refers to the number of photons in the cavity and the letters to the "g)round" and (e)xcited level of the Rydberg-atoms. The interaction is very similar to red-sideband pulses in the ion trap approach.

• detection

Finally the atoms are detected after passing the cavity. This is achieved by state selective ionization. Atoms passing an electric of about 128 V/cm ionize if they are in $|e\rangle$ but not when they are in $|g\rangle$. The electric field is increased as the atom flies further by the non-parallel electrodes. The ions can then be counted quite efficiently (up to 70%). From the timing of the counts with respect to the preparation pulse, one can then determine the quantum state quite reliably.

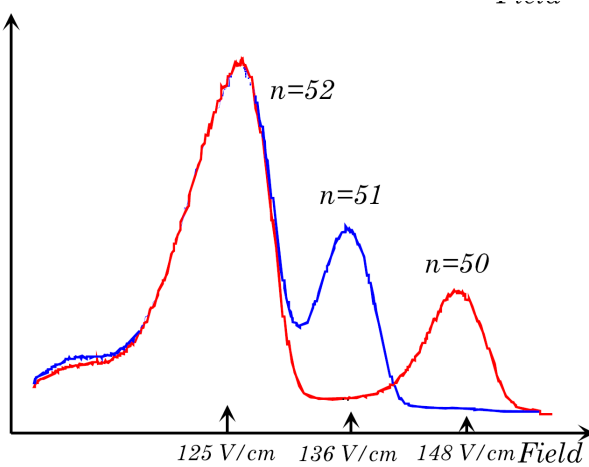


Figure 7.3: Field ionization signal (from a talk by J.M. Raimond)

7.2 The DiVincenzo-criteria for the Paris-experiment

Evaluation of the DiVincenzo criteria for the cavity-atom system of the system:

1. **A scalable physical system with well characterized qubits:** \Rightarrow Qubits are stored in single highly-excited, circular Rydberg atoms. Also photons in a superconducting cavity are used as an auxiliary qubit to couple the atoms to each other. On an abstract level, the system is rather closely related to trapped ions.
2. **The ability to initialize the state of the qubits:** \Rightarrow optical pumping, however, the atoms are not send through the cavity deterministically \rightarrow scalability problem, the cavity is initialised with initialized atoms.
3. **A coherence time much longer than operation time:** The life time of the Rydberg-atoms is 30 ms and more, the life time of the photons in the cavity is in the order of 1 ms. Gate time: $\sim 20 \mu s$.
4. **An universal set of quantum gates:**
 - single qubit operations: Transitions are carried out by microwave

fields.

- two qubit operations: Atom-cavity interaction, either off-resonant or resonant coupling can be used.
5. **A qubit-specific measurement:** Detection is carried out with state selective ionization.

7.3 Experiments

We discuss now three experiments:

1. Creation of Bell states

Here we send first an atom through the empty cavity and let it interact such that the system undergoes the transformation

$$|0, ge\rangle \xrightarrow{(\pi/2)_1^-} (|0, ge\rangle + |1, gg\rangle)/\sqrt{2}. \quad (7.1)$$

In a second step we map the atom-cavity-entangled state onto an atom-atom entangled state:

$$(|0, ge\rangle + |1, gg\rangle)/\sqrt{2} \xrightarrow{(\pi)_2^-} (|0, ge\rangle + |0, eg\rangle)/\sqrt{2}. \quad (7.2)$$

Fig. 7.5 shows the proof of the entanglement in the usual manner (c.f. Eq. 3.4 and Fig. 3.1).

2. A phase gate

We use the computational basis $\{|0, g\rangle, |0, i\rangle, |1, g\rangle, |1, i\rangle\}$ where $|i\rangle$ is an additional auxiliary state. If the cavity is empty only the $|1, g\rangle$ -state is affected and undergoes a 2π -rotation (via the $|0, e\rangle$ -state) such that the state gets a phase shift of π (see Figs. 7.6 and 7.7). This is quite analogous to the situation in ion traps (c.f. the Cirac-Zoller proposal and its realization by Monroe et al. in 1995). The auxiliary state $|i\rangle$ is required here such that only one state is affected. Otherwise the $|0, e\rangle$ state would be coupled, too. Note that with composite pulses the auxiliary-level is not required. Note also that for testing the procedure, we enclose the phase gate into two Ramsey pulses to transfer the phase information into population information (c.f. Eq. 3.15).

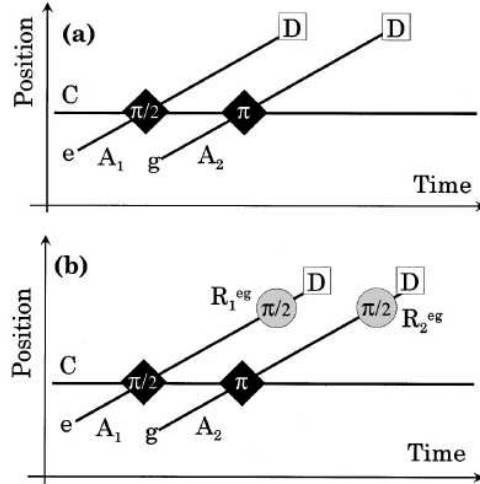


FIG. 6. Temporal sequence of the EPR pair preparation. Space lines of A_1 , A_2 , and C in a position versus time diagram. The black diamonds indicate a resonant Rabi rotation (with the angle as a label). The open squares represent the detection events. The gray circles represent classical Ramsey pulses. (a) Timing of the EPR state preparation with a direct measurement of energy anticorrelations. (b) Timing of the transverse correlation experiment.

Figure 7.4: Entanglement procedure. (from Raimond, Brune, Haroche, Rev. Mod. Phys **73** 565 (2001))

3. Creation of a three particle entangled GHZ-state

A GHZ-state can now be created by inserting the C-NOT into the Bell-creation sequence: an atom prepared in the superposition of $(|g\rangle + |i\rangle)/\sqrt{2}$ is sent through the cavity and is subjected to another $\pi/2$ -pulse before the measurement. In this way the state of the additional particle is flipped depending on the cavities intermediate state.

$$\begin{aligned}
 |0, gge\rangle &\xrightarrow{(\pi/2)_1^-} (|0, gge\rangle + |1, ggg\rangle)/\sqrt{2} \\
 &\xrightarrow{(\pi/2)_2} (|0, gge\rangle + |0, gie\rangle + |1, ggg\rangle + |1, gig\rangle)/\sqrt{4} \\
 &\xrightarrow{\text{Phasegate}} (|0, gge\rangle + |0, gie\rangle + |1, ggg\rangle - |1, gig\rangle)/\sqrt{4} \\
 &\xrightarrow{(\pi/2)_2} (|0, gie\rangle + |1, ggg\rangle)/\sqrt{2} \\
 &\xrightarrow{(\pi)_3^-} (|0, gie\rangle + |0, egg\rangle)/\sqrt{2}.
 \end{aligned} \tag{7.3}$$

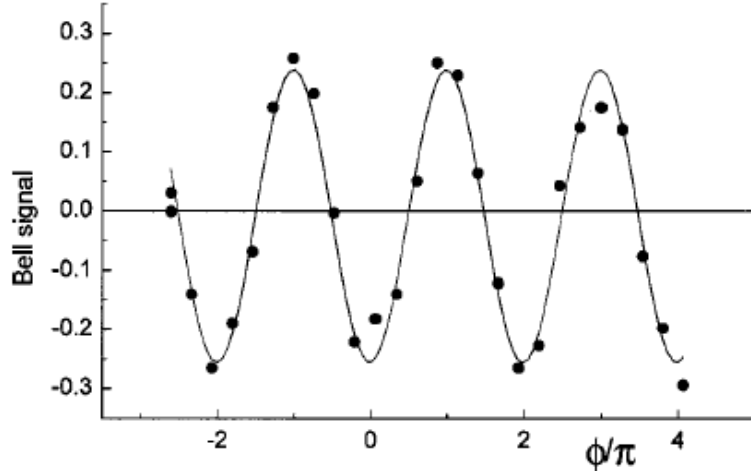


FIG. 7. “Bell signal” plotted versus the relative phase ϕ (in units of π) of pulses R_1^{eg} and R_2^{eg} . The line is a sine fit.

Figure 7.5: Parity signal of the Bell states. (from Raimond, Brune, Haroche, Rev. Mod. Phys **73** 565 (2001))

Note that we use here the binary notation as compared to the figure caption of Fig. 7.9.

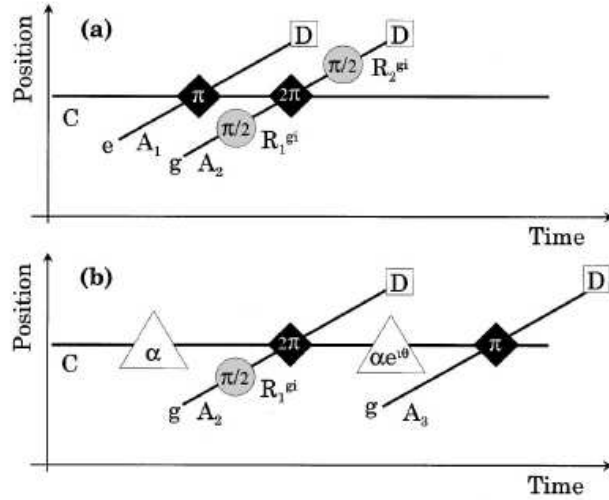


FIG. 8. Timing of the quantum phase gate experiment. Same conventions as in Fig. 6. (a) Check of the atomic coherence phase shift. A single photon state is prepared in C by atom A_1 . (b) Check of the field phase shift. The triangles represent coherent field injection in the cavity mode [amplitudes α and $\alpha e^{i\theta}$].

Figure 7.6: Procedure for the phase gate. (from Raimond, Brune, Haroche, Rev. Mod. Phys **73** 565 (2001))

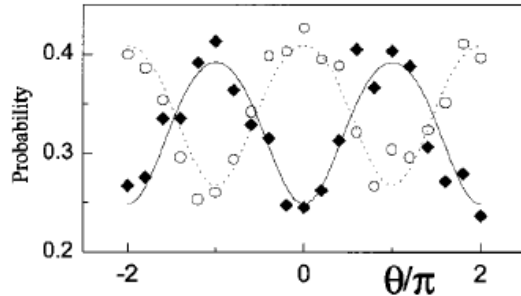


FIG. 10. Test of the field phase shift. Conditional probabilities $P(e_3/i_2)$ (circles) and $P(e_3/g_2)$ (diamonds) versus θ (units of π) for detecting A_3 in i if A_2 has crossed C in i or g . Points are experimental and lines are fits based on a simple model.

Figure 7.7: Procedure for the phase gate. (from Raimond, Brune, Haroche, Rev. Mod. Phys **73** 565 (2001))

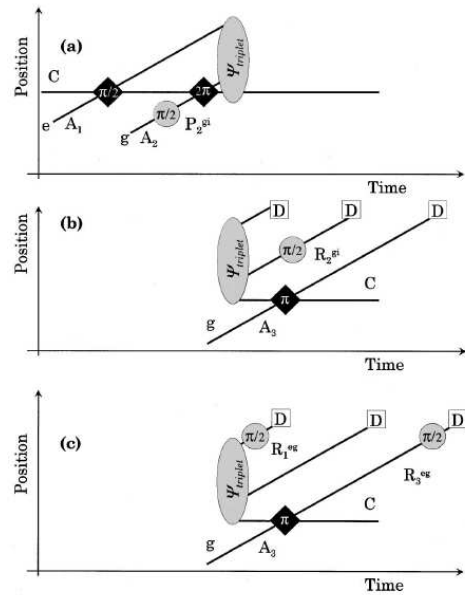


FIG. 13. Timing of the three particle entanglement. (a) State preparation. (b) Test of “longitudinal” correlations. (c) Test of “transverse” correlations. Reprinted with permission from Rauschenbeutel *et al.* (2000). (Copyright 2000, American Association for the Advancement of Science.)

Figure 7.8: Preparation procedure. (from Raimond, Brune, Haroche, Rev. Mod. Phys **73** 565 (2001))

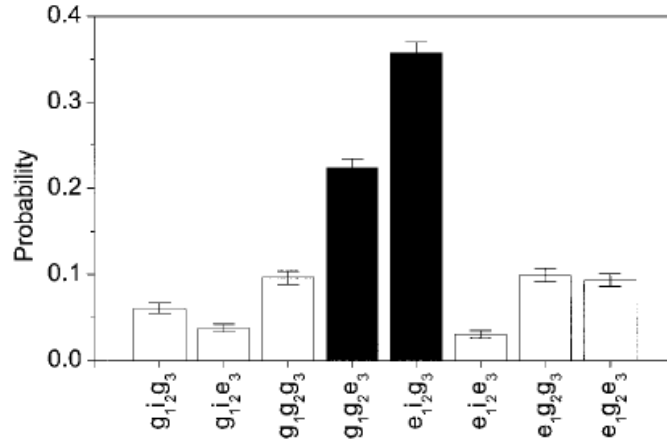


FIG. 14. Longitudinal correlations (experiment I). Histograms of the detection probabilities for the eight relevant detection channels. The two expected channels (g_1, g_2, e_3 and e_1, i_2, g_3) (in black) clearly dominate the others (in white), populated by spurious processes. The error bars are statistical. Reprinted with permission from Rauschenbeutel *et al.* (2000). (Copyright 2000, American Association for the Advancement of Science.)

Figure 7.9: Populations of the produced GHZ-state. (from Raimond, Brune, Haroche, Rev. Mod. Phys **73** 565 (2001))

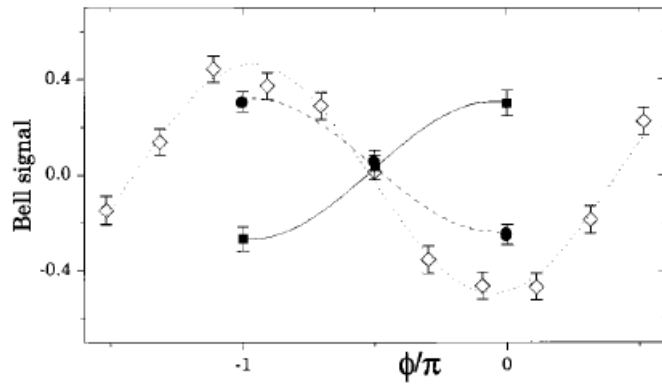


FIG. 15. Transverse correlations (experiment II). Bell signal versus ϕ . Open diamonds: no A_2 atom. Solid circles: atom A_2 detected in i . Solid squares: atom A_2 detected in g . Error bars are statistical. Lines are sine fits. Reprinted with permission from Rauschenbeutel *et al.* (2000). (Copyright 2000, American Association for the Advancement of Science.)

Figure 7.10: Proof of the coherence of the GHZ-state. (from Raimond, Brune, Haroche, Rev. Mod. Phys **73** 565 (2001))

Chapter 8

Superconducting qubits

8.1 Josephson-junctions

Josephson-junctions are the basis of superconducting qubits. A Josephson-junction is a small dielectric barrier between two superconductors. The amount of the (super) current tunnelling through the barrier is given by the phase difference $\gamma = \phi_1 - \phi_2$ between the electronic wavefunction on one side as compared to the one of the other side (as usual in QM, a phase gradient indicates flow of particles, e.g. for a particle with momentum $k = p/\hbar$ we have $\Psi(x, t) = e^{i(kx - \omega t)}$). For a weak junction the current is given by

$$I = I_c \sin \gamma \quad (8.1)$$

, where I_c is the critical Josephson-current. At the absolute temperature zero point the critical current is given by the energy gap of the superconductor (why???). Note that, no current is flowing for $\gamma = 0$ and $\gamma = \pi$. This is analogous to two coupled pendula where there is no energy exchange, if the the pendula are in or out of phase.

If we apply a voltage over the Josephson-barrier the relative phase of evolves according to $\gamma(t) = \gamma_0 + (2e/\hbar)Ut$, where $(2e/\hbar)U$ is the energy difference of a particle (a Cooper pair) being on one or the other side. Inserting this into Eq. 8.1 leads to an AC-current with the frequency

$$\nu = (2e/\hbar)U . \quad (8.2)$$

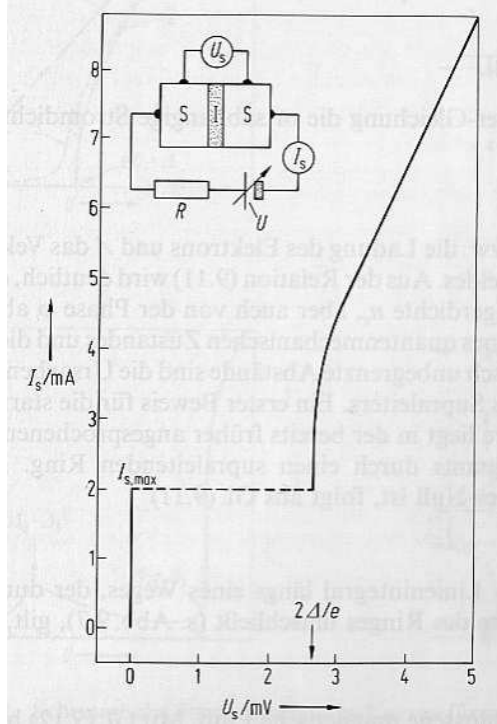


Figure 8.1: Current as a function of the bias voltage. (from ???)

This behaviour is known as the AC-Josephson-effect and is the basis to couple the voltage standard to the frequency standard. An alternative explanation for the the AC-Josephson effect can be obtained from energy conservation reasoning: The Cooper-pairs tunnelling though the barrier gain the energy given by the voltage (the voltage inside the superconductor is constant). Thereby each Cooper-pair radiates a photon whose energy is fixed by this energy gain (given by the voltage) only.

There exist (at least) two approaches to store quantum information with Josephson-junctions:

- **charged qubit:** Here the quantum information is stored as an additional Cooper-pair on a small island of a superconductor separated by two Josephson-junctions (see Fig. 8.3) (a so-called Cooper-pair box). Here an important requirement is that the energy to charge the island $E_C = e^2/2(C_g + C_J)$ is larger than the Josephson-energy $E_J = ???$ given

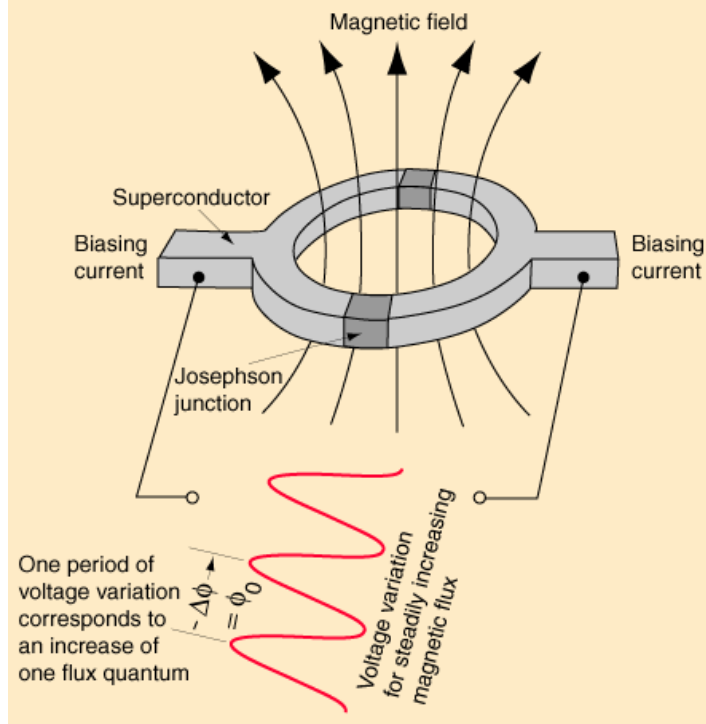


Figure 8.2: A SQUID (Superconducting quantum interference device) (from <http://hyperphysics.phy-astr.gsu.edu/hbase/solids/squid.html>). Electrons entering from one side interfere at the output. Depending on the enclosed magnetic flux they obtain a particular phase shift difference. If this phase difference leads to destructive interference a voltage is built up. A modulation of the magnetic fields leads now to modulated voltage. With this method magnetic fields larger than 10^{-14} T can be measured.

by the tunnelling rate through the junctions (or the critical Josephson current I_C). C_g and C_J are the capacitances of the island to the gate electrode and to the junction, respectively.

- **flux qubit:** Here the quantum information is stored as the direction of a super current in a loop. In the loop the phase of the wavefunction has to be continuous implying that only specific currents are allowed. This leads to a quantization of the the magnetic flux induced by the junction. We can now adjust the external magnetic field such that in the absence of any current in the loop the magnetic field would lead to

phase shift of π in the wave function. This situation is not allowed and the current flows in both directions simultaneously.

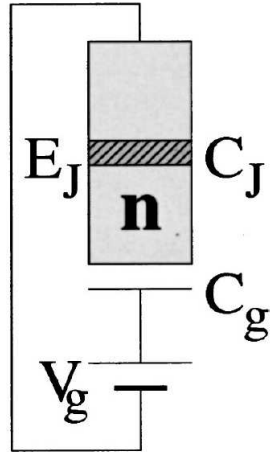


FIG. 1. A Josephson charge qubit in its simplest design formed by a superconducting single-charge box.

Figure 8.3: Layout for a charged qubit. (from Y. Makhlin et al., Rev. Mod. Phys. **73**, 357 (2001))

Literature:

- Y. Makhlin et al., Quantum-state engineering with Josephson-junction devices, Rev. Mod. Phys. **73**, 357 (2001): Review article
- A. Wallraff et al., Strong coupling of a single photon to a superconducting qubit using circuit quantum electrodynamics, Nature 431, 162 - 167 (09 Sep 2004).
- Y. Nakamura, Yu. A. Pashkin, and J. S. Tsai, Coherent control of macroscopic quantum states in a single-Cooper-pair box, Nature 398, 786 (1999).

8.2 The DiVincenzo-criteria for charged qubits

Evaluation of the DiVincenzo criteria for superconducting charged qubits:

1. **A scalable physical system with well characterized qubits:** \Rightarrow Qubits are stored as Cooper-pairs on superconducting islands.
2. **The ability to initialize the state of the qubits:** \Rightarrow Measure the qubit or wait till it is relaxed.
3. **A coherence time much longer than operation time:** Coherence times of ~ 1000 ns have been observed (single and two qubit operation time: ~ 0.1 ns)
4. **An universal set of quantum gates:**
 - single qubit operations: Transitions are carried out either by non-adiabatic switching of the Hamiltonian or by microwave fields.
 - two qubit operations: Coupling via LC-circuits.
5. **A qubit-specific measurement:** Couple the Cooper-pair box to a single electron transistor (SET) capacitively. This works, however, so-far the read-out efficiency (visibility) is in the order of 50%. Alternatively, the Cooper-pair box can be coupled to a high Q-microwave cavity. Here efficiencies in the order 90% are achieved.

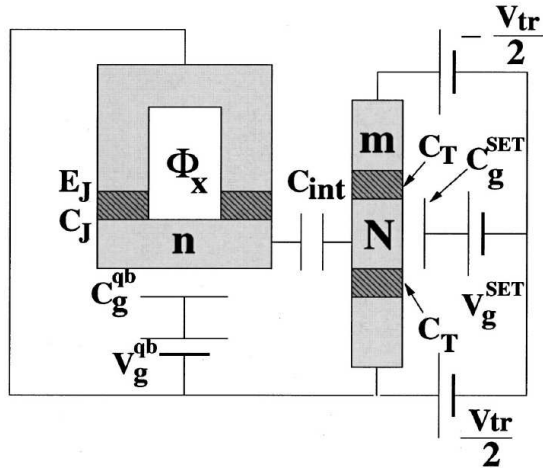


FIG. 14. The circuit consisting of a qubit plus a single-electron transistor used as a measuring device.

Figure 8.4: Layout for a circuit to measure a charged qubit. (from Y. Makhlin et al., Rev. Mod. Phys. **73**, 357 (2001))

The Hamilton function of the circuit displayed in Fig. 8.3 is given by:

$$H = 4E_C(n - n_g)^2 - E_J \cos \gamma . \quad (8.3)$$

n is the Cooper-pairs (in excess) on the island, n_g the ones on the capacitance C_g . In Eq. 8.3 the first term corresponds to the potential energy given by the charging of the superconducting island and the second term corresponds to the kinetic energy represented by the tunnelling process very analogous to the Hamiltonian of atoms in 3D-optical lattices. As for the Mott state we also want the kinetic energy small as compared to the charging energy. In this case ($E_C \gg E_J$), the states with a fixed number of Cooper-pairs are the eigenstates. (For understanding read-out and initialisation it is quite convenient if our logical eigenstates are eigenstates of the actual Hamiltonian.). The Hamiltonian can now be rewritten as:

$$H = \sum_n \left((4E_C(n - n_g)^2 |n\rangle\langle n|) - \frac{1}{2}E_J (|n\rangle\langle n+1| + |n+1\rangle\langle n|) \right) \quad (8.4)$$

The parameter $n_g = C_g V_g / 2e$ (essentially the charge on the auxiliary capacitor) can be used to tune the potential energy. For example, if n_g is set to 0, the ground state of the system corresponds to $n = 0$. If $n_g = 1$ the ground state is the one with $n = 1$. For us of particular interest is also the the case $n_g = 0.5$ (c.f. Fig. 8.5). Here the two eigenstates $|n\rangle = \{0, 1\}$ are degenerate and therefore are coupled maximally by the Josephson-energy, i.e. we have the new eigenstates $|\pm\rangle = (|0\rangle \pm |1\rangle)/\sqrt{2}$. This can be seen by diagonalizing the matrix $(|0\rangle\langle 1| + |1\rangle\langle 0|) = \begin{pmatrix} 0 & 1 \\ 1 & 0 \end{pmatrix}$. Suppose now, we start in $|0\rangle$ (e.g. $n_g = 0$) and rapidly (fast as compared to the Josephson energy (or frequency), however, slowly enough in order not to excite the system) apply now a voltage on C_g such that we achieve $n_g = 0.5$. Here the state $|0\rangle$ is conveniently expressed as the superposition $|0\rangle = (|+\rangle + |-\rangle)/\sqrt{2}$. $|+\rangle$ and $|-\rangle$ differ in energy by the Josephson-energy E_j (The situation is analog to two coupled pendula: the center-of-mass and the breathing mode are split by the coupling constant). Therefore after waiting time of $t = E_J/2d\hbar$, we have $(|+\rangle - |-\rangle)/\sqrt{2} = |1\rangle$! This is a Y -gate. Together with Z -rotations (performed e.g. by adiabatic changes on n_g), we can realize now all single qubit operations. Single qubit operation (i.e. Rabi-oscillations) have been first demonstrated by Nakamura, Pashkin and Tsai. The coupling of two

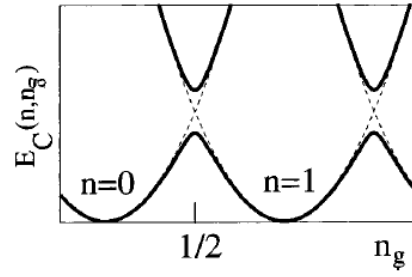


FIG. 2. The charging energy of a superconducting electron box is shown as a function of the gate charge n_g for different numbers of extra Cooper pairs n on the island (dashed parabolas). Near degeneracy points the weaker Josephson coupling mixes the charge states and modifies the energy of the eigenstates (solid lines). In the vicinity of these points the system effectively reduces to a two-state quantum system.

Figure 8.5: "Band structure" of the circuit shown in Fig. 8.3. (from Y. Makhlin et al., Rev. Mod. Phys. **73**, 357 (2001))

charged qubits was demonstrated also in the same group (Pashkin et al., Nature 421, 823 (2003)). Recently, two Josephson junction qubits have been entangled by Steffen et al, Science **313** 1423 (2006).

8.3 Coupling of charged qubit to a cavity

An important step has been achieved by coupling a single charged qubit to a microwave transmission line resonator coherently (Wallraff et al., Nature **431**, 162 (2004))). This device could be used to create and to detect single microwave photons. Alternatively, it can be used also to couple and read out charged qubits. The experiments make use of the huge electric dipole moments of Cooper-pair boxes (in a superposition of two number states, the two electrons tunnel through the barrier back and forth over $\mu\text{m}'s$). In addition, the one-dimensional design of the cavity with a transmission line leads to a very small mode volume. Therefore with the moderate Q -value of 10^4 strong coupling is achieved. Strong coupling means that the time of a coherent oscillation between the Cooper-pair box and the cavity is larger than all decoherence time scales (photon life time and qubit decay time).

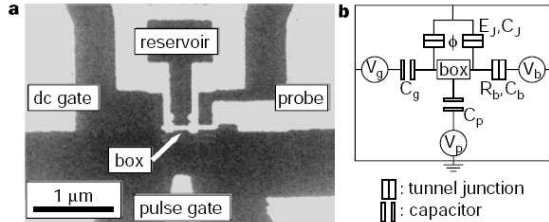


Figure 1 Single-Cooper-pair box with a probe junction. **a**, Micrograph of the sample. The electrodes were fabricated by electron-beam lithography and shadow evaporation of Al on a SiN_x insulating layer (400-nm thick) above a gold ground plane (100-nm thick) on the oxidized Si substrate. The ‘box’ electrode is a 700 × 50 × 15 nm Al strip containing ~10⁸ conduction electrons. The reservoir electrode was evaporated after a slight oxidation of the surface of the box so that the overlapping area becomes two parallel low-resistive tunnel junctions (~10 kΩ in total) with Josephson energy E_J which can be tuned through magnetic flux ϕ penetrating through the loop. Before the evaporation of the probe electrode we further oxidized the box to create a highly resistive probe junction ($R_b \approx 30\text{ M}\Omega$). Two gate electrodes (d.c. and pulse) are capacitively coupled to the box electrode. The sample was placed in a shielded copper case at the base temperature ($T \approx 30\text{ mK}$; $k_B T \approx 3\text{ }\mu\text{eV}$) of a dilution refrigerator. The single-electron charging energy of the box electrode $E_C = e^2/2C_\Sigma$ was $117 \pm 3\text{ }\mu\text{eV}$, where C_Σ is the total capacitance of the box electrode. The superconducting gap energy Δ was $230 \pm 10\text{ }\mu\text{eV}$. **b**, Circuit diagram of the device. The Cs represent the capacitance of each element and the Vs are the voltage applied to each electrode.

Figure 8.6: Setup of the Nakamura-single-qubit-experiment. (from Nakamura, Pashkin, Tsai, Nature **398**, 786 (1999))

This strong coupling leads to a splitting of the resonator transmission by the so-called vacuum Rabi-frequency ($\Omega_{\text{vac}} = 2\pi 11.6\text{ MHz}$) at 6.6 GHz (see Fig. 8.12). The cavity and qubit decay times are in the order of 1 μs . The Hamiltonian of this system is given by:

$$H = \hbar\omega_{\text{CPB}}(\sigma_z)/2 + \hbar\omega_{\text{cav}}(a^\dagger a + 1/2) + \hbar g(a^\dagger \sigma^- + a \sigma^+), \quad (8.5)$$

where the first term is the diagonalized Hamiltonian in Eq. 8.4 for a fixed n_g such that we can approximate it just as a two-level system with frequency ω_{CPB} . a^\dagger , a are the cavity’s creation and annihilation operators, respectively, and σ^+ and σ^- create and annihilate charges on the Cooper-pair-box. On resonance ($\Delta E_{n=0,n=1} = \omega_{\text{cav}}$), we have the new eigenstates $|\pm\rangle = |0,1\rangle \pm |1,0\rangle$ with eigenvalue $E_\pm = \hbar(\omega_{\text{cav}} \pm g)$.

The transition energy of the Cooper-pair box can be inferred by measuring the phase change of a weak probe beam passing the cavity. For this the Cooper-pair energy is tuned via the gate charge n_g and the phase change is recorded (see Fig. 8.10). The intensity of the microwaves can be adjusted

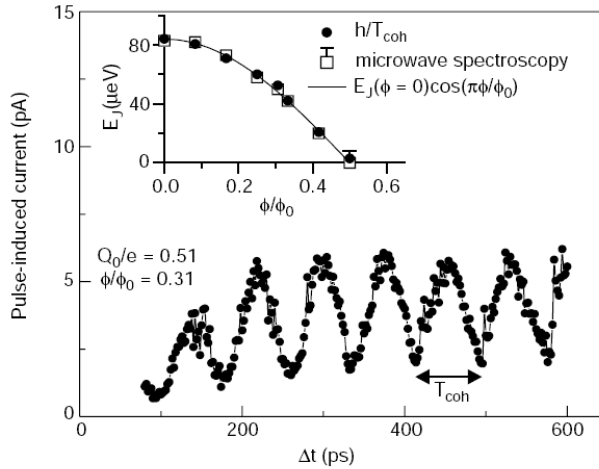


Figure 4 Pulse-induced current as a function of the pulse length Δt . The data correspond to the cross-section of Fig. 3a at $Q_0/e = 0.51$. Inset, Josephson energy E_J versus the magnetic flux ϕ penetrating through the loop. E_J was estimated by two independent methods. One was from the period of the coherent oscillation T_{coh} as h/T_{coh} . The other was from the gap energy observed in microwave spectroscopy⁴. The solid line shows a fitting curve with $E_J(\phi = 0) = 84 \mu\text{eV}$ assuming cosine ϕ -dependence of E_J .

Figure 8.7: Rabi oscillations. (from Nakamura, Pashkin, Tsai, Nature **398**, 786 (1999))

such that on average there is less than 1 photon in the cavity.

Using the strong cavity-Cooper-pair box coupling also the state of the Cooper-pair box can be read out. For this the Copper-pair box is detuned from the cavity via the gate charge n_g . Then depending on the Cooper-pairs boxes state, the interaction between the cavity and the Cooper-pair box creates a positive or negative phase shift. Read-out signals are presented in Fig. 8.13.

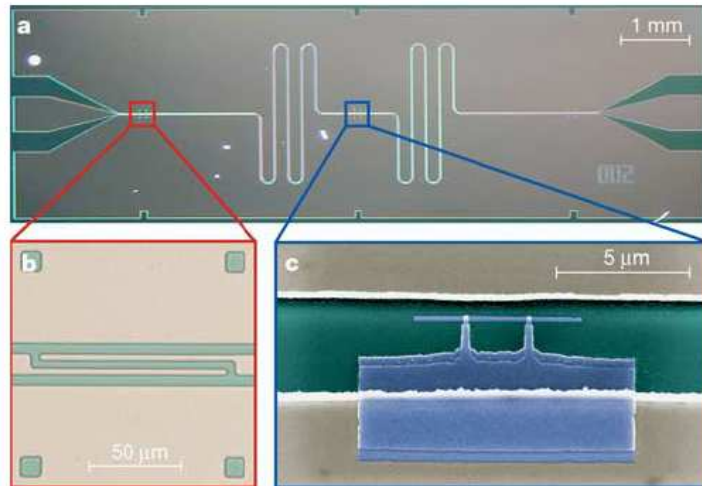


Figure 1 Integrated circuit for cavity QED. **a**, The superconducting niobium coplanar waveguide resonator is fabricated on an oxidized $10 \times 3 \text{ mm}^2$ silicon chip using optical lithography. The width of the centre conductor is $10 \mu\text{m}$ separated from the lateral ground planes extending to the edges of the chip by a gap of width $5 \mu\text{m}$ resulting in a wave impedance of the structure of $Z = 50 \Omega$ being optimally matched to conventional microwave components. The length of the meandering resonator is $l = 24 \text{ mm}$. It is coupled by a capacitor at each end of the resonator (see **b**) to an input and output feed line, fanning out to the edge of the chip and keeping the impedance constant. **b**, The capacitive coupling to the input and output lines and hence the coupled quality factor Q is controlled by adjusting the length and separation of the finger capacitors formed in the centre conductor. **c**, False colour electron micrograph of a Cooper pair box (blue) fabricated onto the silicon substrate (green) into the gap between the centre conductor (top) and the ground plane (bottom) of a resonator (beige) using electron beam lithography and double angle evaporation of aluminium. The Josephson tunnel junctions are formed at the overlap between the long thin island parallel to the centre conductor and the fingers extending from the much larger reservoir coupled to the ground plane.

Figure 8.8: (from Wallraff et al., Nature **431**, 162 (2004))

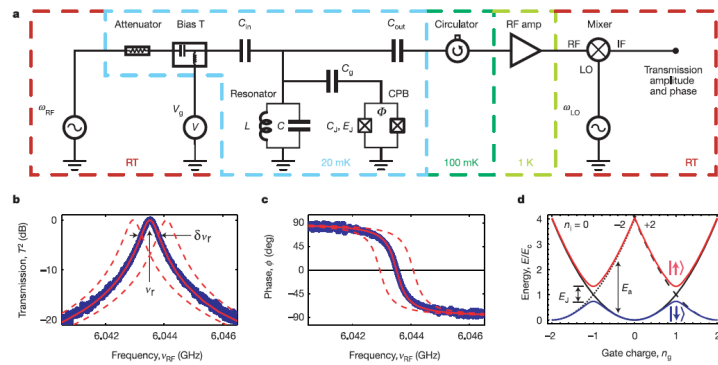


Figure 2 Measurement scheme, resonator and Cooper pair box. **a**, The resonator with effective inductance L and capacitance C coupled through the capacitor C_0 to the Cooper pair box with junction capacitance C_j and Josephson energy E_J forms the circuit QED system which is coupled through C_{out} to the input/output ports. The value of E_J is controllable by the magnetic flux Φ . The input microwave at frequency ω_{RF} is added to the gate voltage V_g using a bias-tee. After the transmitted signal at ω_{RF} is amplified using a cryogenic high electron mobility (HEMT) amplifier and mixed with the local oscillator at ω_{LO} , its amplitude and phase are determined. The circulator and the attenuator prevent leakage of thermal radiation into the resonator. The temperature of individual components is indicated. **b**, Measured transmission power spectrum of the resonator (blue dots), the full linewidth $\delta\nu_r$ at half-maximum and the centre frequency ν_r are indicated. The solid red line is a fit to a Lorentzian with $Q = \nu_r/\delta\nu_r \approx 10^5$. **c**, Measured transmission phase ϕ (blue dots) with fit (red line). In panels **b** and **c** the dashed lines are theory curves shifted by $\pm \delta\nu_r$ with respect to the data. **d**, Energy level diagram of a Cooper pair box. The electrostatic energy $E_c(n - n_g)^2$, with charging energy $E_c = e^2/2C_D$, is indicated for $n = 0$ (solid black line), -2 (dotted line) and $+2$ (dashed line) excess electrons forming Cooper pairs on the island. C_D is the total capacitance of the island given by the sum of the capacitances C_j of the two tunnel junctions, the coupling capacitance C_g to the central conductor of the resonator and any stray capacitance. In the absence of Josephson tunnelling the states with n and $n + 2$ electrons on the island are degenerate at $n_g = 1$. The Josephson coupling mediated by the weak link formed by the tunnel junctions between the superconducting island and the reservoir lifts this degeneracy and opens up a gap proportional to the Josephson energy $E_J = E_{J,\text{max}} \cos(\pi n_g)$, where $E_{J,\text{max}} = \hbar \Delta_J / 8e^2 R_J$, with the superconducting gap of aluminum Δ_J and the tunnel junction resistance R_J . A ground-state band $| \downarrow \rangle$ and an excited-state band $| \uparrow \rangle$ are formed with a gate charge and flux-bias-dependent energy level separation of E_b .

Figure 8.9: (from Wallraff et al., Nature **431**, 162 (2004))

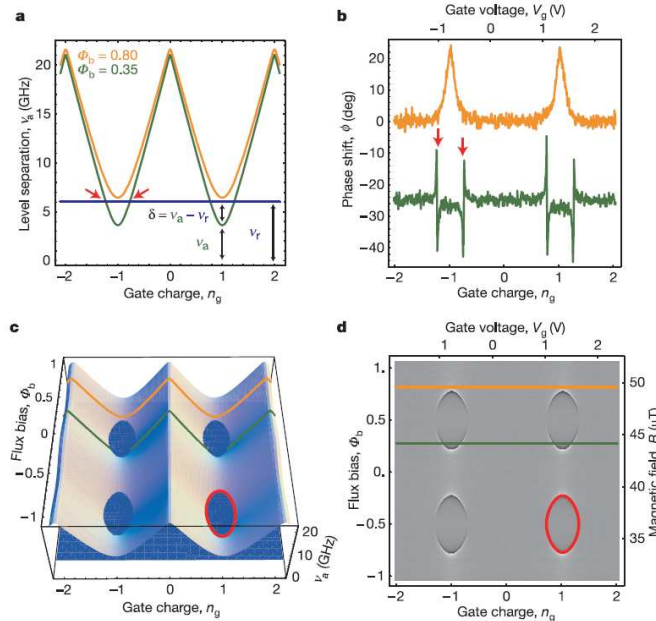


Figure 3 Strong coupling circuit QED in the dispersive regime. **a**, Calculated level separation $\nu_a = \omega_a/2\pi = E_a/\hbar$ between ground $| \downarrow \rangle$ and excited state $| \uparrow \rangle$ of qubit for two values of flux bias $\Phi_b = 0.8$ (orange line) and $\Phi_b = 0.35$ (green line). The resonator frequency $\nu_r = \omega_r/2\pi$ is shown by a blue line. Resonance occurs at $\nu_a = \nu_r$ symmetrically around degeneracy $n_g = \pm 1$; also see red arrows. The detuning $\Delta/2\pi = \delta = \nu_a - \nu_r$ is indicated. **b**, Measured phase shift ϕ of the transmitted microwave for values of Φ_b in **a**. Green curve is offset by -25 deg for visibility. **c**, Calculated qubit level separation ν_a versus bias parameters n_g and Φ_b . The resonator frequency ν_r is indicated by the blue plane. At the intersection, also indicated by the red

curve in the lower right-hand quadrant, resonance between the qubit and the resonator occurs ($\delta = 0$). For qubit states below the resonator plane the detuning is $\delta < 0$, above $\delta > 0$. **d**, Density plot of measured phase shift ϕ versus n_g and Φ_b . Light colours indicate positive ϕ ($\delta > 0$), dark colours negative ϕ ($\delta < 0$). The red line is a fit of the data to the resonance condition $\nu_a = \nu_r$. In **c** and **d**, the line cuts presented in **a** and **b** are indicated by the orange and the green line, respectively. The microwave probe power P_{RF} used to acquire the data is adjusted such that the maximum intra-resonator photon number n at ν_r is about ten for $g^2/\kappa\Delta \ll 1$. The calibration of the photon number has been performed in situ by measuring the a.c.-Stark shift of the qubit levels.

Figure 8.10: (from Wallraff et al., Nature **431**, 162 (2004))

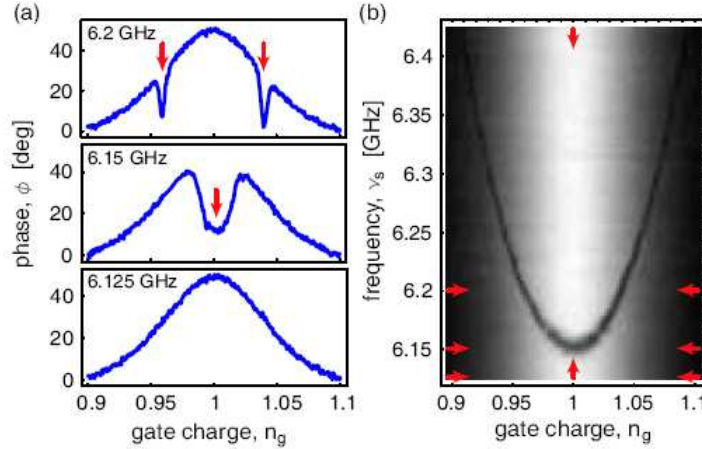


FIG. 2: (color online) (a) Probe microwave phase shift ϕ vs. gate charge n_g at spectroscopy frequency $\nu_s = 6.125$ GHz (lower panel), 6.15 GHz (middle panel) and 6.2 GHz (upper panel). (b) Density plot of ϕ vs. n_g and ν_s , white (black) corresponds to large (small) phase shift. Horizontal arrows indicate line cuts shown in (a), vertical arrows indicate line cuts shown in Fig. 3a.

Figure 8.11: (from Wallraff et al., Nature 431, 162 (2004))

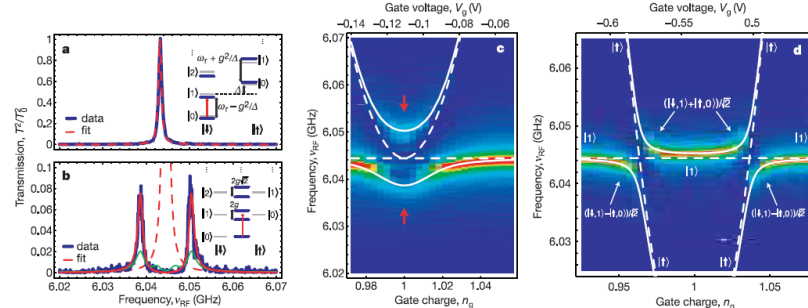


Figure 4 Vacuum Rabi mode splitting. **a**, Measured transmission T^2 (blue line) versus probe microwave probe frequency ν_{RF} for large detuning ($g^2/\Delta \ll 1$) and fit to lorentzian (dashed red line). The peak transmission amplitude is normalized to unity. The inset shows the dispersive dressed states level diagram. **b**, Measured transmission spectrum for the resonant case $\Delta = 0$ at $n_g = 1$ (blue line) showing the vacuum Rabi mode splitting compared to numerically calculated transmission spectra (red and green lines) for thermal photon numbers of $n = 0.06$ and 0.5, respectively. The dashed red line is the calculated transmission for $g = 0$ and $\kappa/2\pi = 0.8$ MHz. The inset shows the resonant dressed states level diagram. **c**, Resonator transmission amplitude T plotted versus probe frequency ν_{RF} and gate charge n_g for $\Delta = 0$ at $n_g = 1$. Blue colour corresponds to small T , red colour to large T . Dashed lines are uncoupled qubit level separation ν_a and resonator resonance frequency ν_r . Solid lines are level separations found from exact diagonalization of H_{LC} . Spectrum shown in **b** corresponds to line cut along red arrows. **d**, As in **c**, but for $E_J/h < \nu_r$. The dominant character of the corresponding eigenstates is indicated.

Figure 8.12: (from Wallraff et al., Nature 431, 162 (2004))

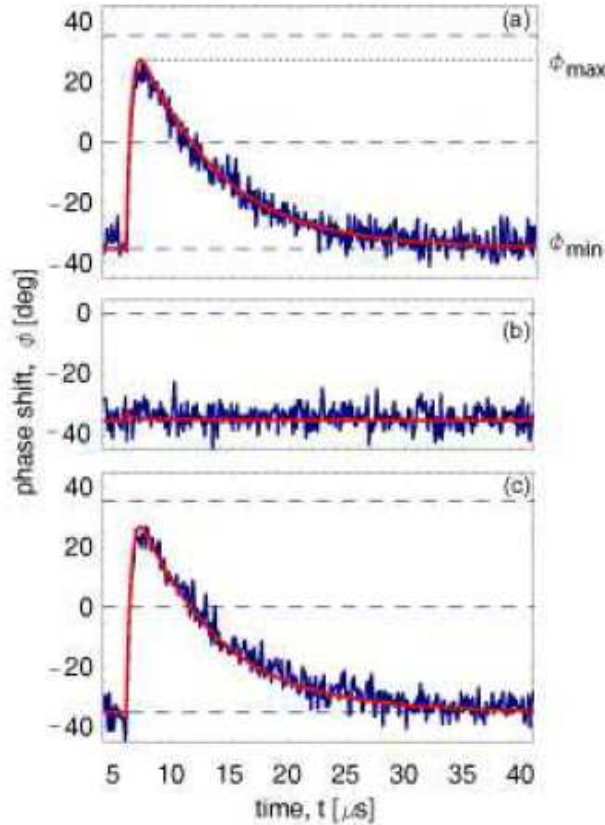


FIG. 2: (color online) Measurement response ϕ (blue lines) and theoretical prediction (red lines) vs. time. At $t = 6\mu\text{s}$ (a) a π pulse, (b) a 2π pulse, and (c) a 3π pulse is applied to the qubit. In each panel the dashed lines correspond to the expected measurement response in the ground state $\phi_{|1\rangle}$, in the saturated state $\phi = 0$, and in the excited state $\phi_{|1\rangle}$.

Figure 8.13: The measurement response was averaged 5×10^4 times. The single shot read-out efficiency is 30%, limited mainly by electronics. (from Wallraff et al., arXiv:cond-mat/0502645 (2005))

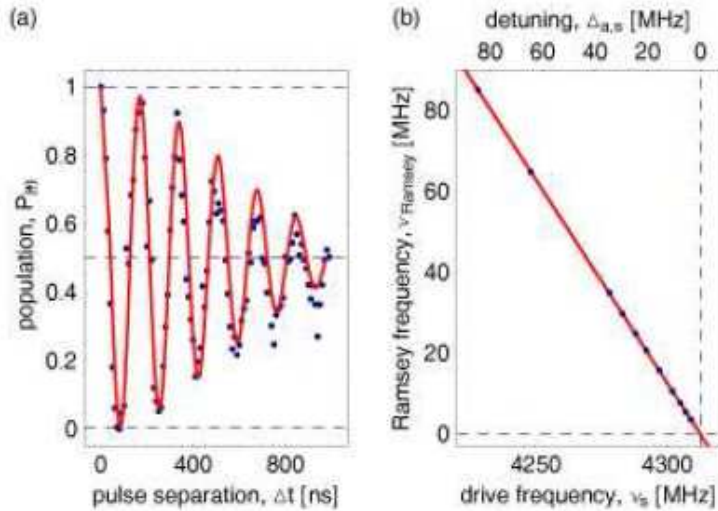


FIG. 5: (color online) (a) Measured Ramsey fringes (blue dots) observed in the qubit population $P_{|1\rangle}$ vs. pulse separation Δt using the pulse sequence shown in Fig. 1b and fit of data to sinusoid with gaussian envelope (red line). (b) Measured dependence of Ramsey frequency ν_{Ramsey} on detuning $\Delta_{\text{a,s}}$ of drive frequency (blue dots) and linear fit (red line).

Figure 8.14: (from Wallraff et al., arXiv:cond-mat/0502645 (2005))

Chapter 9

Spin–qubits with quantum dots

As a solid state approach for quantum computation, we discuss to encode the quantum information in the electron spin of an electron held within a quantum dot (D. Loss and D.P. DiVincenzo, Phys. Rev. A 57, 120 (1998)) in a strong magnetic field. A quantum dot is created by negative charges on electrodes on top of the semiconductor material. Single qubit operations can

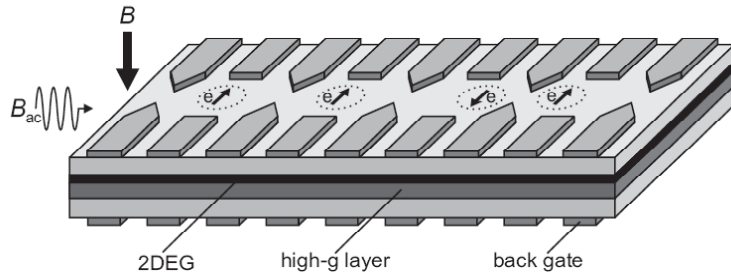


Figure 9.1: (from the PhD-thesis of Jeroen Elzerman, Delft (2004)

be achieved by applying microwave radiation to the dot. Another method is to shake the wavefunction with an electric field. The wavefunction penetrates now periodically a material with a different effective g-factor and thus an oscillating effective magnetic field is created which can drive the qubit transition. Quantum dots can be coupled by lowering the barrier between the two dots for a certain time. This leads to the following Hamiltonian:

$$H = J(t) \vec{S}_1 \cdot \vec{S}_2 = J(t) (\sigma_{x1} \otimes \sigma_{x2} + \sigma_{y1} \otimes \sigma_{y2} + \sigma_{z1} \otimes \sigma_{z2}) \quad (9.1)$$

Here $J(t)$ describes the tunnelling rate (or overlap of the electronic wavefunctions) and $\vec{S}_1 \cdot \vec{S}_2$ the Heisenberg-exchange interaction. Note that this interaction is NOT a consequence of the magnetic moment associated with the electron's spin. This interaction is basically a consequence of the Pauli-exclusion principle and the Coulomb-interaction (see e.g. <http://www.esc.cam.ac.uk/minsci/pdf/partIIorIII.pdf>). The mechanism is the same which leads in the He-atom to a splitting of the singlet and triplet levels in $n = 2$ (for $n = 1$ the triplets even do not exist). However, note that for quantum dots the energy for the singlet is lower than for the triplet (why???). A problem is that driving the single qubit operations with microwave fields or electric fields directly is too slow for the decoherence rates. The exchange interaction, however, is quite strong and can be well in the GHZ-range. Thus DiVincenzo and others (DiVincenzo et al., Nature **408**, 33 (2000)) proposed to encode a single qubit in the following way into three spins (quantum dots):

$$|0_L\rangle = |S\rangle |\uparrow\rangle \quad (9.2)$$

$$|1_L\rangle = \sqrt{2/3}|T_0\rangle |\downarrow\rangle - \sqrt{1/3}|T_+\rangle |\uparrow\rangle \quad (9.3)$$

with $|S\rangle = (|\uparrow\downarrow\rangle - |\downarrow\uparrow\rangle)/\sqrt{2}$, $|T_+\rangle = |\uparrow\uparrow\rangle$, and $|T_0\rangle = (|\uparrow\downarrow\rangle + |\downarrow\uparrow\rangle)/\sqrt{2}$. Numerically it can be shown that with 4 next neighbor exchange interactions for specific times any single qubit operation can be carried out. A CNOT can be carried out with altogether 7 exchange interactions.

9.1 The DiVincenzo-criteria for spin-qubits

Evaluation of the DiVincenzo criteria for spin-qubits in quantum dots:

1. **A scalable physical system with well characterized qubits:** \Rightarrow Qubits are stored in the electron spin of the excess electron in the quantum dot.
2. **The ability to initialize the state of the qubits:** \Rightarrow Measure the qubit or wait till it is relaxed. For the encoding in three spins one has to turn on in addition the exchange interaction between two quantum dots per qubit to a strength such that the ground state (the singlet state) is split by more than the energy corresponding to the temperature.

3. A coherence time much longer than operation time: T_1 -times of $\sim 100 \mu\text{s}$ have been observed (single and two qubit operation time: $\sim 1 \text{ ns}$). Golovach et al. argue in Phys. Rev. Lett. **93**, 016601-1 (2004) that T_2 should be equally large.

4. An universal set of quantum gates:

- single qubit operations: Transitions are carried out either by microwave fields (slow) or use the special three-spin-encoding and the Heisenberg exchange interaction (fast).
- two qubit operations: the Heisenberg exchange interaction can be used to create a $\sqrt{\text{SWAP}}$ -gate, which is universal. This coupling can only be achieved for next neighbors. Therefore the scalability is not very good.

5. A qubit-specific measurement: The quantum dots spin state is transferred to a charge in a neighboring quantum well (an additional charge or not). This can be then read-out with an electrometer (cf. Fig. 9.2).

9.2 Single shot readout of spins in quantum dots

The magnetic moment associated with the electrons spin is quite small. Therefore the Delft-group (Elzerman et al., Nature **430**, 432 (2004) and Hanson et al., PRL **94** 196802 (2005))) convert first the spin state of an electron in a quantum dot into a charge on a neighbouring quantum dot. This auxiliary quantum dot acts then a single electron transistor (Kouwenhoven et al., Rep. Prog. Phys. **64** 701736 (2001)).

We are now looking at an experiment carried out at Harvard in the group of Charlie Marcus (Petta et al., Science 309, 2180 (2005)).

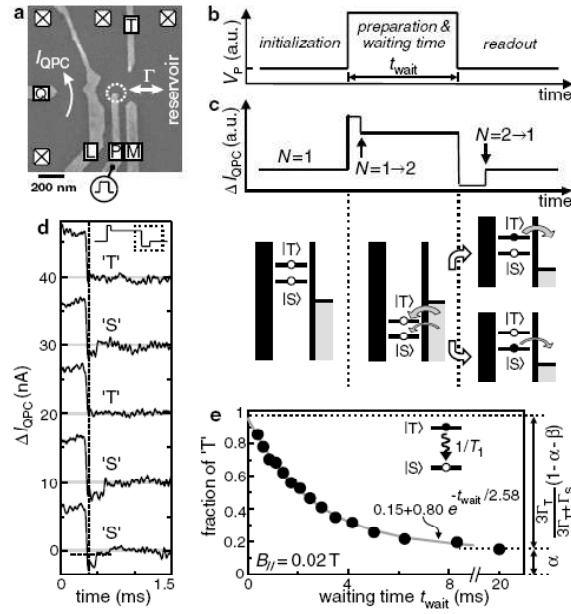


FIG. 2. Single-shot readout of $N = 2$ spin states. (a) Scanning electron micrograph of a device as used in the experiments. (b) Pulse waveform applied to gate P . (c) Response of the QPC current to the waveform of (b). Energy diagrams indicate the positions of the levels during the three stages. In the final stage, spin is converted to charge information due to the difference in tunnel rates for states $|S\rangle$ and $|T\rangle$. (d) Real-time traces of ΔI_{QPC} during the last part of the waveform (dashed box in the inset), for $t_{\text{wait}} = 0.8 \text{ ms}$. At the vertical dashed line, N is determined by comparison with a threshold (horizontal dashed line in bottom trace) and the spin state is declared ' T ' or ' S ' accordingly. (e) Fraction of ' T ' as a function of waiting time at $B_{\parallel} = 0.02 \text{ T}$, showing a single-exponential decay with a time constant T_1 of 2.58 ms.

Figure 9.2: (from Hanson et al., PRL **94** 196802 (2005))

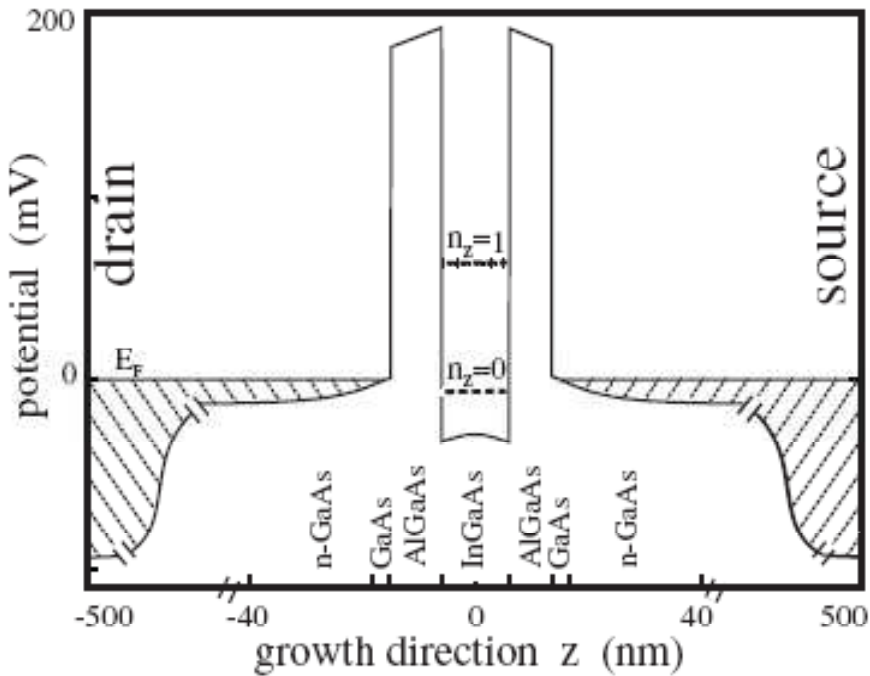


Figure 3. Self-consistent calculation of the energy diagram of the unpatterned double-barrier heterostructure from which the pillars are fabricated [14]. The electron density in the contacts gradually increases moving away from the tunnel barriers, which can be seen from the increasing distance between the Fermi energy and the conduction band edge. The structure is designed such that the lowest quantum state in the vertical z -direction is partially occupied and the second state always stays empty.

Figure 9.3: (from Kouwenhoven et al., Rep. Prog. Phys. **64** 701736 (2001)).

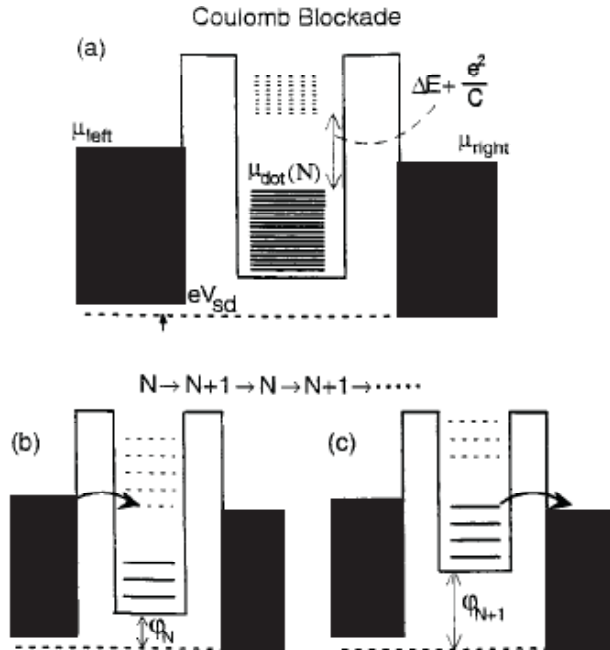


Figure 4. Potential landscape through a quantum dot. The states in the contacts are filled up to the electrochemical potentials μ_{left} and μ_{right} , which are related by the external voltage $V_{\text{sd}} = (\mu_{\text{left}} - \mu_{\text{right}})/e$. The discrete single-particle states in the dot are filled with N electrons up to $\mu_{\text{dot}}(N)$. The addition of one electron to the dot raises $\mu_{\text{dot}}(N)$ (i.e. the highest solid curve) to $\mu_{\text{dot}}(N+1)$ (i.e. the lowest dashed curve). In (a) this addition is blocked at low temperatures. In (b) and (c) the addition is allowed since here $\mu_{\text{dot}}(N+1)$ is aligned with the reservoir potentials μ_{left} and μ_{right} by means of the gate voltage. (b) and (c) show two parts of the sequential tunnelling process at the same gate voltage. (b) shows the situation with N and (c) with $N+1$ electrons on the dots.

Figure 9.4: (from Kouwenhoven et al., Rep. Prog. Phys. **64** 701736 (2001)).

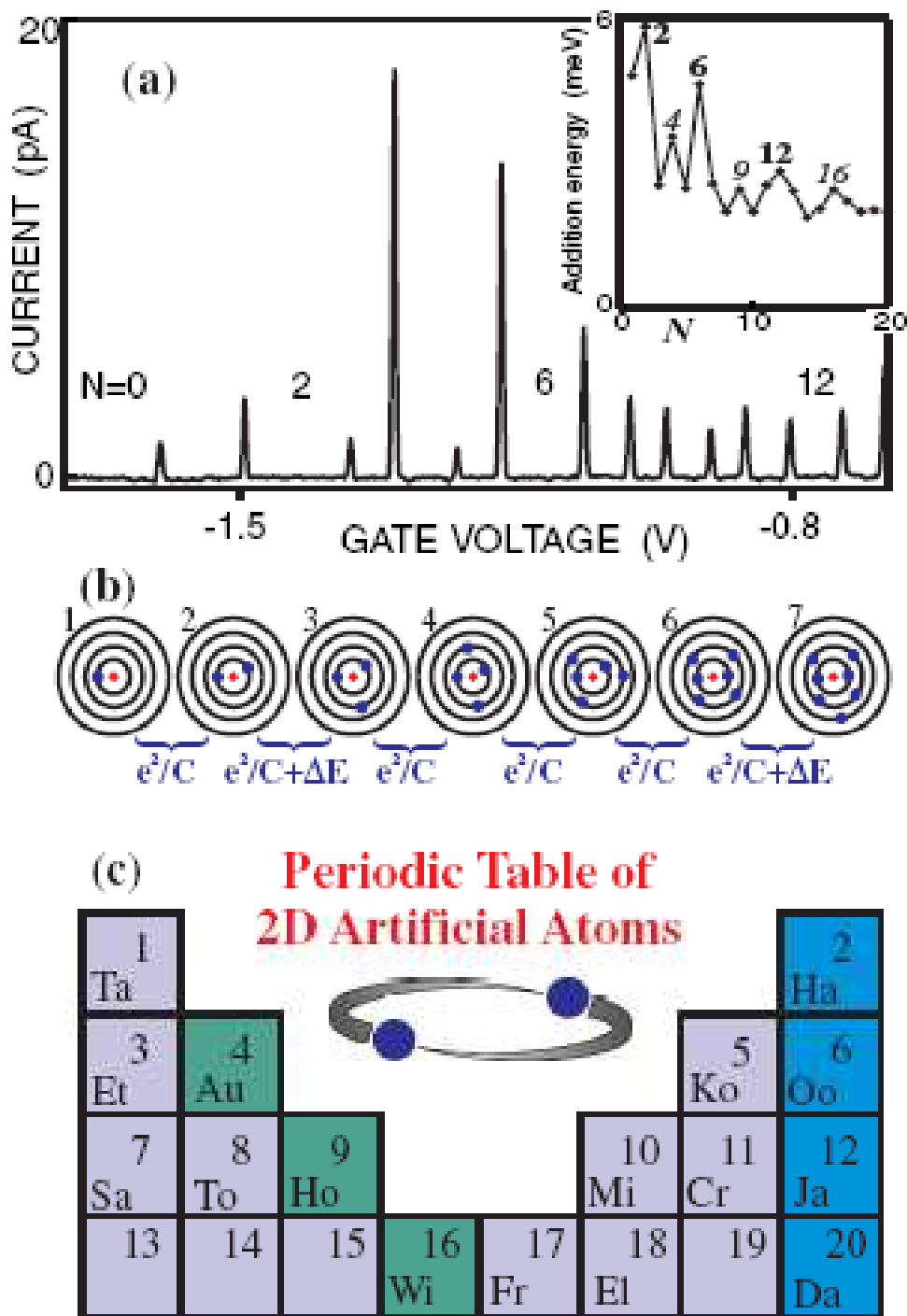


Figure 2. Current flowing through a two-dimensional circular quantum dot on varying the gate voltage. (a) The first peak marks the voltage where the first electron enters the dot, and the number of electrons, N , increases by one at each subsequent peak. The distance between adjacent peaks corresponds to the addition energies (see inset). (b) The addition of electrons to circular orbits is shown schematically. The first shell can hold two electrons whereas the second shell can contain up to four electrons. It therefore costs extra energy to add the third and seventh electron. (c) The electronic properties following from a two-dimensional shell structure can be summarized in a periodic table for two-dimensional elements. (The elements are named after team members from NTT and Delft.)

Figure 9.5: (from Kouwenhoven et al., Rep. Prog. Phys. **64** 701736 (2001)).

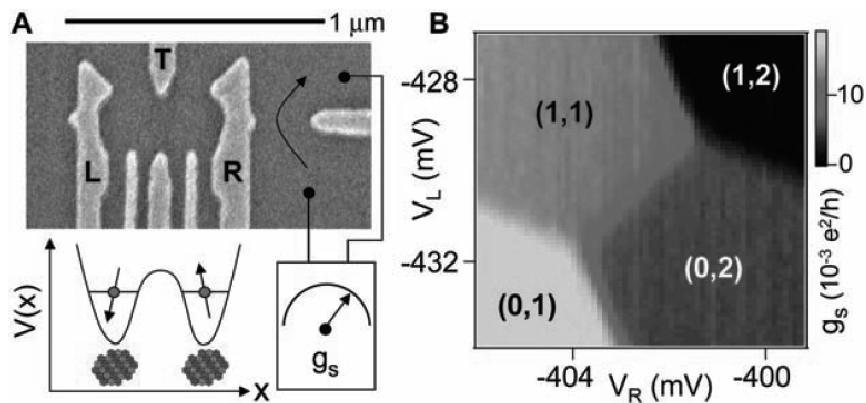


Fig. 1. (A) Scanning electron micrograph of a sample identical to the one measured, consisting of electrostatic gates on the surface of a two-dimensional electron gas. Voltages on gates L and R control the number of electrons in the left and right dots. Gate T is used to adjust the interdot tunnel coupling. The quantum point contact conductance g_s is sensitive primarily to the number of electrons in the right dot. (B) g_s measured as a function of V_L and V_R reflects the double-dot charge stability diagram (a background slope has been subtracted). Charge states are labeled (m,n) , where m is the number of electrons in the left dot and n is the number of electrons in the right dot. Each charge state gives a distinct reading of g_s .

Figure 9.6: Layout. (from Petta et al., Science 309, 2180 (2005)).

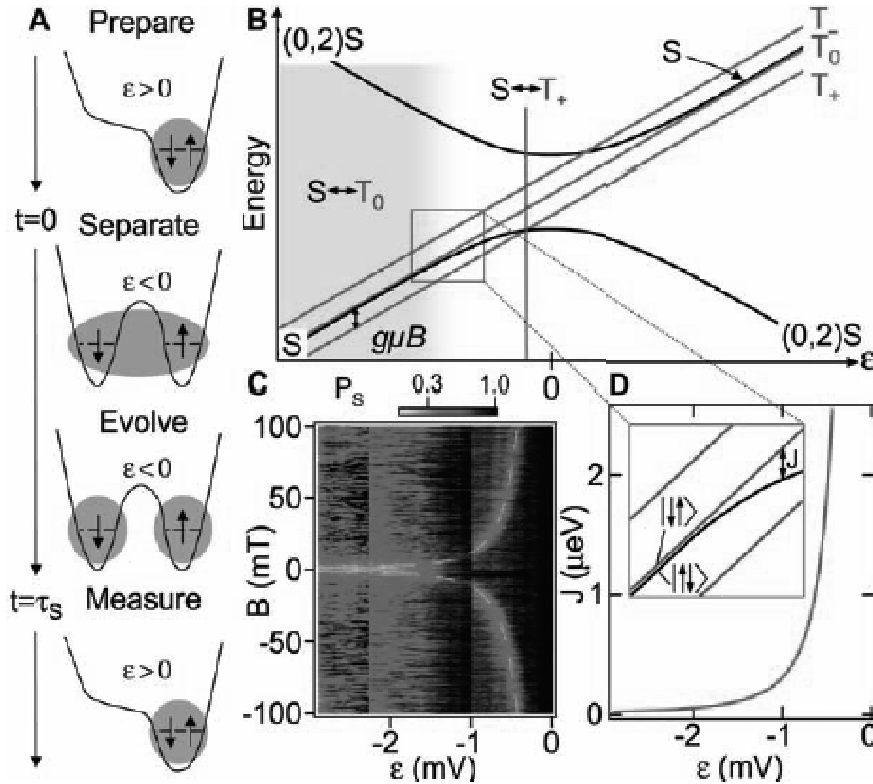


Fig. 2. (A) The control cycle for experiments generally consists of preparation, singlet separation, evolution of various kinds, and projection onto the $(0,2)$ singlet state (measurement). Projective measurement is based on the spin-blockaded transition of T states onto $(0,2)S$, whereas S states proceed freely, allowing S to be distinguished from T by the charge sensor during the measurement step. (B) Energy diagram near the $(1,1)$ -to- $(0,2)$ charge transition. A magnetic field splits T states by the Zeeman energy. At the $S-T_0$ degeneracy (light blue region) and the $S-T_+$ degeneracy (green line), hyperfine fields drive evolution between S and the respective T states. (C) Singlet probability P_S after $\tau_s = 200$ ns, as a function of detuning ϵ and magnetic field B maps out degeneracies of $S-T_0$ ($\epsilon < \sim -1.2$ mV) and $S-T_+$ (dashed green curve). (D) Dependence of exchange on detuning, extracted from the fit of $J(\epsilon) = g^* \mu_B \tilde{B}$ along the $S-T_+$ resonance, assuming $g^* = -0.44$ [dashed curve in (C)]. (Inset) For $J(\epsilon) \gg g^* \mu_B B_{\text{nuc}}$ eigenstates S and T_0 are split by $J(\epsilon)$. At large negative detuning, $J(\epsilon) \ll g^* \mu_B B_{\text{nuc}}$, and S and T_0 are mixed by hyperfine fields but eigenstates $|\uparrow\downarrow\rangle$ and $|\downarrow\uparrow\rangle$ are not.

Figure 9.7: Principle (from Petta et al., Science 309, 2180 (2005)).

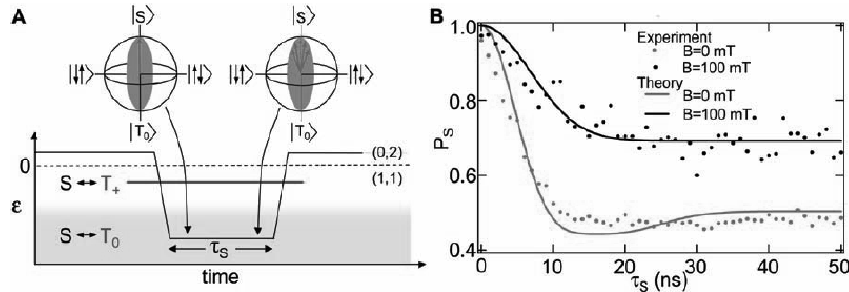


Fig. 3. (A) Pulse sequence used to measure T_2^* . The system is initialized into $(0,2)\text{S}$ and transferred by rapid adiabatic passage to the spatially separated S state. With T_\pm separated by a Zeeman field, S and T_0 mix at large detuning (light blue region), where hyperfine fields drive rotations about the x axis in the Bloch sphere. After a separation time τ_s , the state is projected onto $(0,2)\text{S}$. (B) Singlet probability P_s measured using the calibrated QPC charge sensor, as a function of τ_s at 100 mT (black curve) and 0 mT (red curve). For $\tau_\text{s} \ll T_2^*$, the singlet state does not have ample time to dephase, and $P_\text{s} \sim 1$. For $\tau_\text{s} \gg T_2^*$, $P_\text{s} \sim 0.7$ at 100 mT and $P_\text{s} \sim 0.5$ at 0 mT. A semiclassical model of dephasing due to hyperfine coupling (23) predicts $P_\text{s} \sim 1/2$ at high field and $P_\text{s} \sim 1/3$ at zero field. Fits to the model (solid curves), including a parameter adjusting measurement contrast, give $T_2^* = 10$ ns and $B_{\text{nuc}} = 2.3$ mT.

Figure 9.8: T_2 (from Petta et al., Science 309, 2180 (2005)).

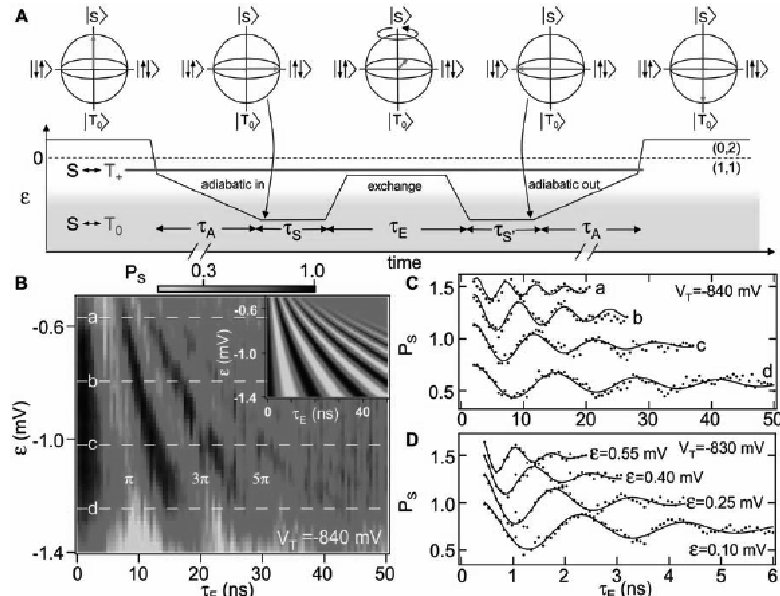


Fig. 4. (A) Pulse sequence demonstrating exchange control. After initializing into $(0,2)\text{S}$, detuning ϵ is swept adiabatically with respect to tunnel coupling through the $\text{S}-\text{T}_+$ resonance (quickly relative to $\text{S}-\text{T}_0$ mixing), followed by a slow ramp ($\tau_\text{A} \sim 1$ μs) to large detuning, loading the system in the ground state of the nuclear fields $|\uparrow\downarrow\rangle$. An exchange pulse of duration τ_E rotates the system about the z axis in the Bloch sphere from $|\uparrow\downarrow\rangle$ to $|\downarrow\uparrow\rangle$. Reversing the slow adiabatic passage allows the projection onto $(0,2)\text{S}$ to distinguish states $|\uparrow\downarrow\rangle$ and $|\downarrow\uparrow\rangle$ after time τ_E . Typically, $\tau_\text{s} = \tau_\text{E} = 50$ ns. (B) P_s as a function of detuning and τ_E . The z -axis rotation angle $\phi = f(\epsilon)\tau_\text{E}/\hbar$ results in oscillations in P_s as a function of both ϵ and τ_E . (Inset) Model of P_s using $f(\epsilon)$ extracted from $\text{S}-\text{T}_+$ resonance condition, assuming $g^* = -0.44$ and ideal measurement contrast (from 0 to 1). (C) Rabi oscillations measured in P_s at four values of detuning indicated.

Figure 9.9: Spin-echo (from Petta et al., Science 309, 2180 (2005)).

Chapter 10

Nuclear Magnetic Resonance

In nuclear magnetic resonance (NMR) the well-known techniques developed for more than 50 years for NMR are applied to quantum computation. In particular, a lot of strategies to compensate for systematic errors were developed for NMR and are extensively used. The method of spin-echo is only one of the basic pulse sequences (invented by O. Hahn (1950) to overcome dephasing in magnetic field gradients). Johnes has a nice lecture on NMR quantum computing online (<http://nmr.physics.ox.ac.uk/pdfs/lhnmrqc.pdf>). In NMR the quantum information is stored in the nuclear magnetic moments of a macroscopic number of particles. The problem, however, is that it is very difficult to prepare a pure initial state. So far experiments work only with the tiny surplus in the energetically lower state. For a two-spin system, we have the equilibrium density matrix ρ^{eq} (see also Fig. 10.1):

$$\rho^{\text{eq}} = \begin{pmatrix} 1 & 0 & 0 & 0 \\ 0 & 1 & 0 & 0 \\ 0 & 0 & 1 & 0 \\ 0 & 0 & 0 & 1 \end{pmatrix} + \begin{pmatrix} \alpha_1 + \alpha_2 & 0 & 0 & 0 \\ 0 & -\alpha_1 + \alpha_2 & 0 & 0 \\ 0 & 0 & \alpha_1 - \alpha_2 & 0 \\ 0 & 0 & 0 & -\alpha_1 - \alpha_2 \end{pmatrix} \quad (10.1)$$

In first order we have a mixture of all possible states. However, the energetically lower states are slightly favored. This is described by the deviation from the white noise (the second term in Eq. 10.1). At room temperature the α 's are in the order of 10^{-6} . Roughly speaking we calculate with all possible input states simultaneously, but get more signal from the energetical lower input state. However, we have to make sure that all the bad states

average out against each other. Different techniques exist. One particular practical technique is called temporal averaging (Knill et al., Phys. Rev. A **57**, 33483363 (1998)). In the most simple case this works for two spins as follows: We perform three runs of the algorithm where we explore as inputs all permutations of the unwanted states. Using the fact that the computation and read-out are represented by linear operators, we are allowed to average the output.

$$\begin{aligned}
 \bar{\rho}_\Delta &= \begin{pmatrix} \beta & 0 & 0 & 0 \\ 0 & \gamma & 0 & 0 \\ 0 & 0 & \delta & 0 \\ 0 & 0 & 0 & \eta \end{pmatrix} \\
 &+ \begin{pmatrix} \beta & 0 & 0 & 0 \\ 0 & \eta & 0 & 0 \\ 0 & 0 & \gamma & 0 \\ 0 & 0 & 0 & \delta \end{pmatrix} \\
 &+ \begin{pmatrix} \beta & 0 & 0 & 0 \\ 0 & \delta & 0 & 0 \\ 0 & 0 & \eta & 0 \\ 0 & 0 & 0 & \gamma \end{pmatrix} \\
 &= \begin{pmatrix} \beta & 0 & 0 & 0 \\ 0 & \gamma + \delta + \eta & 0 & 0 \\ 0 & 0 & \gamma + \delta + \eta & 0 \\ 0 & 0 & 0 & \gamma + \delta + \eta \end{pmatrix}. \tag{10.2}
 \end{aligned}$$

$$\begin{pmatrix} \beta - (\gamma + \delta + \eta) & 0 & 0 & 0 \\ 0 & 0 & 0 & 0 \\ 0 & 0 & 0 & 0 \\ 0 & 0 & 0 & 0 \end{pmatrix}. \tag{10.3}$$

where $\beta = \alpha_1 + \alpha_2$, $\gamma = -\alpha_1 + \alpha_2$ etc.. Moving $(\gamma + \delta + \eta)I$ from $\bar{\rho}_\Delta$ to the identity in Eq. 10.1, we arrive with an effective initial deviation densitymatrix:

$$\begin{pmatrix} \beta - (\gamma + \delta + \eta) & 0 & 0 & 0 \\ 0 & 0 & 0 & 0 \\ 0 & 0 & 0 & 0 \\ 0 & 0 & 0 & 0 \end{pmatrix} \tag{10.4}$$

Because the α 's are small the term corresponding to $\beta - (\gamma + \delta + \eta)$ decreases exponentially with the number of qubits. Therefore NMR is with this concept not scalable and often people say that NMR is "only" simulation of quantum computation. However, in NMR the first (Isaac L. Chuang, et al.

"Experimental realization of a quantum algorithm", Nature 393, 143 (1998)) and so far the most complicated quantum algorithm (L.M.K. Vandersypen et al., "Experimental realization of Shor's quantum factoring algorithm using nuclear magnetic resonance", Nature 414, 883887 (2001)) have been tested.

10.1 The DiVincenzo-criteria for NMR

Evaluation of the DiVincenzo criteria for nuclear magnetic resonance:

1. **A scalable physical system with well characterized qubits:** \Rightarrow Qubits are stored in the nuclear spins of molecules in a liquid.
2. **The ability to initialize the state of the qubits:** \Rightarrow Wait for relaxation (~ 1 minute). Since the typical energy difference of the spin orientations is small as compared to the temperature only a tiny surplus is used.
3. **A coherence time much longer than operation time:** Coherence times of ~ 1000 s have been observed (single and two qubit operation time: 0.01 ms–100 ms)
4. **An universal set of quantum gates:**
 - single qubit operations: radio frequency pulses, addressing in the frequency space.
 - two qubit operations: Coupling of the spins in the molecules via the electron shell +???
5. **A qubit-specific measurement:** Read-out of the surplus of states which started in the correct state \Rightarrow no scalability. The signal to noise scales as NZ^{-N} , where for large temperatures $Z \approx 2$.

For a weak spin-spin coupling (as compared to the Zeeman-energy (100 to 1000 MHz) we have for two spins A and B in good approximation the following Hamiltonian:

$$H = \hbar\omega_A I_{Az} + \hbar\omega_B I_{Bz} + \hbar\omega_{AB} I_{Az} I_{Bz} . \quad (10.5)$$

(For a strong coupling we would have to replace $I_{Az} I_{Bz}$ by $\vec{I}_A \cdot \vec{I}_B$ (c.f. Eq. 9.1)). To get rid of inhomogeneous broadening induced e.g. by magnetic field gra-

dients, we have to use spin echo pulses, known in NMR as refocusing. The third term in Eq. 10.5 is equivalent to a phase gate. It can be seen by writing down the interaction energy in a matrix form:

$$I_{Az} I_{Bz} = \begin{pmatrix} 1 & 0 & 0 & 0 \\ 0 & -1 & 0 & 0 \\ 0 & 0 & -1 & 0 \\ 0 & 0 & 0 & 1 \end{pmatrix} \quad (10.6)$$

Here we used the canonical basis $\{00, 01, 10, 11\}$. Applying a σ_z -rotation on both qubits ($\text{diag}(1, -1, 1, -1)$ and $\text{diag}(1, 1, -1, -1)$) to the first qubit leads to the energy shift:

$$\begin{pmatrix} 3 & 0 & 0 & 0 \\ 0 & -1 & 0 & 0 \\ 0 & 0 & -1 & 0 \\ 0 & 0 & 0 & -1 \end{pmatrix} \quad (10.7)$$

Up to a global phase this corresponds to a phase gate. How to perform a CNOT is explained in Fig. 10.2. One peculiarity in NMR is that the effective spin-spin interaction is on all the time. However, usually in most of the time we do not want any coupling between the qubits. Virtually we can switch off the coupling by performing a spin-echo experiment on all spins. Having look at Eq. 10.6, we see that the total energy shift is zero if the time evolution before the spin-echo-pulses is the same as afterwards.

Box 1. The thermal equilibrium density matrix. Let us assume that the state of the entire system is well described as an ensemble of non-interacting molecules. For example, this is a good approximation in a liquid sample, where the rapid tumbling averages out intermolecular interactions (15). The ensemble averaged state is described by a density matrix, which is a tensor product of the density matrices for each molecule:

$$\hat{\rho} = \hat{\rho}_{\text{molecule } 1} \otimes \hat{\rho}_{\text{molecule } 2} \otimes \hat{\rho}_{\text{molecule } 3} \otimes \dots \quad (14)$$

Because in thermal equilibrium these density matrices are all identical, and because during their further evolution they do not interact, it is sufficient to consider the evolution of a single molecular density matrix to represent the whole sample. The overall system of $O(10^{23})$ N -spin molecules has a huge number of degrees of freedom, but because it is not possible to address the molecules individually, the system acts as though it has only N degrees of freedom. This means that we obtain only a small number of useful quantum bits from the enormous number of underlying degrees of freedom in the sample.

In thermal equilibrium, the N spins of each molecule are arranged in some distribution of energy eigenstates (that is, aligned with or against B_0). These states are described by a $2^N \times 2^N$ diagonal density matrix whose elements give the average populations of the 2^N eigenstates. For example, the equilibrium density matrix for a single spin is:

$$\hat{\rho}_i^{\text{equilibrium}} = \begin{bmatrix} p \downarrow & 0 \\ 0 & p \uparrow \end{bmatrix} \quad (15)$$

where $p \downarrow$ and $p \uparrow$ denote the population probabilities for the two energy levels. In terms of the Boltzmann factor $\alpha_i = \hbar\omega_i/2kT$:

$$\hat{\rho}_i^{\text{equilibrium}} = \frac{1}{2} \begin{bmatrix} 1 & 0 \\ 0 & 1 \end{bmatrix} + \frac{1}{2} \begin{bmatrix} \alpha_i & 0 \\ 0 & -\alpha_i \end{bmatrix} \quad (16)$$

where ω_i is the resonant frequency of the i^{th} spin. For protons at room temperature, $\alpha \approx 4 \times 10^{-5}$ times B_0 in tesla. Although this is a very small number, this small deviation is what almost all NMR experiments measure.

For a molecule with N spins, in thermal equilibrium the density matrix is approximately given by the tensor product of the states of the individual spins:

$$\hat{\rho} = \hat{\rho}_1 \otimes \hat{\rho}_2 \otimes \dots \otimes \hat{\rho}_N \quad (17)$$

For two spins, we find that:

$$\hat{\rho} = \frac{1}{4} \begin{bmatrix} 1 & 0 & 0 & 0 \\ 0 & 1 & 0 & 0 \\ 0 & 0 & 1 & 0 \\ 0 & 0 & 0 & 1 \end{bmatrix} + \frac{1}{4} \begin{bmatrix} \alpha_1 + \alpha_2 & 0 & 0 & 0 \\ 0 & \alpha_1 - \alpha_2 & 0 & 0 \\ 0 & 0 & -\alpha_1 + \alpha_2 & 0 \\ 0 & 0 & 0 & -\alpha_1 - \alpha_2 \end{bmatrix} \quad (18)$$

written in the energy eigenstate basis $| \uparrow\uparrow \rangle, | \uparrow\downarrow \rangle, | \downarrow\uparrow \rangle, | \downarrow\downarrow \rangle$.

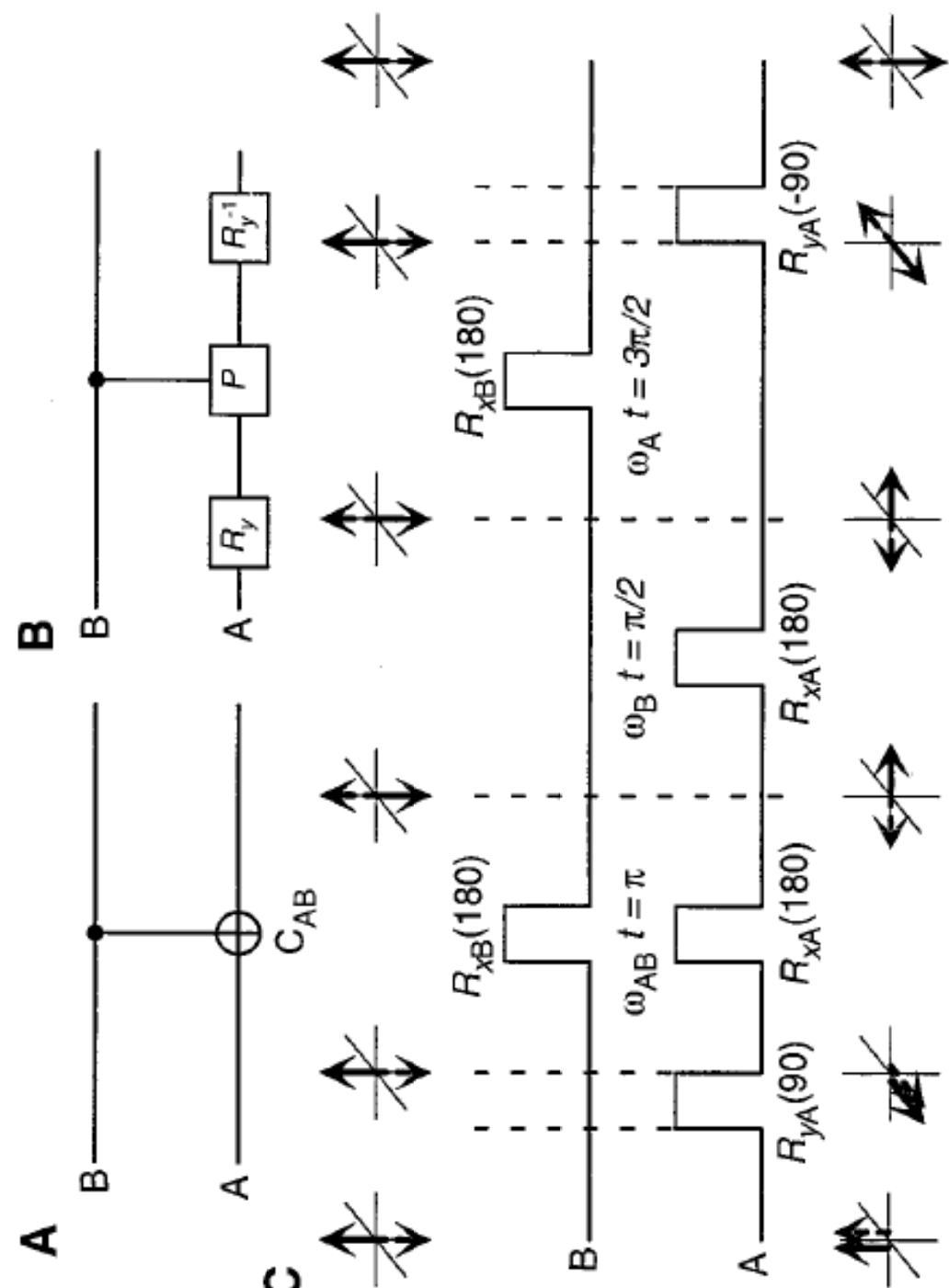
For the $N = 4$ case, the diagonal elements are approximately:

$$\text{diag}(\hat{\rho}_A) = \frac{\alpha}{16} \begin{bmatrix} 1111 & 1111 & 1111 & 1111 & 1111 & 1111 & 1111 & 1111 & 1111 & 1111 & 1111 & 1111 & 1111 & 1111 & 1111 & 1111 \\ 4 & 2 & 2 & 0 & 2 & 0 & 0 & -2 & 2 & 0 & 0 & -2 & 0 & -2 & -2 & -4 \end{bmatrix} \quad (19)$$

where the 16 spin states have been explicitly labeled. Now, a unitary transform on the spin states can be used to selectively exchange populations among the different energy levels; mathematically, this amounts to relabeling the states. Experimentally, this may be accomplished with logic gate pulse sequences (shown below) or by selective rf pulses. Either way, we can produce the final state:

$$\text{diag}(\hat{\rho}'_A) = \frac{\alpha}{16} \begin{bmatrix} 1111 & 1111 & 1111 & 1111 & 1111 & 1111 & 1111 & 1111 & 1111 & 1111 & 1111 & 1111 & 1111 & 1111 & 1111 & 1111 & 1111 \\ 4 & 0 & 0 & 0 & -2 & 2 & 2 & 2 & -2 & -2 & -2 & -4 & 0 & 0 & 0 \end{bmatrix} \quad (20)$$

Figure 10.1: (from Gershenfeld and Chuang, Science 275, 350 (1998)).



1. (A) A controlled-NOT gate acting on two qubits, the controlled-NOT gates implemented by a controlled phase shift gate specified by a unitary matrix C in diagonal elements $\{1, -1\}$ preceded and followed by $\pi/2$ rotations, and the pulse sequence corresponding to the components in (B).

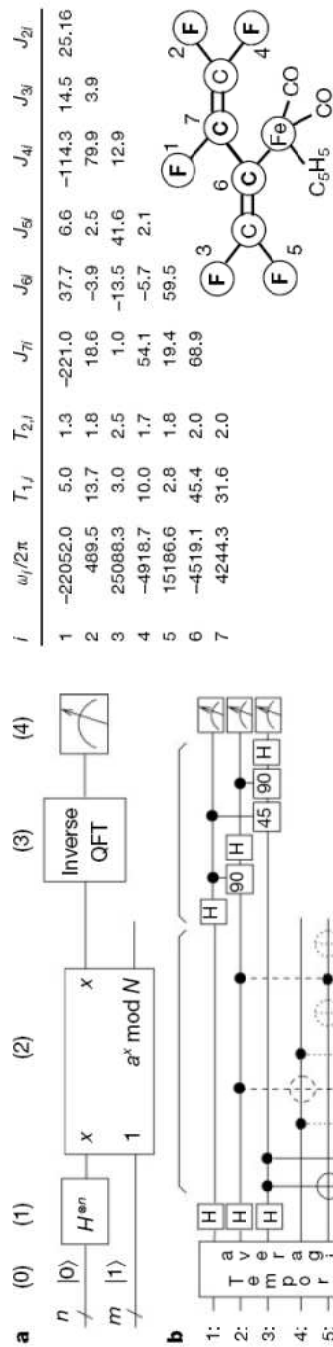


Figure 1 Quantum circuit for Shor's algorithm. **a**, Outline of the quantum circuit. Wires represent qubits, and boxes represent operations. Time goes from left to right. (0) Initialize a first register of $n = 2\lceil \log_2 M \rceil$ qubits to $|0\rangle \otimes \dots \otimes |0\rangle$ (for short $|0\rangle$) and a second register of $m = \lceil \log_2 M \rceil$ qubits to $|0\rangle \otimes \dots \otimes |0\rangle \otimes |1\rangle$. (1) Apply a Hadamard transform H to the first n qubits, so the first register reaches $\sum_{x=0}^{2^n-1} |x\rangle \sqrt{2^{-n}}$. (2) Multiply the second register by $f(x) = a^x \bmod N$ (for some random $a < N$ which has no common factors with N), to get $|\psi_2\rangle = \sum_{x=0}^{2^n-1} |x\rangle |1 \times a^x \bmod N\rangle \sqrt{2^{-n}}$. As the first register is in a superposition of 2^n terms $|x\rangle$, the modular exponentiation is computed for 2^n values of x in parallel. (3) Perform the inverse QFT on the first register¹⁹, giving $|\psi_3\rangle = \sum_{y=0}^{2^n-1} \sum_{x=0}^{2^n-1} e^{2\pi i y f(x)} |y\rangle |a^x \bmod N\rangle \sqrt{2^{-n}}$, where interference causes only terms $|y\rangle$ with $y = c2^n/r$ (for integer q) to have a substantial amplitude, with r the period of $f(x)$. (4) Measure the qubits in the first register. On an ideal single quantum computer, the measurement outcome is $c2^n/r$ (for some c with high probability), and r can be quickly deduced from $c2^n/r$ on a classical computer via continued fractions². **b**, Detailed quantum circuit for the case $N = 15$ and $a = 7$. Control qubits are marked by filled circles; $(+)$ represents a NOT operation and 90° and 45° represent \hat{z} rotations over these angles. The gates shown in dotted lines can be removed by optimization, and the gates shown in dashed lines can be replaced by simpler gates (see Methods).

Figure 10.3: (from Vandersypen et al., Nature **414**, 813 (2001)).

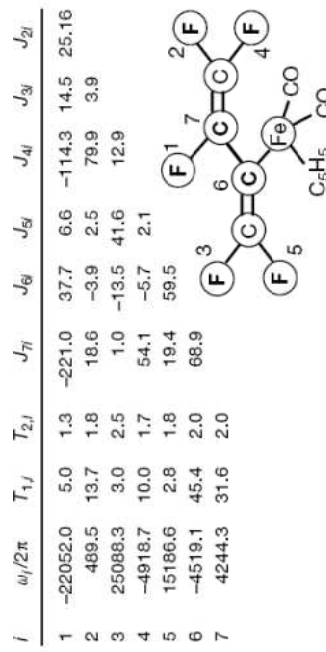


Figure 2 Structure and properties of the quantum computer molecule, a perfluorobutadienyl iron complex with the inner two carbons ^{13}C -labelled. Based on the measured $J_{13\text{C}-13\text{C}}$ values, we concluded that the placement of the iron is as shown, different from that derived in ref. 28 from infrared spectroscopy. The table gives the $\omega_i/2\pi$ (in Hz) at 11.7 T, relative to a reference frequency of ~ 470 MHz and ~ 125 MHz for ^{19}F and ^{13}C , respectively, the longitudinal (T_1 , inversion recovery) and transverse (T_2 , estimation from a single spin-echo sequence) relaxation time constants (in s), and the J -couplings (in Hz). Ethyl (2- ^{13}C -Bromoacetate (Cambridge Isotope Laboratories, Inc.) was converted to ethyl 2-fluoroacetate by heating with AgF , followed by hydrolysis to sodium fluoroacetate using NaOH in MeOH . This salt was converted to 1,1,1,2-tetrafluoroethane using MgF_6 , and was subsequently treated with two equivalents of *n*-butyl lithium followed by I_2 to provide trifluoriodoethene. Half of the ethene was converted to the zinc salt, which was recombined with the remaining ethene and coupled using $\text{Pd}(\text{Ph}_3\text{P})_4$ to give (2,3- ^{13}C)hexafluorobutadiene. The end product was obtained by reacting this butadiene with the anion obtained from treating $[(\pi-\text{C}_6\text{H}_5)_2\text{Fe}(\text{CO})_2]_2$ with sodium amalgam²⁹. The product was purified with column chromatography, giving a total yield of about 5%. The sample, at 0.88 ± 0.04 mol%, in perdeuterated diethyl ether was dried using 3- \AA molecular sieves, filtered through a 0.45- μm syringe filter, and flame-sealed in the NMR sample tube using three freeze-thaw vacuum degassing cycles. All experiments were performed at 30 °C.

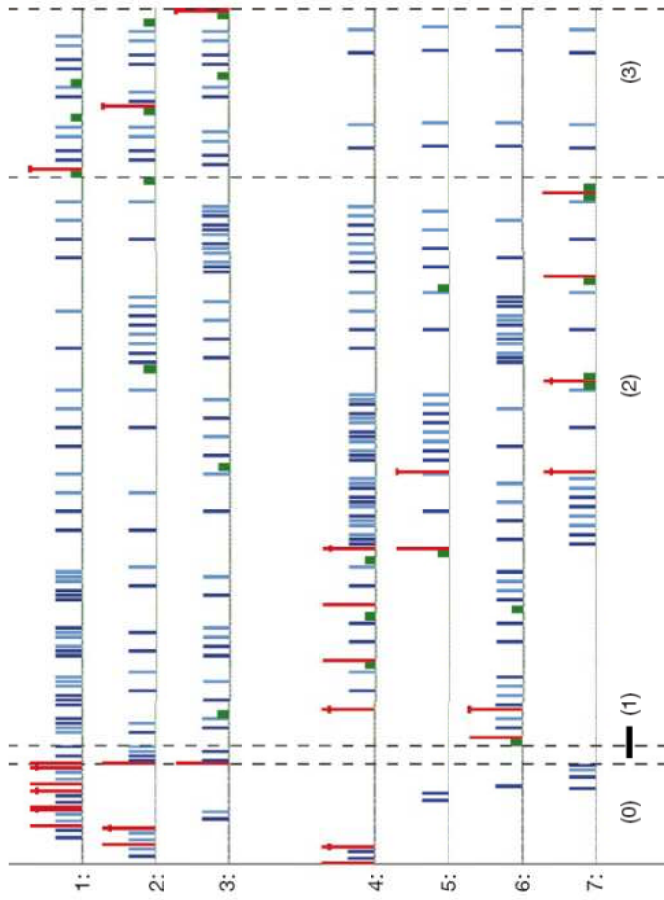


Figure 4 Pulse sequence for implementation of the quantum circuit of Fig. 1 for $a = 7$. The tall red lines represent 90° pulses selectively acting on one of the seven qubits (horizontal lines) about positive \hat{x} (no cross), negative \hat{x} (lower cross) and positive \hat{y} (top cross). Note how single 90° pulses correspond to Hadamard gates, and pairs of such pulses separated by delay times correspond to two-qubit gates. The smaller blue lines

denote 180° selective pulses used for refocusing³⁰ about positive (darker shade) and negative \hat{x} (lighter shade). Rotations about \hat{z} are denoted by smaller and thicker green rectangles, and were implemented with frame-rotations. Time delays are not drawn to scale. The vertical dashed black lines visually separate the steps of the algorithm; step (0) shows one of the 36 temporal averaging sequences.

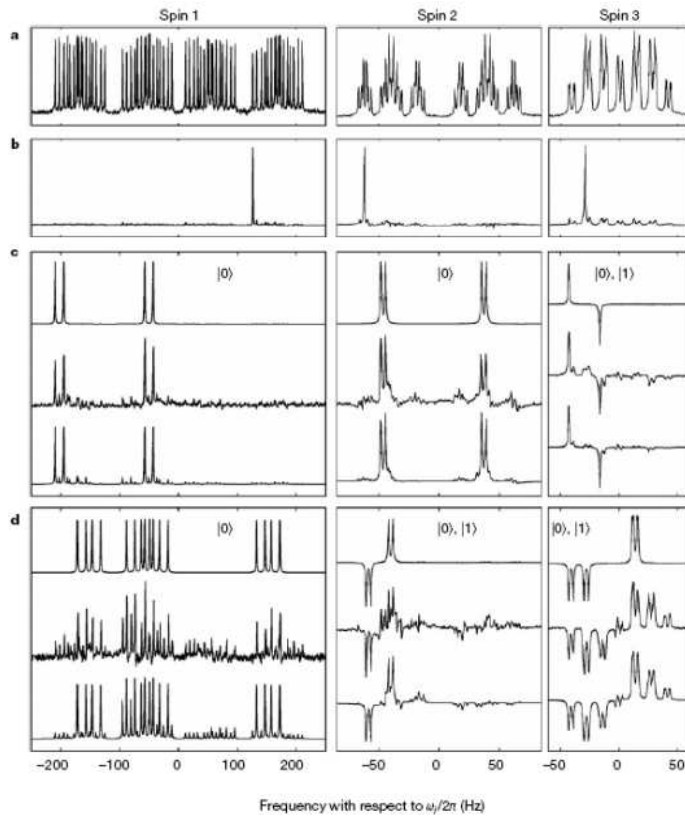


Figure 3 NMR spectra at different stages in the computation. **a**, Experimentally measured thermal equilibrium spectra (real part), acquired after a read-out pulse on spin i has tipped the spin from $|0\rangle$ ($+\hat{z}$) or $|1\rangle$ ($-\hat{z}$) into the \hat{x} - \hat{y} plane, where it induces a voltage oscillating at $\omega_i/2\pi + \Sigma_j \pm J_{ij}/2$ (where the sign depends on the state of the other spins) in a transverse r.f. coil placed near the sample. This voltage was recorded by a phase-sensitive detector and Fourier transformed to obtain a spectrum, with the phase set such that positive (negative) lines correspond to a spin in $|0\rangle$ ($|1\rangle$) before the readout pulse. Frequencies are in hertz, and with respect to $\omega/2\pi$. **b**, Experimental spectra for the

effective pure ground state. As desired, only one line is retained in each multiplet with its position depending on strength and sign of the J -couplings. Here, the transition corresponds to all other spins in $|0\rangle$. The state ρ_7 is obtained from this state by applying a NOT on spin 7. **c**, Output spectra of the easy case of Shor's algorithm ($a = 11$). The top traces are the ideally expected spectra, the middle traces are the experimental data, and the bottom traces are simulations which incorporate decoherence effects (see text). Each trace was rescaled separately. **d**, Similar set of spectra as in **c**, but for the difficult case ($a = 7$).

Figure 10.5: (from Vandersypen et al., Nature **414**, 813 (2001)).

Chapter 11

Linear optics

Zeilinger and Gisin

Chapter 12

Deutsch-Josza algorithm

The Deutsch-Josza (DJ) algorithm is "the" simplest algorithm where a quantum computer offers some advantage over a classical machine. The DJ-aglorithm can decide whether a function is even or odd. In the simplest case we look at the functions which map one bit onto another one. There are four possible functions:

function	input	output	
$f_1(x)$	$\{0, 1\}$	$\{0, 0\}$	
$f_2(x)$	$\{0, 1\}$	$\{1, 1\}$	
$f_3(x)$	$\{0, 1\}$	$\{0, 1\}$	
$f_4(x)$	$\{0, 1\}$	$\{1, 0\}$	(12.1)

These functions can be divided into two classes: The constant (even) functions f_1 and f_2 and the balanced (odd) functions f_3 and f_4 . The task is now with the smallest possible function calls to find out whether a function (hidden in a black box) is constant or balanced. With a classical machine one needs always two calls to decide on that questions. Namely one needs to call the function with 0 and 1 as an input. Often this problem is translated into the question on how many sides of a coin you have to look. The functions correspond here to two false coins (both sides either head or tail / constant) and two fair ones (one side head, the other tail / balanced). Here it also clear that we have to look on both sides before we can decide whether a coin is false or fair.

We are now going to formulate the problem quantum mechanically. For this we have to generalize the function to take qubits as inputs. Since quantum

$n = \{1, 2, 3, 4\}$	Constant		Balanced	
	case 1	case 2	case 3	case 4
$f_n(0)$	0	1	0	1
$f_n(1)$	0	1	1	0
Logic	Id	NOT_a	$CNOT$	$0 - CNOT$

Table 12.1: Laser pulses for the implementation of the DJ-algorithm on a single ion. In the latter two cases the control bit is qubit a

mechanically all operations are unitary, we have to add another qubit (the work or auxiliary qubit). Therefore we have now two input qubits $|a\rangle$ and $|w\rangle$ und two output qubits. Qubit $|a\rangle$ holds the input variable x . Qubit $|w\rangle$ = (the work qubit) will receive the result of the evaluation $f_n(x)$ plus the initial value of qubit $|w\rangle$ (see Fig. 12.1). Thus the unitary U_{f_n} representing the implementation of the function is defined in the following way:

$$U_{f_n}|z_w, x_a\rangle = |f_n(x) \oplus z, x\rangle. \quad (12.2)$$

This leads then to the unitaries displayed in Tab. 12.1

The algorithm consists then out of the following steps (c.f. Fig.??):

1. initialize the system in the state $|0_a\rangle \otimes |1_w\rangle$.
2. put the input $|a\rangle$ into $\frac{1}{\sqrt{2}}(|0\rangle + |1\rangle)$ and the work-qubit $|w\rangle$ into $\frac{1}{\sqrt{2}}(|0\rangle - |1\rangle)$ with $\pi/2$ -pulses.
3. evaluate the function by implementing U_{f_n} .
4. apply $-\pi/2$ -pulse on $|a\rangle$ to close the interferometer.
5. read out $|a\rangle$

How does the DJ-algorithm perform the task to distinguish between constant and balanced functions? To understand this it is helpful to realize that the evaluation of the function is inserted between two Ramsey-pulses. That means the function is evaluated for $x = |0\rangle$ and $x = |1\rangle$ simultaneously. What happens now is that if the function is constant nothing can happen to the relative phase between $x = |0\rangle$ and $x = |1\rangle$. This can be understood as U_{f_1} and U_{f_2} act only on qubit $|w\rangle$. For the balanced case, however, one gets a relative phase of π between $x = |0\rangle$ and $x = |1\rangle$. Thus we will find qubit

	Logic	Laser pulses
f_1	$R_{\bar{y}_w} R_{y_w}$	—
f_2	$R_{\bar{y}_w}$ SWAP $^{-1}$ NOT $_a$ SWAP R_{y_w}	$R^+(\frac{\pi}{\sqrt{2}}, 0)R^+(\frac{2\pi}{\sqrt{2}}, \varphi_{\text{swap}})R^+(\frac{\pi}{\sqrt{2}}, 0)$ $R(\frac{\pi}{2}, 0)R(\pi, \frac{\pi}{2})R(\frac{\pi}{2}, \pi)$ $R^+(\frac{\pi}{\sqrt{2}}, \pi)R^+(\frac{2\pi}{\sqrt{2}}, \pi + \varphi_{\text{swap}})R^+(\frac{\pi}{\sqrt{2}}, \pi)$
f_3	$R_{\bar{y}_w}$ CNOT R_{y_w}	$R^+(\frac{\pi}{\sqrt{2}}, 0)R^+(\pi, \frac{\pi}{2})R^+(\frac{\pi}{\sqrt{2}}, 0)R^+(\pi, \frac{\pi}{2})$
f_4	$R_{\bar{y}_w}$ Z-CNOT R_{y_w}	$R(\pi, 0)R^+(\frac{\pi}{\sqrt{2}}, 0)R^+(\pi, \frac{\pi}{2})R^+(\frac{\pi}{\sqrt{2}}, 0)R^+(\pi, \frac{\pi}{2})R(\pi, 0)$

Table 12.2: Laser pulses for the implementation of the DJ-algorithm on a single ion.

$|a\rangle$ in $|0\rangle$ for the constant functions and in $|1\rangle$ for the balanced functions. In all cases we will find the work qubit $|w\rangle$ in 1.

After the algorithm the work qubit $|w\rangle$ contains no information. Therefore we gained only one bit of information, namely whether the function was constant or balanced. Here the advantage of quantum computing lies only in the fact that we can ask not only the question what is on one side of the coin, but whether there is a difference of the two sides. We could ask also a different question. E.g. what is $f_n(x)$? This would be accomplished simply by executing the function starting in $|00\rangle$ and reading out qubit $|w\rangle$.

Implementations:

1. NMR \Rightarrow Chuang et al., Nature **393**, 143 (1998).
2. Ion traps \Rightarrow Gulde et al., Nature **421**, 48-50 (2003).
3. Vibrational levels of molecules Li₂ \Rightarrow Vala et al., PRA **66**, 062316 (2002).
4. Fiber optics \Rightarrow E. Brainis et al., PRL **90**, 157902 (2003).

The only scalable approach right now is the ion-trap implementation.

	Constant		Balanced	
	case 1	case 2	case 3	case 4
expected $ \langle 1 x \rangle ^2$	0	0	1	1
measured $ \langle 1 x \rangle ^2$	0.019(6)	0.087(6)	0.975(4)	0.975(2)
expected $ \langle 1 z \rangle ^2$	1	1	1	1
measured $ \langle 1 z \rangle ^2$	—	0.90(1)	0.931(9)	0.986(4)

Table 12.3: Results of the DJ–algorithm (ion trap, from Gulde et al., Nature **421**, 48-50 (2003)).

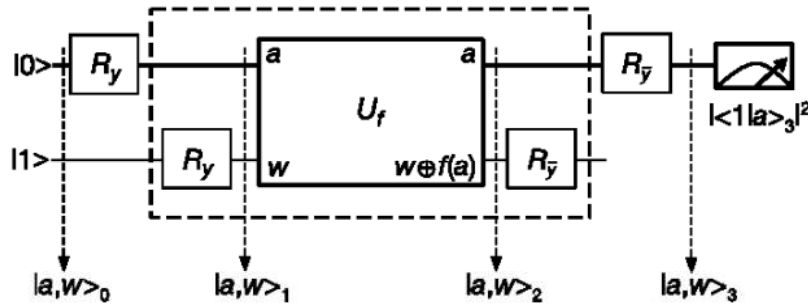


Figure 1 Quantum circuit for implementing the Deutsch–Jozsa algorithm with basic quantum operations. The upper line shows the input qubit $|a\rangle$ ('which side of the coin' information), the lower line an auxiliary working qubit $|w\rangle$ (corresponding to the channel on which the answer is provided). The rotations R_y (see Methods for details) create superpositions $|a\rangle_1 = (|0\rangle + |1\rangle)/\sqrt{2}$ and $|w\rangle_1 = (|0\rangle - |1\rangle)/\sqrt{2}$ from the inputs $|a\rangle_0 = |0\rangle$ and $|w\rangle_0 = |1\rangle$. The box U_{f_n} represents a unitary operation specific to each of the functions f_n , which applies f_n to a and adds the result to w modulo 2. Table 1 lists the logic operations required for transforming $|w\rangle$ into $|w \oplus f_n(a)\rangle$. The output of the box is $|a, w\rangle_2 = (|0, w_{in} \oplus f_n(0)\rangle + |1, w_{in} \oplus f_n(1)\rangle)/\sqrt{2}$. Up to an overall sign $|w\rangle$ is left unchanged, but the positive superposition $(|0\rangle + |1\rangle)/\sqrt{2}$ on $|a\rangle$ is transformed into a negative superposition $|a\rangle_2 = (|0\rangle - |1\rangle)/\sqrt{2}$ if f is balanced; otherwise it is unchanged. After the final rotations R_y , a measurement on $|a\rangle$ is performed with result $|a\rangle_3$ = either $|0\rangle$ or $|1\rangle$. Because of the sign change in $|a\rangle_2$ if f is balanced, $|\langle 1 | a \rangle_3|^2 = f_n(0) \oplus f_n(1)$, that is, $|a\rangle_3$ yields the desired information whether the function f_n is balanced or constant. The working qubit w resumes its initial value $|w\rangle_3 = |w\rangle_0 = |1\rangle$.

Figure 12.1: (from Gulde et al., Nature 421, 48-50 (2003))

Figure 2 Proton spectrum after completion of the DJ algorithm and a single read-out pulse X_A , with an effectively pure initial state $|00\rangle$ and with a thermal initial state (inset). The low(high)-frequency lines correspond to the transitions $|00\rangle \rightarrow |10\rangle$ ($|01\rangle \rightarrow |11\rangle$). The frequency is relative to 499.755.169 Hz, and the amplitude has arbitrary units. The spectrum is the Fourier-transformed time varying voltage $V(t)$, induced in the pick up coil by the precession of spin A about $-\mathbf{B}_0$, at frequency ω_A , after the read-out pulse X_A . $V(t)$ is given by $V(t) \approx V_0 \text{ Triple}^{-i\omega_A t} e^{-i\omega_A t} \rho(0) e^{i\omega_A t} \rho(t) e^{i\omega_A t}$, where $\sigma_{xx} = (\omega_A - \omega_A)/i$, where σ_{xx} are Pauli matrices, and $\rho(0)$ is the density matrix of the state immediately before the readout pulse. By this convention, a spectral line for spin A is real and positive (negative) when spin A is $|0\rangle$ ($|1\rangle$) right before the X_A readout pulse. Experiments were performed at Stanford University using an 11.7-Tesla Oxford Instruments magnet and a Varian Unity Inova spectrometer with a triple-resonance probe. ^{13}C -labelled CHCl_3 was obtained from Cambridge Isotope Laboratories.

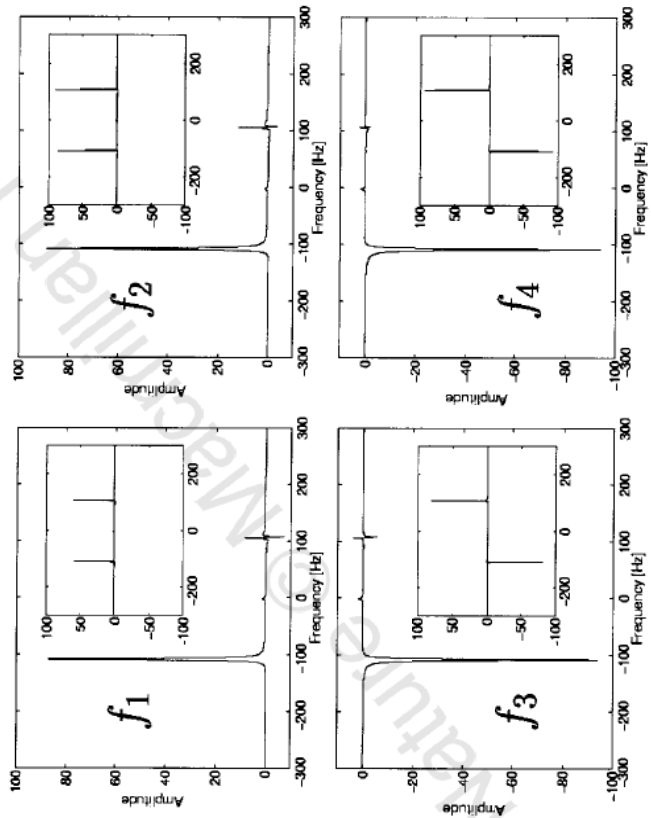


Figure 12.2: (from Chuang et al., Nature 393, 143 (1998)).

Figure 3 Experimentally measured and theoretically expected deviation density matrices after completion of the D-J algorithm. The diagonal elements represent the normalized populations of the states $|00\rangle$, $|10\rangle$, $|11\rangle$ and $|11\rangle$ (from left to right). The off-diagonal elements represent coherences between different states. The magnitudes are shown with the sign of the real component; all imaginary components were small. The deviation density matrix was obtained from the integrals of the proton and carbon spectral lines, acquired for a series of 9 experiments with different read-out pulses for each spin (quantum state tomography²⁴). The observed experimental non-idealities can be quantified as follows. In the experiments, the normalized pure-state population (ideally equal to 1), varied from 0.998 to 1.019. The other deviation density matrix elements (ideally 0), were smaller than 0.075 in magnitude. The relative error ϵ on the experimental pure-state output density matrix ρ_{exp} , defined as $\epsilon = \|\rho_{\text{exp}} - \rho_{\text{theory}}\|/\|\rho_{\text{theory}}\|$, varied between 8 and 12%.

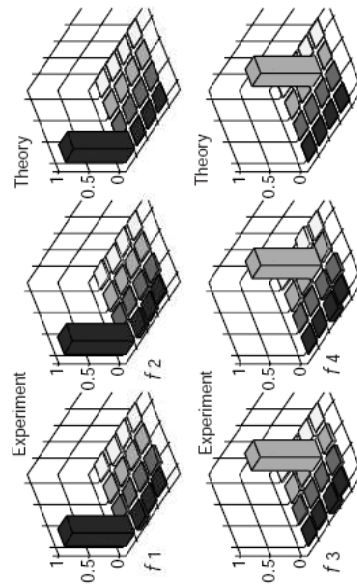


Figure 12.3: (from Chuang et al., Nature **393**, 143 (1998)).

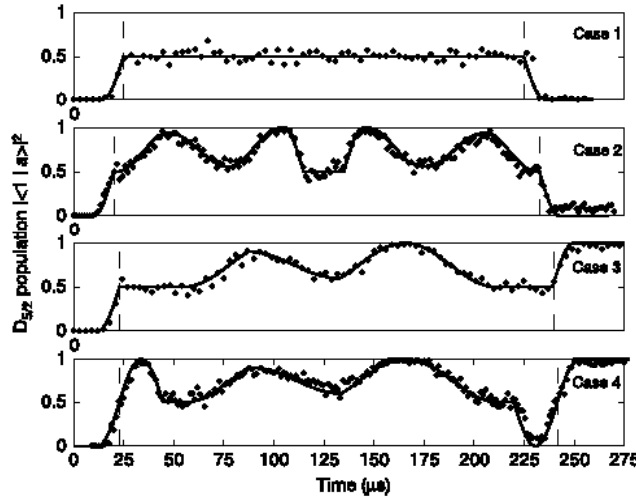


Figure 3 Time evolution of $|\langle 1 | a \rangle|^2$. Points are the probabilities, each inferred from 100 measurements, the line shows the ideal evolution. No parameters were adjusted to fit the data. The implementation of the functions $R_{\bar{y}_a} U_{f_a} R_{y_a}$ takes place between the dashed lines. An initial R_{y_a} and a final $R_{\bar{y}_a}$ rotation on $|a\rangle$, implemented by carrier pulses, complete the algorithm. Taking case 3 as an example, R_{y_a} lasts from 12 μ s to 22 μ s. Then $R_{\bar{y}_a} U_{f_a} R_{y_a}$ on $|a,w\rangle$ is implemented from 54 μ s to 212 μ s with the laser tuned to the blue sideband. The laser phase is switched at 87, 133 and 166 μ s according to Table 3. The final $R_{\bar{y}_a}$ pulse is applied from 240 to 250 μ s.

Figure 12.4: Traces for the implementation of the DJ-algorithm on a single ion (from Gulde et al., Nature **421**, 48-50 (2003)).

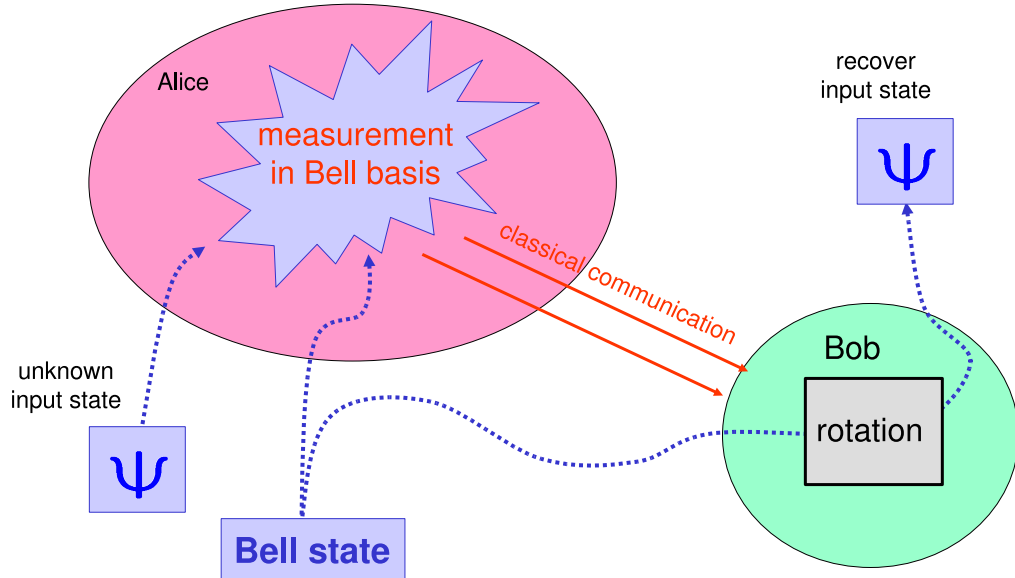
Chapter 13

Teleportation

In physics teleportation means the transfer of quantum information between two qubits without an open quantum channel at the time of the transfer. To help understanding the peculiarities of teleportation, we introduce two parties: Alice and Bob. The teleportation consists now of the following steps (c.f. 13.1)

- Creation of an entangled pair of qubit. Alice holds one qubit and Bob another one. It is important to realize that only for this a quantum channel between Alice and Bob is required.
- Alice receives the quantum information to be teleported in a qubit. Actually, the quantum information can be created much later than the creation of the entangled pair (in the Innsbruck ion trap experiment (M. Riebe *et al.* *Nature* **429**, 734–737 (2004)) it was upto 10 ms later)
- Alice measures the source qubit together with her part of the entangled qubit in the so-called Bell basis. For this Alice applies a CNOT-gate to her two qubits. This measurement projects the target qubit (Bobs part of the entangled state) into one of four possible states (see the Math below). Interestingly these four states of the target qubit are either directly the original state of the source qubit or rotated by σ_z , σ_x or $\sigma_z\sigma_x$. Which deviation is present is encoded in the two classical bits received from the Bell measurement.
- The result of the Bell measurement is communicated to Bob via a

classical channel, Bob applies the corresponding rotation and holds now the original state. Note that neither Alice nor Bob have received any information on this state during the whole procedure. Also there is no information on the teleported quantum state left in the source qubit. Both things are necessary conditions that allow for the survival of the quantum state.



Bennett et al., *Phys. Rev. Lett.* 70, 1895 (1993)

Figure 13.1: Principle of the teleportation procedure.

We are going now to describe this mathematically: The first qubit (rightmost) will be the source, the second the auxiliary and the third one the target qubit. After the creation of the Bell-state we have entangled the auxiliary qubit (held by Alice) with the target qubit (held by Bob):

$$|\varphi\rangle = \frac{1}{\sqrt{2}} (|01\rangle + |10\rangle) \otimes |\psi\rangle = \frac{1}{\sqrt{2}} (|01\rangle + |10\rangle) \otimes (\alpha|0\rangle + \beta|1\rangle) . \quad (13.1)$$

$|\psi\rangle = (\alpha|0\rangle + \beta|1\rangle)$ is the to be teleported state in the first qubit. We expand now the terms and obtain:

$$|\varphi\rangle = \frac{1}{\sqrt{2}} (\alpha|010\rangle + \alpha|100\rangle + \beta|011\rangle + \beta|101\rangle) \quad (13.2)$$

We will try now to express the first two qubits in the Bell–basis $|\Phi^\pm\rangle = \{\frac{1}{\sqrt{2}}(|00\rangle \pm |11\rangle), |\Psi^\pm\rangle = \frac{1}{\sqrt{2}}(|01\rangle \pm |10\rangle)\}$ (by adding some zeros):

$$\begin{aligned}
 |\varphi\rangle &= \frac{1}{2\sqrt{2}} [2\alpha|010\rangle + \alpha|001\rangle - \alpha|001\rangle \\
 &\quad + 2\alpha|100\rangle + \alpha|111\rangle - \alpha|111\rangle \\
 &\quad + 2\beta|011\rangle + \beta|000\rangle - \beta|000\rangle \\
 &\quad + 2\beta|101\rangle + \beta|110\rangle - \beta|110\rangle] \\
 &= (\alpha|0\rangle + \beta|1\rangle)|\Psi^+\rangle - (\alpha|0\rangle - \beta|1\rangle)|\Psi^-\rangle \\
 &\quad + (\alpha|1\rangle + \beta|0\rangle)|\Phi^+\rangle - (\alpha|1\rangle - \beta|0\rangle)|\Phi^-\rangle \\
 &= |\psi\rangle|\Psi^+\rangle - \sigma_z|\psi\rangle|\Psi^-\rangle \\
 &\quad + \sigma_x|\psi\rangle|\Phi^+\rangle - \sigma_z\sigma_x|\psi\rangle|\Phi^-\rangle
 \end{aligned} \tag{13.3}$$

Thus the state $|\psi\rangle$ appears in the target qubit upto a rotation depending on the Bell–state observed between the source qubit and the auxilary qubit. Furthermore, we see that all four Bell–states have the same weight. Therefore the Bell measurement gives no information on $|\psi\rangle$. Only Bob who has the target qubit and the result of the Bell–measurement available can reconstruct $|\psi\rangle$.

According to our current knowledge, physical systems are fully described by their quantum state. Therefore, we can conclude that in the teleportation procedure the identity of one particle is transferred to another one.

13.1 Photon experiments

????

13.2 Ion trap experiment(s)

The production of the entangled state is quite straight forward: we could use a CNOT where the control bit is in a superposition of $|0\rangle$ and $|1\rangle$. In the

experiments, however, a quicker and more robust way is used (see items 4–6 in Table 13.1).

How do we realize a Bell-measurement? The idea is to run the sequence which creates from a logical eigenstate with a $\pi/2$ pulse on the control bit and a subsequent CNOT an entangled state backwards. In this way all four Bell states are mapped onto the four different logical eigenstates. A further difficulty is that the read-out of the source and auxiliary qubit are not allowed to destroy the coherence of the target ion (which is only $5\ \mu\text{m}$ from the auxiliary ion away). It is not obvious how to scatter thousands of photons on one ion while not scattering any on the neighboring ion. The idea used in the Innsbruck experiments was to move the quantum information in the target ion from the $|S_{1/2}\rangle - |D_{5/2}\rangle$ manifold to the Zeeman structure of the $D_{5/2}$ level with a π pulse on the $|S_{1/2}, m_j = -1/2\rangle \rightarrow |D_{1/2}, m_j = -5/2\rangle$ transition. Thus the S state population ends in the $|D_{1/2}, m_j = -5/2\rangle$ state while the population in the $|D_{1/2}, m_j = -1/2\rangle$ remains unaffected. Now this qubit is protected and applying blue light for the state detection does not disturb this qubit. In the Boulder experiment on Beryllium ions this was solved differently. Here the ion string was separated in the segmented trap such that the distance between the ions was big enough so that no spurious detection photons disturbed the target qubit.

To make the experiment feasible phase coherence must be kept over the whole sequence. Therefore generalized spin echo sequences were used in both experiments. Furthermore, in the Innsbruck experiments the algorithm was slightly modified by shifting around some $\pi/2$ pulses. The reason was initially only an aesthetic one, however, later one realised that with this procedure dephasing affected all states on the Bloch sphere similarly with this symmetrized pulse sequence. With the straight forward pulse sequence logical eigenstates would have been teleported much better than superposition states.

Table 13.1 shows the pulse sequence used in the Innsbruck ion trap experiments.

	Action	Comment
1	Light at 397 nm	Doppler preparation
2	Light at 729 nm	Sideband cooling
3	Light at 397 nm	Optical pumping
Entangle	4 $R_3^+(\pi/2, 3\pi/2)$ 5 $R_2^c(\pi, 3\pi/2)$ 6 $R_2^+(\pi, \pi/2)$	Entangle ion #3 with motional qubit Prepare ion #2 for entanglement Entangle ion #2 with ion #3
	7 Wait for $1\mu s - 10\,000\,\mu s$ 8 $R_3^H(\pi, 0)$	Stand-by for teleportation Hide target ion
	9 $R_1^c(\vartheta_\chi, \varphi_\chi)$	Prepare source ion #1 in state χ
Rotate into Bell-basis	10 $R_2^+(\pi, 3\pi/2)$ 11 $R_1^+(\pi/\sqrt{2}, \pi/2)$ 12 $R_1^+(\pi, 0)$ 13 $R_1^+(\pi/\sqrt{2}, \pi/2)$ 14 $R_1^+(\pi, 0)$ 15 $R_1^c(\pi, \pi/2)$ 16 $R_3^H(\pi, \pi)$ 17 $R_3^c(\pi, \pi/2)$ 18 $R_3^H(\pi, 0)$ 19 $R_2^+(\pi, \pi/2)$ 20 $R_1^c(\pi/2, 3\pi/2)$ 21 $R_2^c(\pi/2, \pi/2)$	Get motional qubit from ion #2 Composite pulse for phasegate Composite pulse for phasegate Composite pulse for phasegate Composite pulse for phasegate Spin echo on ion #1 Unhide ion #3 for spin echo Spin echo on ion #3 Hide ion #3 again Write motional qubit back to ion #2 Part of rotation into Bell-basis Finalize rotation into Bell basis
Read-out	22 $R_2^H(\pi, 0)$ 23 PMDetection for $250\,\mu s$ 24 $R_1^H(\pi, 0)$ 25 $R_2^H(\pi, \pi)$ 26 PMDetection for $250\,\mu s$ 27 $R_2^H(\pi, 0)$ 28 Wait $300\,\mu s$ 29 $R_3^H(\pi, \pi)$	Hide ion #2 Read out ion #1 with photomultiplier Hide ion #1 Unhide ion #2 Read out ion #2 with photomultiplier Hide ion #2 Let system rephase; part of spin echo Unhide ion #3
	30 $R_3^c(\pi/2, 3\pi/2 + \phi)$	Change basis
	31 $R_3^c(\pi, \phi)$ 32 $R_3^c(\pi, \pi/2 + \phi)$ 33 $R_3^c(\pi, \phi)$	$i\sigma_x \} = i\sigma_z$ conditioned on PMDetection #1 $i\sigma_y \}$ $i\sigma_x$ conditioned on PMDetection #2
	34 $R_3^c(\vartheta_\chi, \varphi_\chi + \pi + \phi)$	Inverse of preparation of χ with offset ϕ
	35 Light at 397 nm	Read out of ion #3 with camera

Table 13.1: Pulse sequence used in the Innsbruck ion trap experiments.

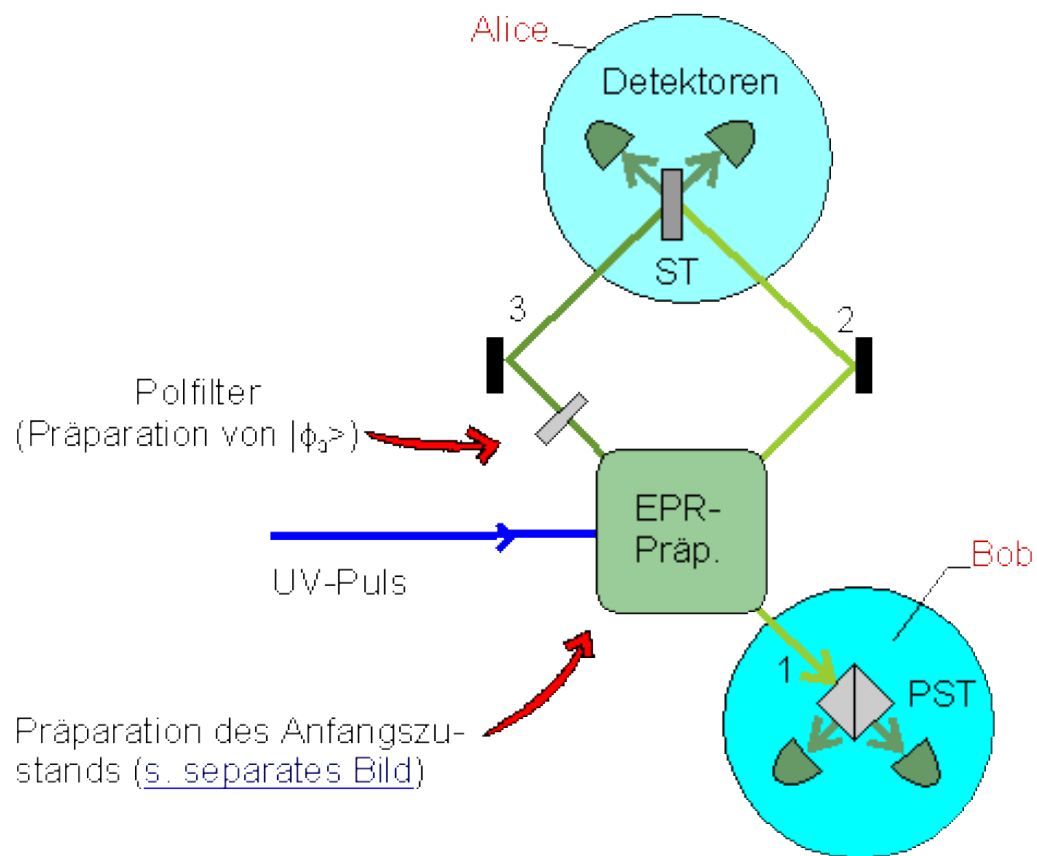


Figure 13.2: Basic implementation of the Zeilinger experiment (D. Bouwmeester et al. Nature **390**, 575-9 (1997)).

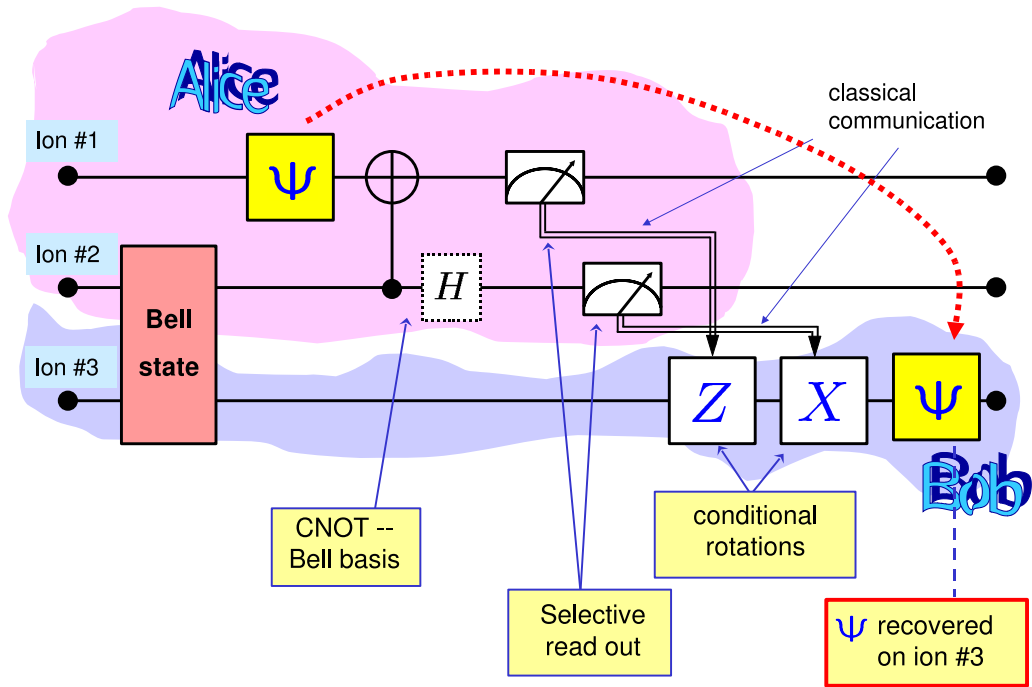


Figure 13.3: Visualization of the teleportation algorithm as implemented in the ion trap experiment(s). (M. Riebe *et al.* Nature **429**, 734–737 (2004) (trapped calcium ions) and M.D. Barret *et al.* Nature **429**, 737–739 (2004) (trapped beryllium ions))

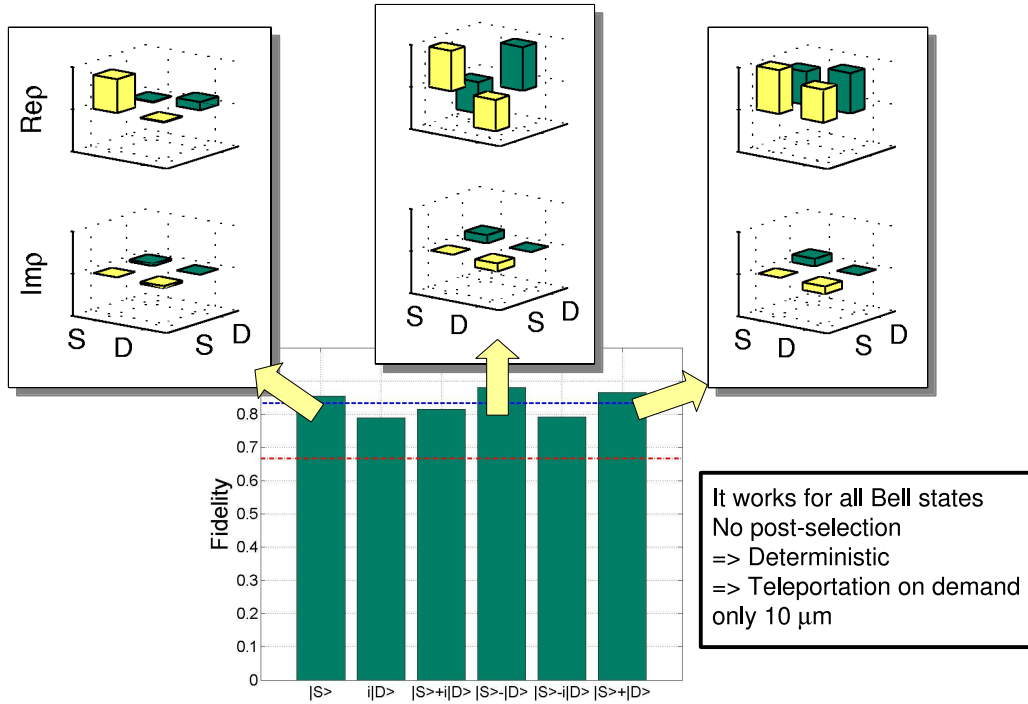


Figure 13.4: Result of the ion trap experiment. Six test states were “teleported” with fidelities in the order of 0.83. Note that using classical techniques (measuring the source and then preparing the target qubit) maximally an average fidelity of $2/3$ is achievable.

Chapter 14

Simulation of quantum systems